

# **Modeling and Measurement of Radon and Thoron Emission from Naturally Occurring Radioactive Materials**

*By*

**BIJAY KUMAR SAHOO**

PHYS01200704011

Bhabha Atomic Research Centre, Mumbai

*A thesis submitted to the  
Board of Studies in Physical Sciences*

*In partial fulfillment of requirements  
For the Degree of*

**DOCTOR OF PHILOSOPHY**

*of*

**HOMI BHABHA NATIONAL INSTITUTE**



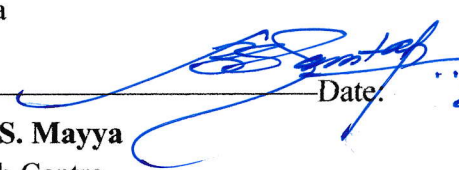
**April, 2014**

# Homi Bhabha National Institute

## Recommendations of the Viva Voce Committee

As members of the Viva Voce Committee, we certify that we have read the dissertation prepared by **Bijay Kumar Sahoo** entitled "Modeling and Measurement of Radon and Thoron Emission from Naturally Occurring Radioactive Materials" and recommend that it may be accepted as fulfilling the dissertation requirement for the degree of Doctor of Philosophy.

 Date: 26.4.14  
Chairman: **Dr. B.K. Dutta**  
Bhabha Atomic Research Centre,  
Mumbai - 400 085, India

 Date: 26.04.14  
Guide/Convener: **Dr. Y.S. Mayya**  
Bhabha Atomic Research Centre,  
Mumbai - 400 085, India

 Date: 26.04.14  
Member1: **Dr. P.K. Sarkar**  
Bhabha Atomic Research Centre,  
Mumbai - 400 085, India

 Date: 26/4/2014  
Member2: **Dr. R.M. Tripathi**  
Bhabha Atomic Research Centre,  
Mumbai - 400 085, India

 Date: 26/04/2014  
External Examiner: **Dr. R.C. Ramola**  
HNB Garhwal University,  
Tehri, Uttarakhand, India

Final approval and acceptance of this dissertation is contingent upon the candidate's submission of the final copies of the dissertation to HBNI

I hereby certify that I have read this dissertation prepared under my direction and recommend that it may be accepted as fulfilling the dissertation requirement.

Date: 26-04-2014  
Place: Mumbai

Guide

  
Prof. B. N. Jagatap

## **STATEMENT BY AUTHOR**

This dissertation has been submitted in partial fulfillment of requirements for an advanced degree at Homi Bhabha National Institute (HBNI) and is deposited in the Library to be made available to borrowers under rules of the HBNI.

Brief quotations from this dissertation are allowable without special permission, provided that accurate acknowledgement of source is made. Requests for permission for extended quotation from or reproduction of this manuscript in whole or in part may be granted by the Competent Authority of HBNI when in his or her judgment the proposed use of the material is in the interests of scholarship. In all other instances, however, permission must be obtained from the author.



(Bijay Kumar Sahoo)

## DECLARATION

I, hereby declare that the investigation presented in the thesis has been carried out by me. The work is original and has not been submitted earlier as a whole or in part for a degree /diploma at this or any other Institution / University.



(Bijay Kumar Sahoo)

## List of Publications arising from the thesis

### Journal

1. A model to predict radon exhalation from walls to indoor air based on the exhalation from building material samples, B.K. Sahoo, B.K. Sapra, J.J. Gaware, S.D. Kanse, Y.S. Mayya, *Sci of Total Environment*, **2011**, 409, 2635-2641
2. Two dimensional diffusion theory of trace gas buildup in soil chambers for flux measurements, B.K. Sahoo, Y.S. Mayya, *Agric. and Forest Meteorol*, **2010**, 150, 1211-1224.
3. Radon exhalation studies in an Indian Uranium tailings pile, B.K. Sahoo, Y.S. Mayya, B.K. Sapra, J.J. Gaware, K.S. Banerjee, H.S. Kushwaha, *Radiation Measurements* **2010**, 45, 237-241.
4. Estimation of radon emanation factor in Indian building materials, B.K. Sahoo, D. Nathwani, K.P. Eappen, T.V. Ramachandran, J.J. Gaware, Y.S. Mayya, *Radiation Measurements*, **2007**, 42, 1422-1425.

### Conferences

1. Development of a fitting algorithm for the joint estimation of radon flux and diffusion coefficient, B.K. Sahoo, B.K. Sapra, Y.S. Mayya, *Proceeding of IARPNC*, **2012**, 82
2. A study on thoron exhalation from monazite beach sands at High Background Radiation Areas, Kerala, B.K. Sahoo, S.D. Kanse, J.J. Gaware, B.K. Sapra, Y.S. Mayya, *Conference proceeding of International Conference 7-HLNRRRA (High Levels of Natural Radiation and Radon Areas)*, **2010**, 56-57
3. Measurement of radon flux and tailings parameters to quantify the source term of radon exhalation from U tailings pile at Jaduguda, B.K. Sahoo, Y.S. Mayya, B.K. Sapra, J.J. Gaware, H.S. Kushwaha, *Proceeding of IARPNC*, **2010**, 35
4. Radon flux from a uranium tailings pond- A comparative study between measured and estimated values, B.K. Sahoo., K.P. Eappen, K.S. Banerjee, T.V. Ramachandran, D. Sengupta, Y.S. Mayya, *Proceedings of sixteenth National Symposium on Environment*, **2008**, 251-256.



(Bijay Kumar Sahoo)

This Thesis is dedicated

To

*My Wife*

*Chinmayee Sahoo*

## **ACKNOWLEDGEMENTS**

I wish to express my deep sense of respect and gratitude to my thesis supervisor, Dr. Y.S. Mayya who has been a constant source of inspiration during this thesis work. His motivating ideas and fruitful discussions have guided me to shape this thesis. During the early years of my PhD work, he taught me the modeling aspect of radon transport in the porous media. He has given me the freedom to do experiments of my own, has rebuilt my self-beliefs and has inspired me to think on the implications of experimental observations. He has helped me in many ways and it's very hard to count those.

Special thanks to my Doctoral Committee chairman Dr. B. K. Dutta, for helping me to maintain the focus by way of critical discussions and constructive suggestions. I also thank the Doctoral Committee members Dr. P.K. Sarkar and Dr. R.M. Tripathi for their helpful suggestions during the annual reviews. I am grateful to Dr. B. K. Sapra, Head, E&BDS, RP&AD for her guidance in evolving various perspectives, constant encouragement during the entire course of this work and making various technical and editorial remarks in the thesis.

I acknowledge the UCIL and Health Physics Unit, Jaduguda for extending the tailings ponds facility for sample collections and carrying out experiments. I also acknowledge the help and support rendered by Dr. T.V. Ramachandran and Dr. K.P. Eappen during the early part of my work. I am indebted to Shri J.J. Gaware for his support in instrumentation and for being always available for sharing ideas on executing various experiments at Jaduguda. I am specifically thankful to Dr. Rosaline Mishra, Mr. Sandeep Kanse and Mrs. Rajeswari Pradhan for their help in editing the thesis.

I should also acknowledge the fruitful interactions and discussions I had on various occasions with my colleagues and friends, Mr. Arshad Khan, Dr. S.Anand, Mr. Manish Joshi, Mr. Tarun Agarwal, Mr. Ashok Kumar and Mr. Chinna esakki. It is very difficult to name all those who have helped in providing logistic, laboratory and administrative support during the various stages of the executing work reported in this thesis. I apologize for any omission.

Finally, I would like to convey my heartiest regards to my family members whose moral support helped me in achieving the goal.

A handwritten signature in black ink, appearing to read 'Bijay Kumar Sahoo', with a horizontal line underneath the name.

(Bijay Kumar Sahoo)

# Contents

<b>Synopsis</b> .....	i
<b>List of Figures</b> .....	xvi
<b>List of Tables</b> .....	xx
<b>1. Introduction</b> .....	1
1.1. Background.....	1
1.2. Decay series of radon ( $^{222}\text{Rn}$ ) and thoron ( $^{220}\text{Rn}$ ).....	2
1.3. Radiological significance of $^{222}\text{Rn}$ / $^{220}\text{Rn}$ and their decay product.....	4
1.4. Sources of $^{222}\text{Rn}$ and $^{220}\text{Rn}$ .....	5
1.5. Mechanism of $^{222}\text{Rn}$ / $^{220}\text{Rn}$ emission.....	5
1.5.1. Emanation of $^{222}\text{Rn}$ and $^{220}\text{Rn}$ .....	7
1.5.2. Transport and exhalation of $^{222}\text{Rn}$ and $^{220}\text{Rn}$ .....	7
1.6. Factors affecting $^{222}\text{Rn}$ and $^{220}\text{Rn}$ emission.....	9
1.7. Motivation for the present study.....	10
1.8. Scope of the present study.....	12
<b>2. Literature Review</b> .....	14
2.1. Introduction.....	14
2.2. Technique for outdoor emission studies.....	15
2.2.1. Adsorption technique .....	15
2.2.2. Micrometeorological technique.....	17
2.2.3. Diffusion theory based technique.....	17

2.2.4. Chamber technique.....	21
2.2.4.1. Historical NSS Model.....	22
2.2.4.2. Non-Steady State Diffusion Model (1-D).....	23
2.2.4.3. Steady State Diffusion Model (2-D).....	26
2.3. Technique for indoor emission studies.....	28
2.3.1. Can technique.....	28
2.3.2. Continuous monitor coupled chamber technique.....	30
2.4. Literature on emission perturbation studies.....	32
<b>3. A Two Dimensional, Diffusion Process based Model for Soil-Chamber Response...</b>	<b>33</b>
3.1. Introduction.....	33
3.2. Mathematical Formulation.....	34
3.2.1. Pre-deployment situation.....	35
3.2.2. Post-deployment situation.....	38
3.3. Derivation of the solution.....	41
3.3.1. Solution in soil matrix.....	43
3.3.2. Solution in chamber headspace.....	45
3.3.3. Explicit form of Laplace Transformed Concentration and Flux.....	46
3.3.4. Temporal increase of the headspace concentration.....	50
3.3.5. First order correction.....	51
3.3.6. Direct numerical solutions of the differential equations.....	53
3.4. Implications of the solution.....	53
3.4.1. Comparison between analytical and numerical solution.....	54

3.4.2. Early time behavior: power-law form of the model.....	55
3.4.3. Steady state situation.....	58
3.4.4. Exponential approximation of the model.....	61
3.4.5. Radial profiles of vertical flux and concentration at the interface.....	64
3.4.6. Effect of chamber dimension on headspace concentration.....	67
3.5. Development of a Least –Square Fitting Algorithm in Wolfram Mathematica .....	69
3.6. Summary.....	71

#### 4. **Experimental Validation and Field Applications of the Chamber Response**

<b>Model.....</b>	<b>73</b>
4.1. Introduction.....	73
4.2. Experimental validation.....	74
4.2.1. Materials and Methods.....	74
4.2.2. Results and discussion.....	77
4.3. Field study at Uranium Tailing Ponds, Jaduguda.....	81
4.3.1. Materials and Methods.....	81
4.3.1.1. Measuring radon flux directly at the tailings surface.....	81
4.3.1.2. Measurement of radon diffusion length( $L$ ) .....	83
4.3.1.3. Measurement of radium content ( $R$ ) and radon emanation coefficient( $E$ ).....	85
4.3.1.4. Estimating flux by measurement of $L$ and $E$ .....	87
4.3.1.5. Estimating flux by calculating $L$ and $E$ via empirical formulae.....	87
4.3.2. Results and Discussion.....	88

4.3.2.1.	Determination of exhalation flux.....	88
4.3.2.2.	Determinations of radon diffusion length.....	90
4.3.2.3.	Relating radium content to radon flux.....	91
4.4.	Field study at coastal beaches, High Background Radiation Areas.....	92
4.4.1.	Materials and Methods.....	92
4.4.2.	Results and Discussion.....	93
4.5.	Summary.....	94
<b>5.</b>	<b>Studies on Radon Emission Perturbations due to Soil Seals.....</b>	<b>96</b>
5.1.	Introduction.....	96
5.2.	Theoretical aspect to emission perturbation near sealed surfaces.....	97
5.2.1.	Formulation of diffusion equation.....	99
5.2.2.	Derivation of the solution.....	100
5.2.2.1.	Determination of coefficient, $A(s)$ .....	101
5.2.3.	Surface concentration and flux.....	105
5.2.4.	Concentration depth profile.....	108
5.2.5.	Implications of study to flux mapping.....	109
5.3.	Experimental Validation.....	109
5.3.1.	Materials and Methods.....	109
5.3.2.	Results and discussion.....	111
5.4.	Summary.....	114

<b>6. Studies on Radon Emission from Building Materials to Indoor Air</b> .....	115
6.1. Introduction.....	115
6.2. Model development.....	116
6.2.1. Formulation and solution to diffusion equation for a building material block.....	116
6.2.2. Comparison between 3-D and 1-D solution.....	120
6.2.3. Empirical extrapolation.....	123
6.3. Validation of the model.....	126
6.3.1. Comparison with 1-D model prediction.....	126
6.3.2. Comparison with experimental observations.....	127
6.4. A case study from literature on inhalation dose assessment.....	132
6.5. Summary.....	133
<b>7. Concluding Remarks of the Thesis</b> .....	134
7.1. Contributions.....	135
7.2. Conclusion.....	138
7.3. Future Scope.....	139
<b>A. List of Symbols</b> .....	140
<b>B. Finite Difference Programming of the 2-D Chamber Problem</b> .....	144
<b>C. Fitting Algorithm of the 2-D Model in ‘Wolfram Mathematica’</b> .....	156
<b>References</b> .....	158

## **Synopsis**

Radon is a natural radioactive gas that occurs ubiquitously in the environment. There are three natural isotopes of radon namely  $^{222}\text{Rn}$  (radon),  $^{220}\text{Rn}$  (thoron), and  $^{219}\text{Rn}$  (actinon) formed from the alpha decay of radium as a part of the decay series of  $^{238}\text{U}$  (uranium),  $^{232}\text{Th}$  (thorium), and  $^{235}\text{U}$  (actinium), respectively. Due to the lower relative abundance of  $^{235}\text{U}$  by weight, actinon is extremely rare in the atmosphere and can generally be neglected. Radon tends to build up in enclosed spaces like underground mines or houses and has been found to be a ubiquitous indoor air pollutant. Inhalation of radon ( $^{222}\text{Rn}$ ), thoron ( $^{220}\text{Rn}$ ) and their decay products contributes a largest fraction (~52%) of natural background radiation dose to humans [1]. Based on the results of recent case-control studies in Europe & North America [2-3], the World Health Organization [4] indicated that exposure due to  $^{222}\text{Rn}$ ,  $^{220}\text{Rn}$  and their decay products in dwellings could be the second most important cause of lung cancer, next to smoking. These findings and inference have led to a renewed interest in the subject of radon studies. Most importantly, it has given impetus to large scale programme [5] aimed at delineating population exposures to estimate the magnitude of radon risk in populations and also to evolve various control measures to minimize this risk. A central component of this programme deals with identifying various sources of these radioactive gases, studying their emission mechanism from sources and developing techniques to measure and reduce their emission into environment.

Most important sources of these radioactive gases are the emission from soil, rocks and ore bodies present in the earth crust, and to some extent, the emission from various building materials such as bricks, cement, tiles etc [1, 6]. These sources are commonly known as Naturally Occurring Radioactive Materials (NORMs). Similarly, the waste products generated from uranium mine and milling facilities, zircon plants, coal and phospo-

gypsum industries are some of the important sources of these gases, resulting from technological activities. These sources are commonly known as NORM residues or alternatively as Technologically Enhanced Naturally Occurring Radioactive Materials (TENORMs).

Radon and thoron emission take place from these sources by two processes. The first stage is emanation from the material grain and the second is exhalation from the matrix. ‘Emanation’ is a process by which  $^{222}\text{Rn}$  atom escapes from the solid mineral grains to the air-filled pores and ‘Exhalation’ is the process by which  $^{222}\text{Rn}$  atoms are transported from air-filled pores to the atmosphere. Although the origin of the nomenclature “exhalation” is not clearly traceable, it is intended to capture the mechanism of gas exchange by diffusion and convection in a porous system, which in some loose way, is analogous to respiratory gas exchange process. Notwithstanding its origin, the usage has come to stay mainly for the purpose of distinguishing the macroscopic transport from the microscopic process of emanation from grains. Although the detailed processes responsible for radon emanation from grains is not fully understood, it is believed that the main contribution comes from the recoil process [7]. Influence of temperature on radon emanation is relatively small but moisture content has a large impact on it [8]. This is because a radon atom recoiling into a pore that is filled or partially filled with water has a higher probability of being stopped in the pore volume (without crossing the pore space) thereby being available for exhalation into the atmosphere. Transport of radon from pore space to the environment takes place mainly by diffusion, and in some cases, because of darcian flow induced by pressure difference [9] between the soil air and the atmosphere. There are many other external factors that can influence the diffusivity and hence the exhalation rate. Rainfall, snowfall, freezing and increase in atmospheric pressure results in decrease of exhalation rate, whereas increase in wind speed and temperature can increase it [10].

Measurements of  $^{222}\text{Rn}$  and  $^{220}\text{Rn}$  exhalation fluxes provide primary information on radon hazard potential of the sources which, in turn, is helpful in classifying them in respect of their impact on human health. Besides, the flux estimations are useful for (i) validating the radon emission and transport models in soils, (ii) quantifying the source term for predicting the radon and its decay products concentration through dispersion modeling, (iii) evolving various control measures such as to determine the adequacy of ventilation in indoor environment, (iv) determining the thickness of cover materials for reduction of emission rate.

Due to the spatial variability of the radioactivity content and soil characteristics coupled to temporal changes in the environmental conditions, the fluxes vary considerably from place to place and from time to time in the outdoor environment. As a result, it is generally a challenging task to assign reliable representative fluxes over large domains averaged over long times. Quite often, there is no alternative way but to carry out large number of measurements at different places and at different times to assign reliable fluxes to a region. This calls for techniques which are accurate, simple to deploy, portable and are minimally dependent upon environmental effects. In this regard, a widely used method is the accumulator technique in which the open face of a chamber closed on the other end, is placed on the surface of interest and the monitored concentration of the accumulated radon in the chamber head space is used for estimating the flux. In order to carry out reliable measurements, one is required to develop protocols based on sound theoretical reasoning.

There exist certain limitations and arbitrariness in the current practices of the use of accumulators. These pertain to the deployment methods, choice of chamber dimensions, gas measurements protocols and the models used for interpreting the concentration data [11]. Most the above aspects are related to quantitative understanding of the concentration build-up process and how it affects the flux one intends to measure, through various feedback

effects. In literature, most often it is assumed that the concentration builds up linearly with time; this basically assumes neglecting back diffusion effects [12]. In order to account for observed deviations from linear responses, several empirical forms of functions (linear-quadratic, exponential etc.) are fitted to the obtained data in the absence of a quantitative theory of the chamber response. As pointed out by Livingston et al. [11], the empirical approaches can significantly underestimate the radon flux. This limitation has given rise to an urgent need for developing a process-based model that can be used for benchmarking the domains of validity of other models as well as to provide a theoretical basis of the accumulator technique. Similarly studies by Scalenghe and Marsanand and Weigand [13-14] show that, there is a significant perturbation of radon and other trace gas emissions due to anthropogenic sealing of soil surface. This raises a question for the field user: how far from a sealed surface should accumulators be deployed for making representative emission measurements in urban regions? Answer to the question hinges upon a model that deals with emission perturbations in the vicinity of soil seals such as buildings, concrete grounds and roads.

In the context of indoor radon emission studies, several authors [15-16] assumed that radon emission fluxes from building material samples and that from walls made up of these materials, are equal. This assumption can lead to erroneous estimates of wall fluxes and corresponding indoor radon concentrations. In order to put the issue in proper perspective, it is necessary to carry out systematic modeling of radon emission from building materials samples *vis a vis* the walls made up of those building materials.

The knowledge gaps identified in the preceding discussions provide clear directions to define the objective of this thesis, which is stated as follows: “To formulate process based models, develop their solutions and validate them through experiments for addressing quantitatively, the shortcomings in the existing radon emission estimation methods, both

from soils surfaces and indoor walls”. The validation process involves several laboratory experiments, field campaigns and measurement of multiple parameters that enter as input variables in model calculations. An important byproduct of the study is the demonstration of a novel in-situ method for obtaining the effective diffusion coefficient of radon in soil by combining experiments with the present theory. On the whole, the thesis combines theoretical analysis and experimental methods for bridging the knowledge gaps in the techniques used for the estimation of radon emission fluxes from soils and building materials. These developments are presented through seven chapters. The highlights of these chapters are given below:

**Chapter 1 (*Introduction*)** describes the basic concepts relating to the physical and chemical properties of radon and thoron and their behavior in the environment. The prevailing state of knowledge on the radiological risks to humans attributable to the inhalation of radon, thoron and their decay products is briefly discussed. Various sources of these gases and the mechanisms of their emission into environment are clearly presented. The basic quantities and terminologies occurring frequently in radon, thoron emission studies, namely flux density, mass exhalation rate, surface exhalation rate, emanation coefficient, diffusion coefficient and porosity unambiguously defined. Clear case is made for the need for the present work by highlighting the importance of these quantities in assessing radiological risks due to radon and thoron.

**Chapter 2 (*Literature Review*)** critically reviews the techniques available for the measurement of radon emission fluxes from NORMs, and their limitations. Broadly speaking, there exist two distinctly different techniques for emission flux measurements: These are:

- (i) Techniques for quantifying the outdoor (terrestrial) emissions from soil surfaces,
- (ii) Techniques for quantifying the indoor emission from building materials.

In respect of (i), soil chambers, also known as accumulators are deployed on soil surfaces. These systems are common both for radon flux measurements as well as for the measurement of emission fluxes of other greenhouse trace gases such as CO<sub>2</sub>, NO<sub>2</sub> etc [17]. In these systems, the changes in the post-deployment mixing scenario and the concentration feedback effects give rise to nonlinear increase of radon concentration with respect to time in the chamber headspace. Excepting for a few numerical studies [18], no analytical functional forms are available for use as a data fitting function for the experimentalist to account for the nonlinear response. In view of this limitation, several restrictive protocols have been devised while operating the chambers in order to keep the response as close to linearity as possible. These protocols are largely based on empirical rules of thumb rather than reasoned on the basis of process based quantitative models. The chapter discusses the existing process based models such as the 2-D steady-state model of Mayya [19] and 1-D non-steady state model of Livingston et al. [11] using diffusion theory, which respectively provide the final steady-state and an early time estimates of the chamber response. In order to operate the chamber without restriction on time and chamber dimensions, 2-D non-steady state solutions are required, which account for both changed mixing scenario and lateral diffusion effects. The solutions should be amenable for use as fitting functions for the experimentalist. The analytical development is quite complex involving the applications of results from the theory of dual integral equations and higher transcendental functions [20]. The elucidation of these derivations forms an important part of the work presented in this thesis.

With regard to the item (ii) above, namely, the measurement of indoor radon/thoron emission fluxes from building materials, one often measures the fluxes from the samples

enclosed in closed containers or cans. In this context, Solid-State Nuclear Track Detector (SSNTD) based Can technique [21] is commonly used. While it is simple and inexpensive, it has several shortcomings such as thoron interference during radon measurements and unknown leak from the can which cannot be easily accounted for. The literature survey also indicates several other prevailing fallacies in the use of calibration factors for SSNTDs and in the interpretations of exhalation data. It is often assumed that the surface flux of radon measured in a can is the same as the radon flux from the wall made up of this material [15-16]. This assumption is in serious error and the correct estimation of wall fluxes based on sample measurements requires the use of 3-D diffusion theory. Further, sample measurements are not unique measures of wall flux in view of possible variations in diffusion lengths of radon from material to material. This necessitates a model which can predict radon flux from the wall based on radon flux data in samples.

The literature survey clearly highlights the need for developing models for correctly estimating radon fluxes from terrestrial soil surfaces and indoor wall materials. This forms the underlying motivation for the detailed exposition of two new models presented in this thesis, namely a process based chamber response model and a building material-to-wall flux extrapolation model. The subsequent chapters dwell at length on the analytical derivations, experiments conducted to validate the models and the various practical implications of the results.

**Chapter 3** (*A Two Dimensional, Diffusion Process based Model for Soil-Chamber Response*) describes the mathematical formulation and the solution procedure, of a two dimensional model, based on Non Steady-State (NSS) diffusion theory, for radon accumulation in a chamber deployed on the soil surface. The formulation includes setting up of coupled, time dependent, diffusion equations along with appropriate initial and boundary

conditions, in vertical and lateral coordinates, both in soil pore space and chamber head space. The radon transport in the porous soil media is handled by the concept of effective diffusion coefficient with appropriate production and sink terms to account for formation and decay. The transport in chamber head space is handled by molecular diffusion model, having concentration and flux matching at the interface. The solution procedure involves simultaneous use of Laplace and Hankel transforms, dual integral equation techniques[20], asymptotic expansion of singular integrals and contour integral based Laplace inversion methods, to obtain analytical expressions. The chapter includes comparison of the analytical formulae with the numerical solution to the differential equation obtained using finite difference methods. The contrasting features in respect of stable and radioactive species, the dependency of response in respect of deployment times and chamber dimensions, the practical implications of the saturating concentrations and limiting behavior are discussed in detail. Attention is drawn to the fact that an analytical formula for the instantaneous flux drop due to changed mixing scenario emerges naturally from the solutions. As the rigorous solution involves higher transcendental functions that may not be convenient for routine use, saturating exponential approximation is developed as a simple fitting function to the concentration data for extended deployment periods in field experiments. The framework provided by the theory for estimating the pre-deployment flux and additionally, the soil diffusion coefficient by utilizing the data from extended periods of observations, is succinctly discussed. The chapter concludes by emphasizing the role of the model in (i) advancing the state of knowledge of the functioning of soil-chambers, (ii) improving the method of flux determination and (iii) introducing a new application, namely, the determination of radon diffusion coefficient, in-situ, in soil.

**Chapter 4** (*Experimental Validation and Field Applications of the Chamber Response Model*) presents the experiments carried out to validate the 2-D model of the chamber method and also the results of various field applications of the technique for the measurement of radon and thoron fluxes from soils. For validation of the model, three set of experiments were conducted at a uranium mineralized zone using chambers of different dimensions. The first set of experiments was aimed at comparing the transient build-up of headspace concentration to its saturation value during an extended deployment period, with that predicted by theory based on measured soil parameters such as  $^{226}\text{Ra}$  content, radon emanation factor, diffusion coefficient, bulk density and moisture content. In this case, a relatively small chamber was used in which chamber feedback effect was expected to be high (extreme scenario). There was good agreement between the predicted and observed radon build up profiles in the chamber headspace which provided the first demonstration of the validity of the 2-D model. The second set of experiments was aimed at estimating the pre-deployment flux and soil diffusion coefficient from the experimental observations of the headspace concentration. For this case, a relatively large chamber was used in order to ensure sufficient data collection for both short and long times, which, in turn, is used for testing the relative performance of the linear model with the new model. The chamber was deployed at several locations of a uranium tailings repository and the measured chamber concentration data were fitted to the analytical formula derived in the previous chapter to elicit both the pre-deployment flux and the effective diffusion coefficient. The chapter presents the details of the alternative method [1] of estimating these two quantities based on the measurements of several soil parameters at the same locations. An excellent matching was found between the model predicted and measured radon fluxes as well as the effective diffusion coefficient. The third validation experiment was aimed at comparing the radon fluxes and soil diffusion coefficients obtained by using two different chambers, in

conjunction with the 2-D NSS model, at a given location. For this case, two consecutive experiments were conducted at a given location under nearly similar environmental conditions using a small and large chamber. Least square fitting of 2-D model to the above two different data set yielded nearly equal radon flux and soil diffusion coefficient (within a deviation of about 8 %). Since the chamber feedback relaxation times are widely different for the two chambers, this agreement clearly assures the validity of the model over different size of chambers.

Two campaigns conducted to map radon, thoron fluxes from soils are also presented in Chapter 4, to demonstrate the practical applicability of 2-D model based chamber technique. The first study deals with the evaluation of the radon emission source term for a uranium residue repository at Jaduguda. Systematic experiments were conducted at about 40 locations to map the radon release from the residue repository and quantify the source term of radon release. The second study deals with mapping of thoron emission flux from beach sands in High Background Radiation Areas, Kerala and Orissa. Measurement were carried out at 28 different locations spanning over a distance of about 30 km on the beaches in Karunagapalli-Kollam area of coastal Kerala and about 30 different locations in the coastal regions of Chhatrapur, Orissa. The chapter discusses the implications of these studies for assessing the environmental impact of elevated emissions of radon and thoron from these sources.

**Chapter 5 (*Studies on Radon Emission Perturbations due to Soil Seals*)** presents an important application of the chamber theory to experimentally determine the rapidly changing flux profiles in the vicinity of soil seals. Concrete buildings, pavements, made grounds, roads etc are practical examples of such anthropogenic seals and there is increasing interest in evaluating their effect on radon, and other trace gas emission fluxes [13-14]. An

important question to be addressed is: how far the flux is perturbed due to a seal for making representative measurements in the uncovered regions. To address this problem, first, a radon diffusion model is formulated for the case of a semi-infinite seal covering a soil surface. As the boundary conditions are inhomogeneous, the problem is analytically solved using dual integral equation techniques. The results provide closed-form expressions for the concentration build-up near the edge of the seal and the flux variations in the region away from the seal on the free surface. Subsequently, the model predictions were subjected to experimental test by carrying out radon emission measurement at the vicinity of the parapet of a building, which is considered as a close, real life, example of a semi-infinite seal. As it was required to measure fluxes at distances as small as 10 cm, conventional large chamber (diameter  $\sim 30$  cm) techniques were not suitable. Hence a small chamber of diameter 5 cm was deployed in all the measurements. This necessarily included nonlinear buildup effects even at relatively short times and hence the use of 2-D NSS model (described in Chapter 3) becomes inevitable to extract flux information from the concentration data. The experimental results were found to be in good agreement with the model predictions and demonstrated the fact of enhancement of radon emission flux at edge of the seal (by a factor of 5) due to seal induced perturbation. The effect of perturbation is gradually reduced as one moves away from the seal and the radon emission flux attains its normal value (within 5%) at about 1 meter ( $\sim$  value of radon diffusion length) away from seal. This chapter highlights two new contributions made in these studies, namely (i) demonstration of the use of small chambers for high resolution spatial profiling of radon flux made possible by the 2-D chamber theory developed in Chapter-3 and (ii) a validated model of flux around seals for estimating perturbation effects at sampling locations in urban regions for emission mapping.

**Chapter 6** (*Studies on Radon Emission from Building Materials to Indoor Air*) describes the development of a model to predict indoor radon emissions from walls using the emission

data of building material samples. The study considers the specific case of brick samples on which radon emission measurements have been made by closed can techniques and it is now required to predict the radon contribution in the indoor air due to emissions from walls made of these bricks. The chapter describes a two-step approach to achieve this objective. In the first step analytical solutions are obtained for the radon diffusion equation including source and sink terms, separately for the cases of three-dimensional cuboidal shaped building materials (such as brick, concrete block) and one dimensional wall system. The results indicated the radon emission flux from wall can be as high as seven times that from building materials samples, depending upon the dimension of the building materials, wall thickness and diffusion length. In the second step, sample to wall flux ratios were calculated for various physically realistic combination of the parameters. An empirical best fit formula in the form a saturating exponential function, was then derived for the flux ratio, as a function of the ratio of the diffusion length and wall thickness. The empirical result was validated against actual measurements at a construction site to demonstrate its practical applicability. The chapter discusses the implication of this study to indoor radon problems for providing regulatory guidelines on the suitability of materials used for construction, from the radiological risk perspective.

**Chapter 7 (*Concluding Remarks of the Thesis*)** highlights the major contributions and achievements made in this research work. These may be listed as follows:

- The development of a diffusion process based two-dimensional, Non -Steady-State model for describing soil chamber response;
- Experimental validations and implementation of the 2-D model for radon flux and soil diffusion coefficients measurements;

- Demonstration of practical applicability of the technique for large scale flux mapping through several field campaigns;
- Modeling flux perturbations due to soil seals and its validation through space resolved flux profiling using small chambers in conjunction with 2-D theory,
- Development of indoor radon prediction model for building materials.

The chapter concludes by noting how the above developments constitute definite progress towards providing mathematical basis for understanding the radon, thoron emissions in general and to their metrology, in particular. It is no longer necessary to make ad-hoc assumptions and arbitrary protocols in deploying soil chambers, since, precise response function is now made available. The experimental studies amply demonstrate that one can use both small and large chambers, deploy them for short and large times, as demanded by specific experimental requirements, without having to worry about the type of model to fit the data. Similarly, the thesis makes a serious attempt to improve our ability of assessing the indoor radon potentials of building materials by bridging the existing gap between the emission data from a sample and that from a wall, through systematic theoretical analyses. It is not an exaggeration to say that the thesis combines considerable mathematical depth with experimental acumen to address some of the outstanding issues in the area of radon and thoron. Considering the increasing concern shown by professional bodies as well as the general public on the radiological risks due to radon exposure, it is important that the metrological aspects are given due consideration in terms of scientific rigor aimed at improving their accuracy while still retaining their simplicity. This forms the recurring theme of this thesis and it is hoped that the various developments presented here will go a long way in strengthening our confidence in the assessment methods, so as to provide a realistic perspective of the radon, thoron issues in the country and elsewhere in the world.

---

## **References**

- [1] UNSCEAR, 2000. Report to the General Assembly, United Nation, New York.
- [2] Krewski D, et al., 2005. *Epidemiology*,16 (2),137-145.
- [3] Darby S, et al., 2005. *British Medical Journal*,330 (7485), 223-226.
- [4] WHO, 2009. WHO hand book on indoor radon: a public health perspective, World Health Organization, Geneva 27, Switzerland.
- [5] Gruber, V., Bossew, P., Cort, M. De, Tollefsen, T., 2013. *J. Radiol. Prot.* 33 51  
[doi:10.1088/0952-4746/33/1/51](https://doi.org/10.1088/0952-4746/33/1/51)
- [6] Nazaroff, W.W., Nero, A.V., Jr, 1988. Radon and its decay products in indoor air. Eds John Wiley and Sons Inc., New York. 57-112.
- [7] Sasaki, T., Gunji, Y., Okuda, T., 2004. *J. Nucl. Sci. Technol.*, 41, 993-1002.
- [8] Sakoda, A., Ishimori, Y., Yamaoka, K., 2011. *Appl. Radiat. Isot.* 69, 1422–1435
- [9] Schery, S.D., Holford, D.J., Wilson, J.L., Phillips, F.M., 1988. *Radiat. Prot. Dosim.* 24, 191-197.
- [10] Rogers, V.C., Nielson, K.K., 1991. *Hlth. Phys.* 60, 807.
- [11] Livingston, G.P., Hutchinson, G.L., Spartalian, K., 2006. *Soil Sci. Soc. Am. J.* 70, 1459-1469.
- [12] Hutchinson, G., Mosier, A.R., 1981. *Soil Science Society of America Journal* 45, 311–316.
- [13] Scalenghe, R., Marsan, A. F., 2009. *Landscape and Urban Planing*, 90, 1-10.
- [14] Wiegand, J., Schott, B., 1999. *Nuovo Cimento Soc. It. Fisica C* 22, 449-455.
- [15] Mahur, A.K., Kumar, R., Mishra, M., Sengupta, D., Prasad, R., 2008. *Applied Radiation and Isotopes*, 66(3),401-406.

- [16] Ujić, P., Čeliković, I., Kandić, A., Vukanac, I., Đurašević, Dragosavac, D., Žunić. Z.S., 2010. *Applied Radiation and Isotopes*, 68(1), 201-206.
- [17] Jassal, R.S., Black, T. A., Nestic, Z., Guay, D.G., 2012. *Agricultural and Forest Meteorology*, 161, 57– 65
- [18] Hutchinson, G.L., Livingston, G.P., Healy, R.W. and Striegl, R.G., 2000. J. *Geophys. Res.* 105(D7), 8865-8875.
- [19] Mayya, Y.S., 2004. *Rad. Prot. Dos.*, 111(3), 305-318.
- [20] Sneddon, I.N., 1972. *The Use of Integral Transforms*. MCGraw Hill, 292-352.
- [21] Abu-jarad, F. A., 1988. *Nucl. Tracks Radiat. Meas.*, 15 (1-4), 525-534
-

---

## List of Figures

<b>Fig. 1.1:</b> Process of radon emission from soil matrix to atmosphere.....	6
<b>Fig. 2.1:</b> Schematic diagram of the use of a charcoal adsorption canister.....	15
<b>Fig. 2.2:</b> Schematic diagram of a depth profile of radon concentration in pore space of soil matrix (scaling is not done) .....	18
<b>Fig. 2.3:</b> Coordinate system taken for formulation of radon diffusion equation (1-D) in a building wall.....	19
<b>Fig. 2.4:</b> Schematic diagram of the “Can” technique.....	28
<b>Fig. 2.5:</b> Schematic diagram of the continuous radon monitor (AlphaGUARD) coupled chamber technique for radon exhalation measurements.....	30
<b>Fig. 3.1:</b> Schematic diagram of a cylindrical chamber deployed at the surface of the soil matrix. The dashed arrow represents the vertical ( $z$ ) axis in the cylindrical coordinate system. ‘ $H$ ’ and ‘ $a$ ’ are height and radius of the chamber respectively. $f_0$ is the steady state pre-deployment flux of the trace gas.....	39
<b>Fig.3.2:</b> Comparison of the 0 <sup>th</sup> and 1 <sup>st</sup> order modeled mean concentration of radon at the chamber-soil interface. (The values of parameters used are: $a=15$ cm, $H=30$ cm, $C_\infty = 1$ , $D_s=0.02$ cm <sup>2</sup> s <sup>-1</sup> , $D =0.1$ cm <sup>2</sup> s <sup>-1</sup> , $n_e=0.3$ , $\lambda =2.1 \times 10^{-6}$ s <sup>-1</sup> ).....	52
<b>Fig. 3.3:</b> Temporal variation of mean concentration of radon in the chamber headspace predicted by finite difference method and 2-D analytical and numerical inversion models...	55
<b>Fig. 3.4:</b> Variation of radon flux at chamber-soil interface with dimensionless radial distance from the center of the chamber for short and extended deployment times.....	65

---

<b>Fig. 3.5:</b> Spatial variation in radon concentration at the chamber-soil interface as a function of the dimensionless radial distance from the center of the chamber for deployment periods ranging from 1 min to 7.9 h.....	66
<b>Fig. 3.6:</b> Temporal variation in the mean concentration of CO <sub>2</sub> in the chamber headspace for chambers of different height ( <i>H</i> ) and fixed radius ( <i>a</i> ).....	68
<b>Fig. 3.7:</b> Temporal variation in the mean concentration of CO <sub>2</sub> in the headspace of chambers with different radii ( <i>a</i> ) and fixed height ( <i>H</i> ).....	69
<b>Fig. 3.8:</b> Graph showing least square fitting of 2-D model to the radon builds up data in chamber headspace.....	70
<b>Fig. 4.1:</b> Comparison of experimental data on the temporal increase of radon concentration in the headspace with that predicted by 2-D theory based on measured soil parameters. Chamber dimensions are: radius 7.5 cm and height 15 cm. Observed data points are connected with lines for guiding the eye.....	77
<b>Fig. 4.2:</b> Least square fit of the exponential form of the 2-D model (Eq. (3.61)) to the experimental observations data for radon concentration in the chamber headspace as outlined in experiment no. 2. Observed data points are connected with lines for guiding the eye.....	78
<b>Fig. 4.3:</b> Soil chamber attached with AlphaGUARD continuous radon monitor set up for radon flux measurement.....	82
<b>Fig. 4.4:</b> Typical build up data of radon concentration in the chamber along with least square fitting of Equation (3.61) for an accumulator of radius, <i>a</i> =7.5 cm and <i>V</i> =3.4 l deployed on the Uranium residue repository.....	83
<b>Fig. 4.5:</b> Schematic diagram of soil probe method for the measurement of radon concentration in tailings using a continuous radon monitor.....	84
<b>Fig. 4.6:</b> Least square fitting of radon depth profile equation to the radon concentration data in soil gas at various depths.....	85

---

<b>Fig. 4.7:</b> Comparison between measured and predicted radon flux densities at 10 locations of the Uranium Tailings Pond.....	89
<b>Fig. 4.8:</b> Comparison of radon diffusion length in uranium tailings obtained by three different methods at 10 locations of the Uranium Tailings Pond.....	90
<b>Fig. 4.9:</b> Correlation between measured radon fluxes and $^{226}\text{Ra}$ content at 40 locations of the Uranium Tailings Pond.....	91
<b>Fig. 4.10:</b> Histogram plot of measured thoron exhalation rate at various locations on monazite beach sands, Kerala.....	94
<b>Fig. 5.1:</b> Schematic diagram of a semi infinite seal on soil surface and coordinate system taken for the problem formulation.....	99
<b>Fig. 5.2:</b> A schematic of the contour taken for solving the complex integral equation given in Eq. (5.11).....	102
<b>Fig. 5.3:</b> A schematic of the contour taken for solving the complex integral equation given in Eq. (5.14a, b).....	104
<b>Fig. 5.4:</b> Graph showing the radon concentration build up below the seal as predicted by the model.....	105
<b>Fig. 5.5:</b> Graph showing the variation of mean radon flux with respect to dimensional distance from edge of the seal.....	107
<b>Fig.5.6:</b> Depth profile of the relative radon concentration below the seal, predicted by model.....	108
<b>Fig. 5.7 :</b> In-situ measurement of radon flux from soil surface at edge of a concrete seal using a chamber connected to AlphaGUARD radon monitor.....	110
<b>Fig.5.8:</b> Plot of model predicted and measured radon flux at various distances from the edge of the seal. Data points are connected with dot lines for guiding the eye.....	113

---

<b>Fig. 5.9:</b> Linear correlation of model predicted and experimentally measured radon fluxes near the sealed surface.....	113
<b>Fig. 6.1:</b> Schematic diagram of a cuboidal shaped building material and the coordinate system used for the model development.....	117
<b>Fig. 6.2:</b> Variation of ' $J_w/J_b$ ' with respect to radon diffusion length ( $l$ ).....	121
<b>Fig. 6.3:</b> Least Square fitting of the empirical model (Eq. (6.14)) to the data on $J_w/J_b$ , plotted against $d/l$ for different combinations of $a, b, h, d$ . The estimated fitting parameter $k$ and the corresponding $R^2$ value showing the goodness of fit are listed in Table 6.1 for each combination.....	124
<b>Fig. 6.4:</b> Comparison of the radon flux estimated using 1-D flux model and empirical model.....	127
<b>Fig. 6.5:</b> Comparison of the measured and 3-D model predicted radon fluxes from cubic concrete blocks.....	130

---

## **List of Tables**

<b>Table 1.1:</b> Half-life and principal radiation energy of $^{222}\text{Rn}$ , $^{220}\text{Rn}$ and their decay products.....	3
<b>Table 3.1:</b> Comparison of radon growth rate constants estimated using Eq. (53) with those obtained by exponential fitting to the headspace concentration predicted by 2-D theory for the chambers. The text in bold represents the best matching of the rise rate constants predicted by the two approaches.....	63
<b>Table 3.2:</b> Estimated radon emission parameters after least square fitting of 2-D model to the radon build up data in the chamber parameters.....	71
<b>Table 4.1:</b> Parameters ( $\bar{C}_c(\infty)$ and $\lambda_e$ ) obtained by fitting the exponential form of the 2-D model (Eq.(51)) to the data points shown in the Fig. 9 and the derived pre-deployment flux ( $f_0$ ) and soil diffusion coefficient ( $D_s$ ) from these parameters.....	79
<b>Table 4.2:</b> Comparison of estimated pre-deployment flux density and time constant for different chambers used in the third set of experiments.....	79
<b>Table 4.3:</b> Relative variations in time constant with respect to change of multiplicative term $a.H$ (product of chamber radius and height).....	80
<b>Table 4.4:</b> Variations in radon saturation concentration with respect to radius of chamber.....	80
<b>Table 4.5:</b> The mean of measured tailings parameters along with standard deviation in winter, summer and rainy seasons for 40 locations of the tailings pond.....	89
<b>Table 5.1:</b> Various parameters of soil estimated using soil samples and measured radon concentration in the pore space of the soil matrix.....	111

---

<b>Table 5.2:</b> Model predicted and experimentally measured radon fluxes at various distances from edge of the seal.....	112
<b>Table 6.1:</b> Lists of estimated parameter ' $k$ ' from the fitting procedure in Fig. 6.3 and the corresponding $R^2$ showing the goodness of fit.....	124
<b>Table 6.2:</b> Measured and predicted radon fluxes for concrete block samples using measured physical parameters. Each sample has dimensions: $a=b=h=10\text{ cm}$ .....	129

# 1. Introduction

---

## 1.1. Background

Radon (Rn) belongs to the family of noble gases in the periodic table. There are three radon isotopes naturally present in the environment,  $^{222}\text{Rn}$  (commonly referred to as radon) of the uranium decay series,  $^{220}\text{Rn}$  of the thorium decay series, and  $^{219}\text{Rn}$  of the actinium decay series. Historically,  $^{220}\text{Rn}$  and  $^{219}\text{Rn}$  are referred to as thoron and actinon, respectively. Although this nomenclature is gradually being phased out since these are chemically the same as  $^{222}\text{Rn}$ , we retain it in this thesis for convenience of distinguishing the radiological properties. In the case of actinon, its short half-life (3.98s) and its very low activity concentration relative to  $^{222}\text{Rn}$  in the environment means that for all practical situations its radiological impact is negligible compared with that of  $^{222}\text{Rn}$ . Consequently, the primary focus has been given to  $^{222}\text{Rn}$  and to some extent to  $^{220}\text{Rn}$  wherever applicable.

The discovery of radon followed soon after the discovery of radium in 1898 by the Curies [1]. The Curies noted that air medium in contact with radium compounds becomes a conductor of electricity. In 1900, Dorn showed that this phenomenon was due to an emanation from radium and Rutherford established that thorium compounds too gave off a similar emanation. Rutherford called the gaseous element from radium “emanation” and gave a symbol “*Em*”. The International Committee on Chemical Elements officially adopted the name “Radon” for this element in 1923. Investigations for its chemical properties and the emanating spectrum from radium were carried out by Ramsay and Rutherford. Soddy and

other scientists showed that chemically radon is akin to the inert gases and it was included in the argon group.

The presence of radon in the free atmosphere was first noted by Elster and Geitel [2] and later by Gish [3]. The study of conduction of electricity in air and other gases led Elster and Geitel to the conclusion that gaseous ions are the carriers of electricity. They later found that radiations from radioactive substances form ions in the surrounding air. Some observations also indicated that the content of radioactive matter in the air over land followed seasonal changes and was due to emission of radioactive gases ( $^{222}\text{Rn}$ ,  $^{220}\text{Rn}$ ) from the soil. Radon being a gaseous element, it diffuses easily in the pore space of the earth's crust and exhales into the atmosphere. Radon tends to build up in enclosed spaces like underground mines or houses and has been found to be a ubiquitous indoor air pollutant.

## 1.2. Decay series of radon ( $^{222}\text{Rn}$ ) and thoron ( $^{220}\text{Rn}$ )

The vast difference in the half-lives of  $^{222}\text{Rn}$  (3.8 days) and  $^{220}\text{Rn}$  (55 sec) plays an important role in their emanation from ground, their distribution in the free atmosphere above the ground and in the indoor air of dwellings and buildings. The progeny of  $^{222}\text{Rn}$  and  $^{220}\text{Rn}$  are isotopes of Polonium, Bismuth, Lead and Thallium, which decay by emission of  $\alpha$  or  $\beta/\gamma$  radiations.  $^{222}\text{Rn}$  decay products are divided into two groups: "short-lived"  $^{222}\text{Rn}$  daughters which are  $^{218}\text{Po}$  (RaA; 3.05 min),  $^{214}\text{Pb}$  (RaB; 26.8 min),  $^{214}\text{Bi}$  (RaC; 19.7 min) and  $^{214}\text{Po}$  (RaC'; 164  $\mu\text{s}$ ) with half-lives below 30 min; and the "long-lived"  $^{222}\text{Rn}$  decay products namely,  $^{210}\text{Pb}$  (RaD; 22.3 yr),  $^{210}\text{Bi}$  (RaE; 5.01 days) and  $^{210}\text{Po}$  (RaF; 138.4 days). There is no long-lived group for  $^{220}\text{Rn}$  daughters. But in comparison with the short lived decay products of  $^{222}\text{Rn}$ , the  $^{220}\text{Rn}$  decay products have relatively longer half-lives. The most important radionuclide in this chain is the lead isotope  $^{212}\text{Pb}$  with a half-life of 10.6 h. The half-lives

and the principal radiation emitted during their decay along with the energy of the emitted particle for both  $^{222}\text{Rn}$  and  $^{220}\text{Rn}$  decay products in given in Table 1.1.

*Table 1.1: Half-life and principal radiation energy of  $^{222}\text{Rn}$ ,  $^{220}\text{Rn}$  and their decay products*

Isotopic Name	Element Name	Half life	Principal radiation & energies (MeV)
$^{222}\text{Rn}$	<b>Radon - 222</b>	<b>3.824 d</b>	<b><math>\alpha</math> 5.490 (100 %)</b>
$^{218}\text{Po}$	Polonium – 218	3.05 min	$\alpha$ 6.003 (100 %)
$^{214}\text{Pb}$	Lead – 214	26.8 min	$\beta$ 0.650 (50 %)
$^{214}\text{Bi}$	Bismuth – 214	19.9 min	$\beta$ up to 3.26 MeV
$^{214}\text{Po}$	Polonium – 214	164 $\mu$ s	$\alpha$ 7.687 (100 %)
$^{210}\text{Pb}$	Lead – 210	22.3 y	$\beta$ 0.015 (81 %)
$^{210}\text{Bi}$	Bismuth – 210	5.01 d	$\beta$ 1.161 (100 %)
$^{210}\text{Po}$	Polonium – 210	138 d	$\alpha$ 5.303 (100 %)
$^{206}\text{Pb}$	Lead – 206	Stable	None
$^{220}\text{Rn}$	<b>Radon - 220</b>	<b>55.6 s</b>	<b><math>\alpha</math> 6.29 (100 %)</b>
$^{216}\text{Po}$	Polonium – 216	0.15 s	$\alpha$ 6.78 (100 %)
$^{212}\text{Pb}$	Lead – 212	10.6 h	$\beta$ 0.35 (81 %)
$^{212}\text{Bi}$	Bismuth–212 (64%)	60.6 min	$\beta$ 2.27 (54 %)
$^{212}\text{Po}$	Polonium – 212	0.305 $\mu$ s	$\alpha$ 8.78 (100 %)
$^{208}\text{Pb}$	Lead – 208	Stable	None

### 1.3. Radiological significance of $^{222}\text{Rn}$ / $^{220}\text{Rn}$ and their decay products

Inhalation of high cumulative levels of  $^{222}\text{Rn}$  and, in particular, its  $\alpha$ -particle-emitting decay products have been linked to an increased risk of lung cancer [4-5]. About 125 years ago, Harting and Hesse [6] diagnosed a sharply higher lung cancer rate among miners, which became known as “Schneeberger Berkrankheit” (Schneeberger mountain sickness). About 45 years later, Ludewing and Lorenzer [7] suggested that the high lung cancer incidence among the Schneeberg mines may be attributed to the high radon concentration of between  $10^3 \text{ Bq m}^{-3}$  and  $5 \times 10^4 \text{ Bq m}^{-3}$ . Exposure to lower levels of residential  $^{222}\text{Rn}$  has also been tied to lung cancer in some studies of  $^{222}\text{Rn}$  in homes [8]. A recently concluded analysis of European Case control studies [9] seem to suggest an increased risk of lung cancer by about 8% (3% to 16%) per  $100 \text{ Bq m}^{-3}$  of  $^{222}\text{Rn}$  concentration which, in turn, is consistent with an estimate of 11% (0% to 28%) found in a combined analysis of North American studies[10]. Based on these recent results, it is now strongly surmised that the inhalation exposure due to these radioactive species is most likely to be the second most important cause of lung cancer, next to smoking [11]. These studies and the observation by WHO has rekindled interest on radon studies in various countries and has undermined the need to evolve various control measures to minimize concentrations of these gases in the environment and hence the exposure. This is possible by identifying various sources of these gases, studying their emission mechanism from sources and developing techniques to measure and reduce their emission into environment.

Even though, both radon and thoron are present in the atmosphere, most studies generally ignore the presence of the latter because of its short half-life. However, thoron may not be negligible under all circumstances, especially in the regions where thorium bearing sediments, better known as High Background Radiation Areas (HBRAs), exist. Examples of

such places are monazite-bearing sands in Kerala, India, and regions of Yangjiang in China, where thoron issues may not be negligible. Considering the general population residing in these regions, these constitute a natural study group for examining the consequences of exposure to thoron. In view of this, several major study programmes have been initiated in these regions to address the thoron problem in a systematic manner [12-13]. Additionally, thoron problem is of unique significance to India in view of our future nuclear power programme involving thorium based fuels. This highlights the growing concern regarding the exposure due to thoron that may not be negligible in the global context especially in situations like India.

#### **1.4. Sources of $^{222}\text{Rn}$ and $^{220}\text{Rn}$**

The occurrence of radon in the living environment of humans may be attributed both to natural sources as well as to sources arising from anthropogenic activities. The emission from soil, rocks and ore bodies present in the earth crust, and to some extent, the emission from various building materials such as bricks, cement, tiles etc [14-15] constitute natural sources. These sources are often referred to as Naturally Occurring Radioactive Materials (NORMs). Similarly, the waste products generated from uranium mine and milling facilities, zircon plants, and coal and phospho-gypsum industries are some of the important anthropogenic sources of radon. These sources are commonly known as NORM residues or often referred to as Technologically Enhanced Natural Occurring Radioactive Materials (TENORMs).

#### **1.5. Mechanism of $^{222}\text{Rn}$ / $^{220}\text{Rn}$ emission**

Radon atoms which are located within solid grains are unlikely to become available for release into the atmosphere due to their very low diffusion coefficients in solids.

However, if they are located in the interstitial space between grains then they may diffuse to the surface. Therefore, releases of radon from a radium bearing matrix to the atmosphere take place by the following processes [15]:

1. Emanation – process by which radon atoms formed from the decay of radium escape from the grains (mainly due to recoil) and get into the interstitial space between the grains.
2. Transport – diffusion and advective flow cause the movement of the emanated radon atoms through the pore space of the soil matrix to the ground surface.
3. Exhalation – radon atoms that have been transported to the ground surface and then emitted into the atmosphere.

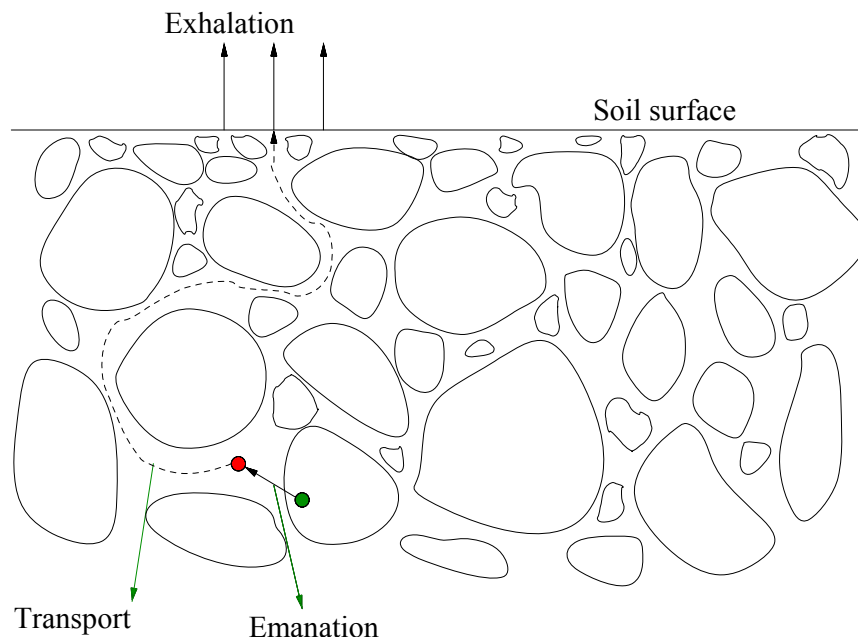


*Fig. 1.1: Process of radon emission from soil matrix to atmosphere*

These processes are illustrated in Fig.1.1. Although the origin of the nomenclature “exhalation” is not clearly traceable, it is intended to capture the mechanism of gas transport by diffusion and advection in a porous system, which in some loose way, is analogous to

respiratory gas exchange process. Notwithstanding its origin, the usage has come to stay mainly for the purpose of distinguishing the macroscopic transport from the microscopic process of emanation from grains.

### **1.5.1. Emanation of $^{222}\text{Rn}$ and $^{220}\text{Rn}$**

Only a fraction of all the radon/thoron atoms generated by the decay of radium contained in a rock or soil grain, is released into pore spaces and gets mobilized. One of the three things, listed below, can happen to a radon/thoron atom after it is formed from the decay of a radium atom in the grain:

1. It may be embedded in the same grain and remain immobilized,
2. It can travel across a pore space and become embedded in an adjacent grain,
3. It can be released into pore space.

The fraction of radon/thoron atoms released into a rock or soil pore space from a radium-bearing grain is termed the '*radon/thoron emanation coefficient*'. Although the detailed processes responsible for radon emanation from grains is not fully understood, it is believed that the main contribution to the emanation comes from the recoil processes [16-21]. Influence of temperature on radon emanation is relatively small but moisture content has a large impact on it [22-27]. This is because a radon atom entering a pore space that is filled or partially filled with water has a higher probability of being stopped in the pore volume without crossing the pore space. It is then available for migration in the matrix.

### **1.5.2. Transport and exhalation of $^{222}\text{Rn}$ and $^{220}\text{Rn}$**

There are primarily two mechanisms responsible for the transport of radon in porous media after its emanation [28]. These are as described below:

1. Radon/thoron can be transported by diffusion due to differences in the spatial distribution of radon concentration (see Fig. 1.1). Diffusive transport is considered to be one of the main processes for exhalation of radon/thoron from building materials, soils and other porous media sources. The quantity called the pore space diffusion coefficient, which accounts for the tortuous paths suffered by the diffusing species in a porous medium, characterizes the strength of diffusion. For radon in typical dry soils, the tortuosity corrected diffusion coefficient is about  $2 \times 10^{-6} \text{ m}^2/\text{s}$ , which is about 4-5 times lower than molecular diffusion coefficient. The property of radioactive decay limits the distance upto which a radon atom would migrate by diffusion. It is characterized by a mean diffusion length, often referred to simply as diffusion length. For typical soils, this distance is about 1 m for radon and about 2 cm for thoron. By implication, radium present in a soil depth of about a meter essentially contributes to exhalation at the surface by diffusion process.. Radium activity contained at greater depths will not have significant contribution to surface flux. This fact makes it possible to mitigate radon emission by the use of soil covers.

2. Radon/thoron can also be transported to large distances by the flow of air, known as advective transport. Advection is not limited to exchange of air between open spaces but can also occur in porous materials (such as soil and building materials) due to pressure differences in the pore air (see Fig. 1.1). The law governing the flow of air in porous media, due to pressure gradients, is known as Darcy's law. Apart from the magnitude of the pressure difference, the advection velocity in soils also depends upon the hydraulic conductivity, which in turn depends on the permeability of soils. Typical soil permeability for air is about  $1.5 \times 10^{-11} \text{ m/s}$  and hydraulic conductivity (permeability /air viscosity) is  $\sim 10^{-6} \text{ m}^3 \cdot \text{s}/\text{kg}$ . In a soil exposed to open atmosphere, atmospheric pressure fluctuations can induce varying pressure differences in soils. The induced pressure pulse travels in soil with a diffusion coefficient of about  $0.1 \text{ m}^2/\text{s}$ , which is far higher than molecular diffusion coefficient of radon

( $10^{-5}$  m<sup>2</sup>/s). As a result, the induced pressure differential diffuses rapidly (within a few minutes) thereby annulling any sustainable pressure difference between the soil and the atmosphere for considerable length of time. In view of this, Darcian flow induced advective transport is generally neglected in comparison to diffusive transport, in radon exhalation studies in open atmospheres.

In contrast to open atmospheres, advective transport is considered to be the most important mechanism for entry of radon/thoron into buildings from the soil, especially in regions having cold climate. This is because, in cold climates, living spaces inside buildings are generally warmer than outside air, thereby inducing a sustained flow of radon filled soil air into living spaces through cracks in the concrete flooring or walls of basement structures. In fact, much of residential radon problem in western countries with colder climates has arisen as a result of the combined effect of pressure driven flow and the inevitable build up of radon in air of the energy efficient housing systems having low air exchange rates.

### **1.6. Factors affecting <sup>222</sup>Rn and <sup>220</sup>Rn emission**

The weather parameters such as air pressure, temperature, rainfall and wind speed affect radon exhalation flux from the soil surface [29-31]. The physical and hydrological properties of the soil and the length of time for which radon fluxes are reported are important in assessing the extent of meteorological effects. In particular, diurnal and seasonal variations in the weather parameters can lead to variations in flux over these time periods.

Usually, the duration of atmospheric pressure changes is much less than the half-life of <sup>222</sup>Rn. The exhalation flux density from the soil surface can be expected to increase when the atmospheric pressure decreases. Since atmospheric pressure changes are cyclic, the increases and decreases in the flux tend to compensate for each other. Thus the long term fluxes are not strongly dependent on atmospheric pressure changes.

Strong winds can cause erosion and are of particular concern for Uranium tailings, where contaminated particles may be carried to surrounding locations. In cold regions, strong winter winds have contributed to freeze-drying effects on soil. Where tailings and cover has been isolated under water cover, wind induced wave action may increase radon transport to the surface by mixing or reducing the cover thickness.

Long-term seasonal variations may influence the annual average radon fluxes. For example, a snow covering and frozen ground can decrease the annual surface flux. Rainfall directly affects soil moisture content. In one study [32] in a tropical region, radon exhalation flux densities were observed to increase as the soil started turning from dry to moist, followed by a rapid decrease as the rainy season started. Average radon exhalation flux densities over the wet season were lower than the dry season, but with greater variability.

### **1. 7. Motivation for the present study**

The radon/thoron emission flux from soils has a considerable variation across the globe. It is far lower in the oceans and snow covered regions as compared to tropical regions. The global average estimate from the continental regions is about 0.85 atom per cm<sup>2</sup>/s [14]. However, the spatial and temporal variability can be several times higher or lower than the global value. Considering this, several programmes [32-35] exist for determining the radon flux from soils and Uranium mill tailings.

Measurements of <sup>222</sup>Rn and <sup>220</sup>Rn exhalation fluxes provide primary information on radon hazard potential of the sources which, in turn, is helpful in classifying them with respect to their impact on human health. Besides, the flux estimations are useful for (i) validating the radon emission and transport models in soils, (ii) quantifying the source term for predicting the radon and its decay products concentration through dispersion modeling [36-37], (iii) evolving various control measures (such as to determine the adequacy of

ventilation in indoor environment, determining the thickness of cover materials for reduction of emission rate) to minimize their concentrations in the environment [38-40].

Due to the spatial variability of radioactivity content and soil characteristics coupled to temporal changes in the environmental conditions, the fluxes vary considerably from place to place and from time to time in the outdoor environment. As a result, it is generally a challenging task to assign reliable representative fluxes over large domains averaged over long times. Quite often, there is no alternative way but to carry out large number of measurements at different places and at different times to assign reliable fluxes to a region. This calls for techniques which are accurate, simple to deploy, portable and are minimally dependent upon environmental effects. In this regard, a widely used method is the chamber technique in which a closed chamber is placed on the surface of interest and the monitored concentration of the accumulated radon in the chamber head space is used for estimating the flux. In order to carry out reliable measurements, protocols need to be developed based on sound theoretical reasoning.

There exist certain limitations and arbitrariness in the current practices of the use of chambers. These pertain to the deployment methods, choice of chamber dimensions, gas measurements protocols and the models used for interpreting the concentration data[41]. Most of the above aspects are related to quantitative understanding of the concentration build-up process and how it affects the flux one intends to measure, through various feedback effects. These issues have been discussed in chapter 2. Similarly studies by Scalenghe and Marsan [42] and Weigand [43] showed that there is a significant perturbation of radon emission due to anthropogenic sealing of soil surface. This raises a question for the field user: how far from a sealed surface should a chamber be deployed for making representative emission measurements in urban regions. Answer to the question hinges upon a model that

deals with emission perturbations in the vicinity of soil seals such as buildings, concrete grounds and roads.

In the context of indoor radon emission, there exist large body of literature[44-54]. However, it has been observed that most of these studies [44, 45, 48, 54] assumed that radon emission fluxes from building material sample and that from wall are equal and predicted their contribution to indoor radon concentration and dose to humans which may not be true in real conditions. Hence, it is very important to understand the radon emission from building materials samples *vis-a-vis* wall made by those building materials.

### **1.8. Scope of the present study**

Given the importance of radon flux measurement techniques both in the context of outdoor and indoor environment, it is necessary to strengthen the understanding of the functioning of these techniques, through carefully constructed mathematical models. The lack of such knowledge also has sometimes resulted in erroneous interpretations and arbitrary protocols. The scope of this thesis, therefore, encompasses not only the development of theoretical models but also their applications for the improvement in measurement techniques and protocols.

Motivated by the above consideration, the development of process based models of radon transport from soils and building materials under various practically relevant situations forms the primary objective of the thesis. The detailed analysis and interpretation of the model results then provide a framework for addressing, in a quantitative manner, the shortcomings in the existing methods of estimating radon emission. The second objective is to validate the models by laboratory experiments and field campaigns involving the measurements of multiple parameters. In the process, several new outcomes emerge: (i) a

novel method of measuring the diffusion coefficient of radon in soil (ii) a chamber technique for highly space resolved flux measurements (iii) development of simple formula for assessing radon potential of building materials. In the final analysis, the work not only provides new theoretical insights and novel techniques for the determination of some of the soil parameters, but also provides definite focus on improving the existing methods for the accurate estimation of radon emission fluxes from soils and building materials.

---

## 2. Literature Review

---

### 2.1. Introduction

As highlighted in the section 1.5, measurements of  $^{222}\text{Rn}$  and  $^{220}\text{Rn}$  exhalation fluxes provide primary information on radon hazard potential of the sources which, in turn, is helpful in classifying them with respect of their impact on human health. There exists large body of literature dealing with various techniques for quantification of sources and concentrations. From a flux measurement point of view, the available techniques can be classified in the following manner:

- (i) Techniques for quantifying the outdoor (terrestrial) emissions from soil surfaces,
- (ii) Techniques for quantifying the indoor emission from building materials.

Although the fundamental detection method of radon is the same, the above distinction is based on difference in collection methods. In the former, the techniques should be field compatible and measurements have to carry out, in-situ, on field, whereas in the latter the measurements are generally carried out in the laboratory on material samples. Further, in both these contexts, several of the measurement techniques used over the years have been outdated and therefore, the review in this chapter is focused on some of the commonly used techniques.

In the context of radon emission from soils, the perturbation effect due to various soil seals (such as buildings, roads, concrete surface etc.) is another important aspect of radon and thoron emission studies. Some of studies carried out in the recent past on the emission

perturbation are also critically reviewed. In sum, an attempt is made in this review to identify the knowledge gap existing in the literature on radon and thoron emission measurement which provide the primary motivation for the work in the subsequent chapters aimed at filling up those gaps. The detailed literature review is discussed below.

## 2.2. Technique for outdoor emission studies

### 2.2.1. Adsorption technique

The adsorption method for  $^{222}\text{Rn}$  exhalation flux involves the use of an adsorption medium (typically activated charcoal) placed in close proximity to the surface being investigated. Fig. 2.1 shows a schematic of a charcoal adsorption canister. Before use, the charcoal is heated in an oven to remove any radon, moisture and other contaminants which may have been adsorbed previously. This drying may be carried out when the charcoal is already in the canister or prior to it being weighed into canisters. Once prepared, the canister is sealed to prevent adsorption of ambient radon or moisture onto the charcoal.

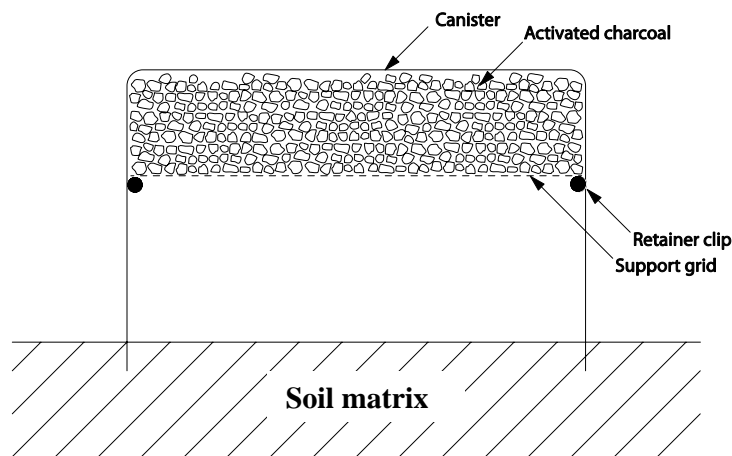


Fig. 2.1. Schematic diagram of the use of a charcoal adsorption canister.

Following exposure, the canisters are again sealed and the activities of the radon progeny  $^{214}\text{Pb}$  and  $^{214}\text{Bi}$  measured, most commonly by gamma spectrometry, following a

short (~3 hours) in growth period for the progeny. Liquid scintillation counting may be used as the measurement technique if a higher counting efficiency is required [55]. The measurement should take place as soon as possible after the progeny in growth period in order to minimize loss due to radon decay. The radon exhalation flux density over the period of exposure can be estimated using the expression:

$$f = \frac{N \cdot t_c \cdot \lambda^2 \cdot \exp(\lambda t_d)}{\varepsilon \cdot A \cdot [1 - \exp(-\lambda t_e)] \cdot [1 - \exp(-\lambda t_c)]} \quad (2.1)$$

where

$f$  is the radon flux density ( $\text{Bqm}^{-2}\text{s}^{-1}$ );

$N$  is the net count rate, after background subtraction, obtained during the counting period (counts per s, or  $\text{s}^{-1}$ );

$t_c$  is the counting period (s);

$\lambda$  is the radioactivity decay constant for  $^{222}\text{Rn}$  ( $\text{s}^{-1}$ );

$t_d$  is the delay period from the end of exposure to the beginning of the counting interval(s);

$\varepsilon$  is the counting efficiency of the system relative to the activity of radon adsorbed ( $\text{Bq}^{-1}\text{s}^{-1}$ );

$A$  is the area of the canister ( $\text{m}^2$ ); and

$t_e$  is the period of exposure of the charcoal in the canister (s) [56]

When exposed to humid or wet environments, the charcoal adsorbs moisture, which causes reduction in the radon collection efficiency [57]. To ensure that water adsorption is not problematic or to allow any required correction, water adsorption can be quantified by weighing the canisters before and after exposure.

### 2.2.2. Micrometeorological technique

Micrometeorological techniques are derived from the mathematical description of turbulent mass and energy transport above relatively large, flat, and homogeneous sources. They are nonintrusive and can provide temporally and spatially integrated estimates of the exchange of most gases of interest in agricultural ecosystems. For detailed information about the use of techniques based on gas diffusion theory and micrometeorological theory, readers are referred to other reviews [58-59]. This technique is widely used in green house gas emission studies and has little scope in radon/thoron emission studies as the environmental concentration is very low for accurate measurements.

### 2.2.3 Diffusion theory based technique

Central to the understanding of response of measuring systems for emission fluxes, is the theory of radon emission from free surfaces. Analytical models [15, 60] based on diffusion theory have been proposed earlier to estimate radon exhalation flux from soil and walls. The model considers that radon diffusion occurs in vertical direction after emanating from soil grain to pore space. Soil properties and radioactivity distributions are assumed to be homogeneous. The steady equation used for deriving the profile of radon pore space concentration ( $C(z)$ ) is given as:

$$D_s \frac{\partial^2 C(z)}{\partial z^2} - \lambda C(z) + \lambda \frac{R \rho_b E}{n_e} = 0, \quad (2.2)$$

Where,  $R$  is  $^{226}\text{Ra}$  content ( $\text{Bq kg}^{-1}$ ) in the soil,  $D_s$  is the diffusion coefficient of radon in the soil matrix ( $\text{m}^2 \text{s}^{-1}$ ),  $\rho_b$  is the dry bulk density ( $\text{kg m}^{-3}$ ) of soil,  $n_e$  is the porosity of the soil matrix,  $E$  is radon emanation factor and  $\lambda$  is the radon decay constant ( $\text{s}^{-1}$ ).

The first term and second term of Eq. (2.2) represent the loss of radon in the pore space of the soil matrix by the process of diffusion and radioactive decay respectively, while

the third term represents the production of radon due to emanation from soil grain to pore volume. The boundary conditions of the problem are taken as:

$$C(z = -\infty) = R\rho_b E / n_e = C_\infty \quad (2.3(a))$$

$$C(z = 0) = 0 \quad (2.3(b))$$

Using the above boundary conditions and defining the radon diffusion length in soil as

$$l_s = \sqrt{D_s / \lambda}$$

the solution of this equation is derived as:

$$C(z) = C_\infty \{1 - \exp(-z/l_s)\} \quad (2.4)$$

Eq. (2.4) represents the vertical profile of radon concentration in the soil matrix and a typical profile of pore space radon concentration is shown in Fig. 2.2. The concentration increases exponentially as soil depth increases and after a certain depth ( $\sim 3l_s$ ) the concentration saturates.

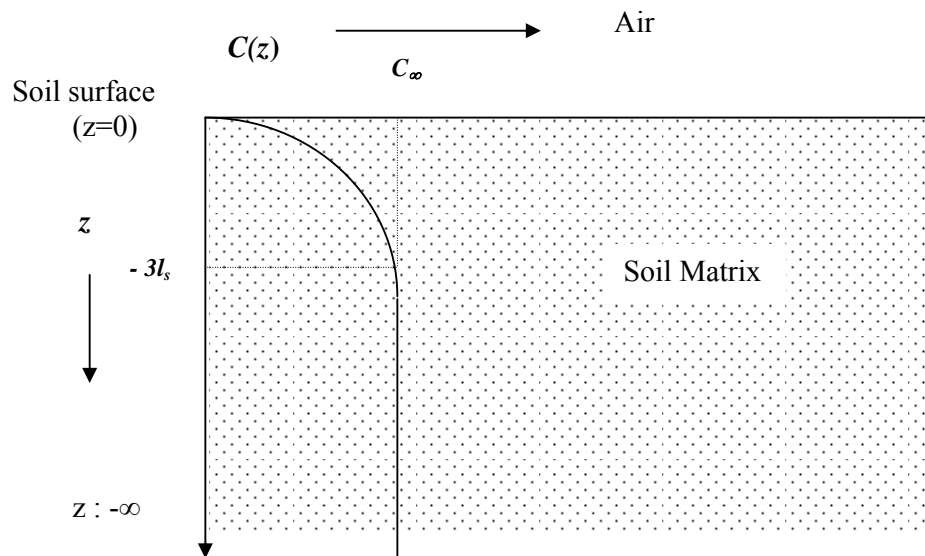


Fig. 2.2: Schematic diagram of a depth profile of radon concentration in pore space of soil matrix (scaling is not done)

The radon emission rate at the soil surface ( $f_s$ ) is determined as:

$$f_s = -n_e D_s \left. \frac{dC(z)}{dz} \right|_{z=0} = \frac{n_e D_s}{l_s} C_\infty = \lambda l_s R \rho_b E \quad (2.5)$$

Eq. (2.5) indicates that it is necessary to measure the soil parameters such as radium content, radon diffusion length in soil, radon emanation factor and bulk density to estimate the radon exhalation flux from the soil surface. Measurement of these parameters is not an easy task and hence this method is not routinely used for estimating the emission rate. The popularity of this method is decreased by imprecision in estimating soil gas diffusivity and by difficulty in determining the vertical gas concentration gradient, especially when gas production or consumption is non-uniformly distributed as a function of soil depth.

Radon exhalation from a wall will take place through two faces. This will result in a symmetric concentration profile with flux at centre of the wall equal to zero. The radon diffusion process may be considered one dimensional ( $z$ -direction) as shown in Fig. 2.3.

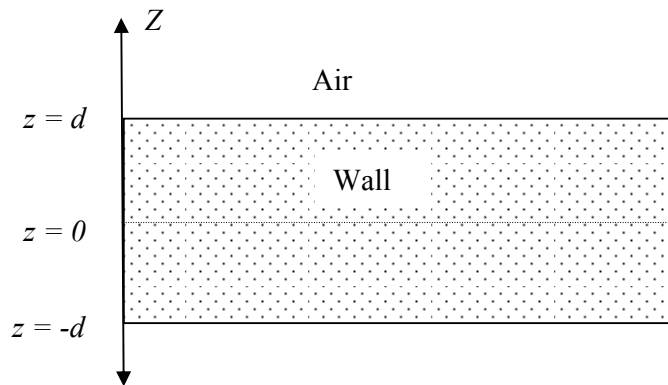


Fig. 2.3: Coordinate system taken for formulation of radon diffusion equation (1-D) in a building wall

The steady-state equation for radon concentration ( $C(z)$ ) in the pore space of the wall matrix may be written as:

$$D_w \frac{\partial^2 C(z)}{\partial z^2} - \lambda(C(z) - C_\infty) = 0 \quad (2.6)$$

where, the notations correspond to parameters for building material instead of soil as defined in the previous problem.

The boundary conditions of the problem may be written as:

$$C(z = \pm d) = 0 \quad (2.7 \text{ a})$$

$$n_e D_w \left. \frac{\partial C}{\partial z} \right|_{z=0} = 0 \quad (2.7 \text{ b})$$

Using these boundary conditions, the solution for Eq. (2.6) may be written as:

$$C(z) = C_\infty \left[ 1 - \frac{\cosh(z/l_w)}{\cosh(d/l_w)} \right] \quad (2.8)$$

Where,  $l_w = \sqrt{D_w / \lambda}$  denotes the radon diffusion length in the wall

Applying Fick's law of diffusion, the radon flux at the surface of the building wall ( $f_w$ ) can be expressed as:

$$f_w = -n_e D_w \left. \frac{dC(z)}{dz} \right|_{z=d} = \lambda l_w R \rho_b E \tanh \frac{d}{l_w} \quad (2.9)$$

Eq. (2.9) indicates that it is necessary to measure the parameters of the building materials such as radium content, radon diffusion length, radon emanation factor and bulk density to estimate the radon exhalation flux from the building wall.

It has been observed that the diffusion theory based technique requires information of various soil parameters to estimate the radon/thoron emission fluxes. Measurement procedures of these soil parameters are tedious and time consuming, thereby limiting application of this technique to only specific studies. There is a requirement of alternative

simple method for measurement of radon/thoron emission directly from soil/wall matrix which will be useful for field users.

#### **2.2.4. Chamber technique**

Chamber techniques have been used to estimate soil-surface gas emissions for more than eight decades and remain the most commonly used approach for measurement of radon flux as well as stable gas emission. They permit measurement of very small fluxes, are relatively inexpensive to build and use, and can be adapted to a wide range of field conditions and experimental objectives. But there remains a lack of uniformity in the nomenclature, construction and deployment protocol of chambers in the contexts of radon (radioactive gas) and green house gases (Stable gases). Chambers used for stable gases [61], known as soil chambers, are typically constructed in two sections, a “collar” that is inserted into the soil and a “cover” that is then sealed to the collar. On the other hand, chambers used to measure radon emission are known as accumulators [62-63] and are typically constructed as a single unit whose open mouth is inserted into the soil. The space above the soil surface bounded by the chamber is typically referred to as the headspace for both types of chambers. The fundamental strategy of the chamber technique is to relate the monitored gas concentration data in the chamber headspace to the pre-deployment flux density by use of a model. In most applications, chambers are operated in a Non-Steady State (NSS) diffusive mode [64] which in turn requires an appropriate NSS model to estimate the pre-deployment flux from the headspace concentration data. The non-steady state model available in literature is discussed below.

#### **2.2.4.1. Historical NSS Model**

The steady-state emission model mentioned earlier is applicable only for a free surface and fails when a chamber is deployed. From the point of time the chamber is sealed onto the surface, transient diffusion effects begin to operate. The non-steady state models recognize this effect and attempt to yield insights into the transient relaxation rates of soils and the feed-back effects from chambers. The historical NSS model used in chamber technique is the linear model [65] which is a zero order model as it does not consider transient effect in soil. This model assumes that emissions into the chamber headspace are constant throughout the deployment period. In fact, the rate of transport of a diffusing gas into the chamber headspace necessarily declines throughout deployment because any increase in the headspace concentration results in an immediate decline in the subsurface vertical concentration gradient driving that transport [66-68, 31, 58]. The error in applying a linear model to inherently nonlinear concentration data has long been assumed negligible if recommended guidelines regarding chamber design, deployment, and sampling are followed to foster the appearance of linearity in the observed concentration data [69-71]; however, it may not be always possible to adhere to these guidelines, or even have an assessment of the extent of uncertainties. In such situations, the resultant error is not negligible and the use of linear models has ensured that pre-deployment emission rates have been systematically and often substantially underestimated in nearly all NSS chamber applications [67-68, 72-73]

In recognition of this issue, nonlinear models, such as the physically based model proposed by Hutchinson and Mosier [66] and the quadratic model explored by Wagner et al.[74], were applied to NSS chamber observations, although both approaches are limited in their applicability or interpretation. For example, the physical significances of the fitted polynomial coefficients of the quadratic model are not necessarily either apparent or meaningful. In turn, the diffusion model advanced by Hutchinson and Mosier[66] is

compromised by its assumption of steady-state conditions at every point in time [75] and, as originally implemented, limited in its applicability [72, 76], although Pedersen [76] and Pedersen et al. [64] mathematically extended this model to permit its application to any number and spacing of observations with time and to reduce its sensitivity to measurement error and this approach is referred as the H–M–P model.

#### 2.2.4.2. Non-Steady State Diffusion Model (1-D)

The non-steady-state diffusive flux estimator (NDFE) introduced by Livingston et al. (2005) is the only gas emissions model derived from time dependent diffusion theory applicable to NSS chamber concentration data. The model considers that molecular diffusion is the principal mechanism driving trace gas exchange between soil and the atmosphere in terrestrial ecosystems [77-78, 67]. Assuming that Fick's laws apply [79] and that the soil has uniform properties across space and time except for a vertically distributed zero-order trace gas source, the rate of this exchange is described by the standard diffusion equation in one dimension:

$$\theta \frac{\partial C(z,t)}{\partial t} = D_p \frac{\partial^2 C(z,t)}{\partial z^2} + \lambda(z) \quad (2.10)$$

where  $C(z,t)$  is the trace gas concentration [ $\text{M L}^{-3}$  air] at time  $t$  [T] and depth  $z$  [L soil] below the soil surface,  $\lambda(z)$  is its depth-dependent zero-order source strength [ $\text{M L}^{-3}\text{soil T}^{-1}$ ],  $\theta$  is the air-filled porosity of soil [ $\text{L}^3$  air  $\text{L}^{-3}$  soil], and  $D_p$  is the soil gas diffusion coefficient [ $\text{L}^3$  air  $\text{L}^{-1}$  soil  $\text{T}^{-1}$ ] as defined by Rolston [58] and Rolston and Moldrup [79]. Authors assumed that at  $t=0$ , a NSS chamber enclosing an air volume  $V$  [ $\text{L}^3$  air] is deployed across soil area  $A$  [ $\text{L}^2$  soil] with its vertical side walls inserted into the soil to sufficient depth so that subsurface gas transport is limited to the vertical domain during the deployment period. The

authors also assumed the chamber air was uniformly mixed throughout, such that the chamber height multiplied by the change in headspace gas concentration ( $C_c(t)$ ) over time was equal to the soil gas flux at the soil–air interface

$$h \left. \frac{\partial C_c(t)}{\partial t} \right|_{z=0} = D_p \left. \frac{\partial C(z,t)}{\partial z} \right|_{z=0} \quad (2.11)$$

From these relationships, the authors developed the non steady-state diffusive flux estimator (NDFE) model

$$\bar{C}_c(t) = C_0 + \frac{f_0 \tau}{h} \left[ \frac{2}{\sqrt{\pi}} \sqrt{\frac{t}{\tau}} + \exp\left(\frac{t}{\tau}\right) \operatorname{erfc}\left(\sqrt{\frac{t}{\tau}}\right) - 1 \right] \quad (2.12)$$

where  $C_0$  is the initial chamber gas concentration [ $\text{M L}^{-3}$  air] at  $t = 0$ ;  $\tau$  is an experimental time constant equivalent to  $h^2(\theta D_p)^{-1}$  with units [T];  $h$  is the height [L air] of the non-steady-state chamber; and ‘*erfc*’ is the complementary error function. A series expansion of Eq. (7) when  $t/\tau$  is small yields

$$\bar{C}_c(t) = C_0 + \frac{f_0 \tau}{h} \left[ \frac{t}{\tau} - \frac{4}{3\sqrt{\pi}} \left(\frac{t}{\tau}\right)^{3/2} + \frac{1}{2} \left(\frac{t}{\tau}\right)^2 - \frac{8}{15\sqrt{\pi}} \left(\frac{t}{\tau}\right)^{3/2} + \dots \right] \quad (2.13)$$

Unlike most expansions that have integer exponents such that each term leads the next by an order of magnitude, this expansion has the atypical form of integer powers of the expansion variable  $t/\tau$  intertwined with half-integer powers. As a consequence, the  $(t/\tau)^{3/2}$  term is not negligible relative to the linear term and is thus the reason why a linear regression fit to the headspace concentration data underestimates  $f_0$  even for small values of  $t/\tau$ . For example, at  $t/\tau = 0.01$ , the  $(t/\tau)^{3/2}$  term is 7.5% of the linear term. Thus, if  $\tau$  has a value of 600 min, a linear model applied to observed concentration data during a deployment period as short as 6

min ( $0.01 \tau$ ) would underestimate  $f_0$  by 7.5% even though the  $C_c(t)$  vs.  $t$  response would resemble a straight line because of the weak curvature of the  $(t/\tau)^{3/2}$  term. It is also noted that the quadratic model advanced by Wagner et al. [74] recognizes the need to account for the curvature in the data, but does so by introducing a quadratic term  $t^2$  instead of  $(t/\tau)^{3/2}$  and assumes that the coefficient of the quadratic term is unrelated to  $f_0$ .

While developing this model, the authors took into consideration, the results of several earlier studies on the factors influencing the chamber performance and hence the accuracy of the estimated flux. Chief among them were the changes in the concentration gradients in the soil matrix and the gas mixing processes in the chamber headspace [80-81, 68]. For example, Hutchinson et al. [68] demonstrated that following chamber deployment, there occur both instantaneous and gradual changes in the pre-deployment flux, the former being due to a change in the mixing scenario in the headspace and the latter due to a continuous decrease in the concentration gradient across the soil-atmosphere boundary. Together, these processes are referred to as the chamber feedback effect. Although these effects were captured in the 1-D framework proposed by Livingston et al. [41], their model, however, is based on the assumptions that the soil gas transport is essentially governed by vertical diffusion and that mixing in the headspace is instantaneous and uniform at all times. Application of this model, therefore, requires that the chamber walls be inserted into the soil at a sufficient depth to ensure that lateral diffusion can be ignored and that the deployment period is limited to avoid saturation. In inhomogeneous soils, or with soils for which the experimentalist has limited experience, these assumptions are potentially at risk. Besides, insertion of the chamber walls into the soils may disturb the existing natural trace gas diffusion processes in the soil matrix, especially if significant lateral concentration gradients exist at short length scales. These difficulties could be largely resolved, however, if chambers

were deployed at the surface and an appropriate NSS model developed. Because lateral diffusion is likely to be as significant as vertical diffusion in surface deployed chambers, it would therefore be necessary to investigate the emission process by treating the problem in terms of a comprehensive two dimensional (2-D) diffusion theoretic framework.

### 2.2.4.3. Steady State Diffusion Model (2-D)

A beginning of a rigorous 2-D analysis for surface deployed chambers was made by Mayya [82] in the context of radon. The author assumed that molecular diffusion is the principal mechanism of radon transport in soil, both vertical as well as the lateral diffusion is considered subsequent to deployment of chamber. Author also assumed that mixing of gases in the headspace occur by both vertical and lateral diffusion, in contrast to NSS diffusion model proposed by Livingston et al. [73] where instantaneous uniform mixing process is considered. It is assumed that a cylindrical chamber of radius  $a$  and height  $H$  is deployed on the surface of the soil. Subsequent to the deployment, lateral diffusion concentration gradient develops due to accumulation in headspace and soil space below the chamber region. In view of this, the post deployment diffusion equations in soil pore space and chamber headspace under final steady state are taken as

$$D_s \left[ \frac{1}{r} \frac{\partial}{\partial r} \left\{ r \frac{\partial C_s}{\partial r} \right\} + \frac{\partial^2 C_s}{\partial z^2} \right] - \lambda C_s + S(z) = 0, \quad 0 \leq r < \infty, \quad -\infty < z \leq 0 \quad (2.14)$$

$$D \left[ \frac{1}{r} \frac{\partial}{\partial r} \left\{ r \frac{\partial C_c}{\partial r} \right\} + \frac{\partial^2 C_c}{\partial z^2} \right] - \lambda C_c = 0, \quad 0 \leq r \leq a, \quad 0 \leq z \leq H \quad (2.15)$$

Where  $C_s$  and  $C_c$  denote the trace gas concentration (moles or Becquerel of target gas per  $\text{m}^3$  of pore air or chamber space) in the pore space of the soil matrix and chamber headspace respectively.  $D_s = \tau D$  [80], where,  $\tau$  is the tortuosity of the soil matrix and  $D$  is the binary molecular diffusion coefficient of the trace gas in air at ambient temperature and pressure.  $S$

( $z$ ), is the zero-order production rate density, (where  $S(z)$  is allowed to vary with depth in such a way that the total production in soil is bounded for stable gases) and  $\lambda$  is a first order loss rate constant, ( $s^{-1}$ ), (which may be taken as zero for stable gases and is the radioactive decay constant in the case of radon) in the pore space of the soil matrix.

With suitable boundary conditions, a steady state solution to average headspace concentration under exponential approximation turns out to be

$$\bar{C}_c(\infty) = \frac{f_0}{H\lambda_e} \quad , \quad (2.16)$$

Where  $\lambda_e$  represents the rate constant ( $s^{-1}$ ) for build-up of concentration in the chamber headspace and is expressed as

$$\lambda_e = \left( \frac{n_e D_s}{aH} \left[ \frac{\lambda H^2}{D} \right]^{1/2} \text{Cot h} \left[ \left\{ \lambda \frac{H^2}{D} \right\}^{1/2} \right] \chi_v \left[ \lambda \frac{a^2}{D_s} \right] + \lambda \right). \quad (2.17)$$

For stable gases ( $\lambda \rightarrow 0$ ), Eq. (13) reduces to

$$\lambda_e = \frac{n_e D_s}{aH} \chi_v(0), \quad (2.18)$$

Although this 2-D model dealt essentially with the final steady state situation, it provided an important insight into the origin of the nonlinear headspace concentration increase over time that occurs in response to changes in the diffusion gradient across the surface particularly near the chamber wall at the soil-chamber interface. Most importantly, the study demonstrated the occurrence of singularities in the emission flux densities both inside and outside the chamber walls. Author quantified this so-called back-diffusion effect in terms of a “time constant” characterizing the concentration increase in the chamber headspace as a function of the chamber dimensions and soil properties. A major limitation of this model is that it does not handle transient effects and therefore fails to explain the early time effects such as the sudden flux drop and other short term effects.

From the above review it is clear that despite considerable advances, a completely satisfactory model for the chamber response is lacking. The correct approach appears to take forward the 2-D Steady-state model to transient situations. Such a model will also provide the correct framework for trace gas emission studies without having to worry about chamber feedback errors, regardless of chamber dimensions. While doing so, it should be kept in mind that the resulting solutions should be reduced to as simple forms as possible for routine field applications. Motivated by these considerations, Chapters-3, 4, deals with a comprehensive analytical theory of the chamber response.

### 2.3. Technique for indoor emission studies

#### 2.3.1. Can technique

For long-term measurement of radon exhalation from building materials or walls "Can technique" was initially proposed by Abujarad [83]. In this technique, a track detector (CR-39 or LR-115) is placed in a small, impervious vessel and sealed to a typical part of the wall or individual (Fig. 2.4).

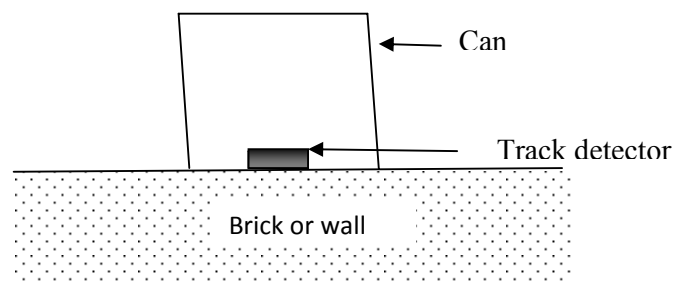


*Fig. 2.4: Schematic diagram of the "can" technique*

The detector is placed at about 2 mm from the surface of the wall or brick inside the 'Can', hidden by a diaphragm (250 polystyrene) but freely exposed to the emergent radon. It

records the decay of radon gas accumulated inside the ‘Can’ plus the decay of Po-218 and Po-214 deposited on the inner walls of the ‘can’. This would reach equilibrium concentration after a week or so. Hence, knowing the geometry of the system and time of exposure, (3 months or more), the equilibrium activity of emergent radon could be obtained. To measure the exhalation rate, the following equation was used:

$$f = \frac{CV\lambda / A}{t_e + (1/\lambda)(e^{-\lambda t_e} - 1)} \quad (2.20)$$

Where

- $f$  : is the radon exhalation per unit area and time (Bq m<sup>-2</sup> h<sup>-1</sup>)  
 $C$  : is the integrate radon exposure as measured by the track (Bq m<sup>-3</sup> h)  
 $V$  : is the volume of the ‘Can’(m<sup>3</sup>)  
 $\lambda$  : is the decay constant of the radon ( h<sup>-1</sup> )  
 $A$  : is the area covered by the ‘Can’ (m<sup>2</sup>)  
 $t_e$  : is the exposure period of the detector inside the ‘can’ (h)

By sticking three or more ‘cans’ to different walls of each room, a good estimation of the exhalation rate from the walls to the inside air of the room can be made.

The technique, however, has few shortcomings recently pointed out by many investigators [49, 82, 84-87]. These are mainly pertaining to underestimation of radon exhalation rate due to back diffusion effect [82], thoron interference [84-86], non-uniformity in the measured values [87] and un-identification of leakage rate during measurements [49]. In view of above issues involved in the ‘can’ technique, focus has now been given to dynamic methods [53, 88-89] of exhalation measurement using online radon monitor.

### 2.3.2. Continuous monitor coupled chamber technique.

Radon mass exhalation from building materials samples is measured by enclosing the sample in a closed chamber and monitoring the build-up of radon concentration in the chamber at regular time intervals using a continuous radon monitor [44, 88-89]. A schematic diagram of the set up is given in Fig. 2.5.

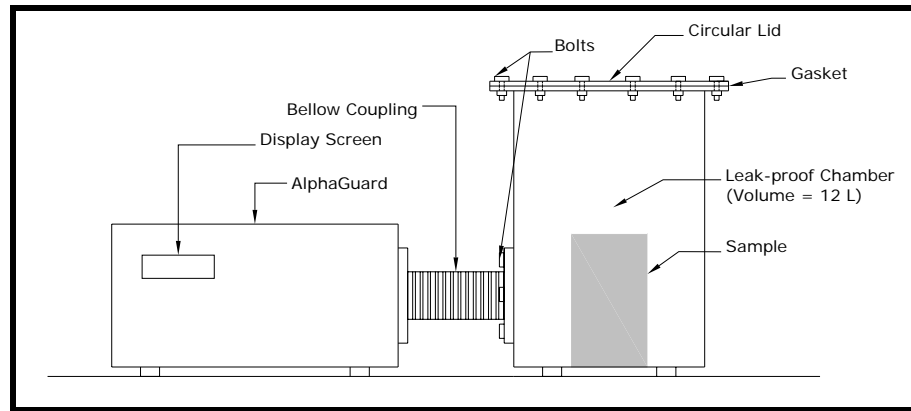


Fig. 2.5: Schematic diagram of the continuous radon monitor (AlphaGUARD) coupled chamber technique for radon exhalation measurements.

Typically about 350 to 500 g of sample is enclosed in a leak tight metallic chamber coupled to a continuous  $^{222}\text{Rn}$  monitor. The radon concentration  $C(t)$  at time  $t$  since closing the chamber builds up according to the formula:

$$C = \frac{J_m M}{V \lambda_e} \left[ 1 - e^{-\lambda_e t} \right] + C_0 e^{-\lambda_e t} \quad (2.21)$$

Where

$J_m$  is the  $^{222}\text{Rn}$  mass exhalation rate of the sample ( $\text{Bq kg}^{-1} \text{h}^{-1}$ )

$C_0$  is the  $^{222}\text{Rn}$  concentration present in the chamber volume at  $t = 0$  ( $\text{Bq m}^{-3}$ );

$M$  is the total mass of the dry sample (kg);

$V$  is the effective volume (volume of chamber + internal volume of  $^{222}\text{Rn}$  monitor – volume of sample) ( $\text{m}^3$ );

$\lambda_e$  is the effective decay constant for  $^{222}\text{Rn}$ , which is sum of the leak rate (if existing) and the radioactive decay constant of  $^{222}\text{Rn}$  ( $\text{s}^{-1}$ ); and

$t$  is the measurement time (s).

Upon least square fitting of the data to the above formula (Eq. 2.21), one may obtain  $J_m$  from the fitted parameters with the knowledge of the dry mass  $M$  of the sample. This technique is one of the superior techniques in recent time as this method automatically takes care of leakage issue during exponential curve fitting and does not have any thoron interference in radon exhalation measurement. The technique is now being largely used all over the world.

Despite the advances on measurement technique of radon exhalation from building materials samples, there does not exist any viable model or analytical approach to extrapolate the radon exhalation from building material samples to that from walls made by those building materials. It is often assumed that the surface flux of radon measured from a building materials is the same as the radon flux from the wall made up of this material [48, 54]. This assumption is in serious error and the correct estimation of wall fluxes based on sample measurements requires the use of 3-D diffusion theory. Further, sample measurements are not unique measures of wall flux in view of possible variations in diffusion lengths of radon from material to material. This necessitates a model which can predict radon flux from the wall based on radon flux data in samples.

#### **2.4. Literature on emission perturbation studies**

The anthropogenic activities associated with the urbanization, leading to large scale soil sealing, is a potential modifier of the gas emission from soil. The emission perturbation

arising out of this phenomenon will affect largely the greenhouse and radioactive gases emission measurements programme [42-43] This is because, the sealed surface tends to inhibit the gas emission from the soil and at the same time, the buildup of trace gases under the sealed surface would result in enhanced emission fluxes around the seal. Because of such emission perturbation, there will be a spatial profile of the emission fluxes across the sealed surfaces. It has been observed that the value of perturbed flux at the edge of the seal is much higher than that of natural flux and it gradually decreases and attains the value of natural flux after some distance away from the seal. The extent of this perturbation would depend upon the dimensions of seal, diffusion parameters of the soil, type of gas, the source and sink distribution underneath the soil. Although this phenomenon has numerically studied in the context of radon [43], however, it has not been studied analytically and especially in the context of trace gases. Hence, there is a need to develop analytical models for the above problem which will enable quantification of the emission perturbation around a sealed surface as a function of distance from the seal and the soil properties. The work will facilitate further studies on the emission perturbation analysis of finite seals in soil matrices having varying properties.

The literature survey clearly highlights the need for developing models for correctly estimating radon fluxes from terrestrial soil surfaces and indoor wall materials. This forms the underlying motivation for the detailed exposition of three new models presented in this thesis, namely, a process based chamber response model, an analytical model for predicting radon emission profile across sealed surface and a building material-to-wall flux extrapolation model. The subsequent chapters dwell at length on the analytical derivations, experiments conducted to validate the models and the various practical implications of the results.

## **3. A Two Dimensional, Diffusion Process based Model for Soil-Chamber Response**

---

### **3.1. Introduction**

Since last few decades, soil-chamber technique remains the most simple and practically viable approach to estimate the radioactive (e.g. radon) as well as stable gases emission from the earth's surface. Chambers used for stable gases are typically constructed in two sections, a "collar" that is inserted into the soil and a "cover" that is then sealed to the collar. On the other hand, chambers used to measure radon emission are typically constructed as a single unit whose open mouth is inserted into the soil. Notwithstanding these differences, the space above the soil surface bounded by the chamber is typically referred to as the headspace for both types of chambers. The fundamental strategy of this chamber method is to relate the increasing gas concentration data in the chamber headspace to the pre-deployment flux density by application of a non-steady state (NSS) model. As mentioned in Chapter-2, the traditional NSS models have certain limitations regarding the chamber deployment and accurate estimation of pre-deployment flux. There is a requirement of another process based NSS model which will simplify the chamber deployment protocol and will provide the correct value of pre-deployment flux.

The response of the chamber to an impressed trace gas flux rests principally on the process of diffusion and mixing in the chamber head space. However, the diffusion process in the chamber head space cannot be separated from that occurring in the soil region. At the

same time, the surface of the soil outside the chamber region acts as trace gas sink (due to a maintained concentration in the atmosphere) which inevitably induces both horizontal and lateral diffusion phenomena. Considering all these aspects, a quantitative understanding of radon build up in head space can be achieved only by treating the problem in terms of a non-steady-state 2-region diffusion equation with appropriate coupling of boundary conditions at the interfaces. The solution developed should be analytical in character so as to provide usable fitting functions for the experimentalist. With this in view, a systematic exposition of the chamber response theory is provided in this chapter.

### **3.2. Mathematical Formulation**

As the problem is quite complex involving two dimensional treatments across multiple regions (Soil space & Chamber space) in non-steady state situations, certain assumptions have to be made to render the problem analytically tractable. These are listed below.

(i) It is assumed that diffusion, governed by Fick's law, is the essential mode of gas transport within the pore space of the soil matrix. This implies that we neglect the pressure driven Darcian flow of the trace gas. In the outdoor atmosphere, pressure fluctuations occur around the mean pressure. These fluctuations, however, are rapidly relaxed in the soil medium as a result of which pressure differential is not sustained for any considerable length of time. In this situation diffusion dominates over pressure driven flow, which justifies the assumption. Although this is a reasonable approximation made by most [90, 41] dealing with trace gas emission modeling, it may not be true in general and hence should be treated as an assumption.

(ii) It is also assumed that the soil properties (e.g. porosity and moisture) are homogeneous throughout the soil matrix and the source is distributed homogeneously in the soil. Soil depth is assumed infinite.

(iii) The chamber is sealed to the surface rapidly and sufficiently gently without causing artificial disturbances to the soil and atmospheric matrices. It is further assumed that the depth of the insertion of the chamber into soil is minimal ( $\sim 1$  cm) in order to meet the criterion of surface deployment.

(iv) The environmental conditions (e.g. soil moisture content, atmospheric pressure, temperature and turbulence) have remained the same both before and after the chamber deployment.

These assumptions imply the existence of a steady-state emission flux from the soil surface before the deployment. However, the steady-state situation changes to a transient state flux after the deployment of the chamber. In order to analyze the latter, it is necessary to quantify the state of the gas profile in the soil matrix prior to deployment.

### **3.2.1. Pre-deployment situation**

Consider a porous matrix such as soil, in which the trace gas (e.g. radon) is continuously released to the pore volume of the matrix with a zero-order production rate density,  $P(z)$ , (for the sake of generality,  $P(z)$  is allowed to vary with depth in such a way that the total production in soil is bounded for stable gases) and there is a first order loss rate constant,  $\lambda$  ( $s^{-1}$ ), (which may be taken as zero for stable gases and is the radioactive decay constant in the case of radon). Assuming that the gas is transported in the pore volume by the process of diffusion through the pores, one may define a local flux density  $F_p$  representing the activity of trace gas crossing per unit pore area per unit time. Let  $C_p$  be the pore space trace

gas concentration at any point at a given time. The general diffusion equation is obtained by a limiting process of the time rate of change of trace gas in an infinitesimal pore volume arising due to the difference between the generation rate and losses due to a first order loss rate constant  $\lambda$  which can be written as:

$$\frac{\partial C_p}{\partial t} = P(z) - \nabla \cdot F_p - \lambda C_p \quad (3.1)$$

For a one-dimensional system, the diffusion flux is expressed in terms of the concentration gradient by applying Fick's law of diffusion as follows:

$$F_p = -D_s \frac{\partial C_p}{\partial z} \quad (3.2)$$

Where,  $D_s$  is the trace gas diffusion coefficient in the pore space in the soil matrix. In a strictly dry matrix, it is the product of molecular diffusion coefficient in air ( $D_M$ ) in the pore space and tortuosity ( $\tau$ ) that accounts for the tortuous path traversed by the trace gas atoms along the pores. However, in general, soil pore contains moisture and trace gas will diffuse both in the air and water phases resulting in lowering of the diffusion coefficient ( $D_s$ ) in the pore space of the soil matrix.

Substitution of Eq.(3.2) in Eq.(3.1) yields the following diffusion equation:

$$\frac{\partial C_p}{\partial t} = P(z) + D_s \frac{\partial^2 C_p}{\partial z^2} - \lambda C_p \quad (3.3)$$

While the flux  $F_p$  above refers to unit pore area, the emission flux density at the soil surface refers to the bulk area that includes both pore area and the area covered by the solid materials. Upon assuming the fractional pore area at the surface to be the same as the fractional pore volume of the bulk of the soil matrix, the soil-surface emission flux density ( $f_o$ ) may be related to the pore space concentration as follows:

$$f_0 = n_T F_p = -n_T D_s \left. \frac{\partial C_p}{\partial z} \right|_{z=0} \quad (3.4)$$

Where  $n_T$  is the total porosity of the matrix (i.e. total pore volume/ bulk volume).

In dry soil matrix, the pores will be filled only with air, and hence  $C_p$  will be the same as the concentration  $C_a$  in pore air. In the case of soil pore containing moisture, the trace gas in the pore volume will be distributed partly in air and partly in water in proportion to the water/air partition coefficient of trace gases. It is more convenient to recast the diffusion equation in terms of  $C_a$  so as to develop consistent formulations and interface boundary conditions to address multi-layer problem involving covers having different moisture contents and material properties. This can be done by following the mathematical formulation given by [91]. If  $C_w$ ,  $C_a$ , denote trace gas concentration in water and in air and if  $n_w$ ,  $n_a$  are air-filled and water filled porosities respectively, then material conservation requires that:

$$n_T C_p = n_a C_a + n_w C_w \quad (3.5)$$

Now applying the law of equilibrium partitioning which relates  $C_w$  to  $C_a$ , one can write:

$$C_w = K \cdot C_a \quad (3.6)$$

where,  $K$  is the water/air partition coefficient. Upon combining Eq.(3.6) with Eq.(3.5), one arrives at

$$n_T C_p = C_a (n_a + K n_w) = n_e \cdot C_a \quad (3.7)$$

where,

$$n_e = (n_a + K n_w). \quad (3.8)$$

The quantity  $n_e$  denotes the partition corrected porosity. It may be expressed more conveniently in terms of the volumetric moisture saturation ( $m$ ), defined as  $m = n_w / n_T$ , as follows:

$$n_e = n_T [1 - (1 - K)m]. \quad (3.9)$$

With this, Eq. (3.3) may be recast in terms of  $C_a$  as follows:

$$\frac{\partial C_a}{\partial t} = D_s \frac{\partial^2 C_a}{\partial z^2} - \lambda C_a + S(z) \quad (3.10)$$

Where  $S(z) = \frac{n_T}{n_e} P(z)$  is the new source term that includes the effect of gas partitioning

between air and water phase in the soil pore space. Under steady state condition, denoting trace gas concentration in soil air space as  $C_s^{(0)}(z)$ , the diffusion equation in pre-deployment situation may be written as:

$$D_s \frac{\partial^2 C_s^{(0)}(z)}{\partial z^2} - \lambda C_s^{(0)}(z) + S(z) = 0 \quad (3.11)$$

The above Eqs. (3.10) and (3.11) are the most general equations for trace gas diffusion in soil pore, partly filled with water. This form of equation provides the correct framework to deal with concentration and flux continuity condition across multiple regions. Now in terms of  $C_s^{(0)}(z)$ , Eq. (3.4) may be expressed to find the emission flux density at soil surface as:

$$f_0 = -n_e D_s \left. \frac{\partial C_s^{(0)}}{\partial z} \right|_{z=0} \quad (3.12)$$

Eq. (3.12) indicates that, for a steady trace gas concentration profile in the soil space, there is a steady emission flux density at the soil surface before deploying the chamber.

### 3.2.2. Post-deployment situation

It is postulated that prior to deployment of the chamber, there exists a steady emission flux of the trace gas at the soil surface as given in Eq. 3.12. This flux is maintained by the process of columnar diffusion in the pore space of the soil matrix and rapid removal of the emitted gas at the surface due to atmospheric mixing. Upon deployment of chamber, lateral diffusion in the soil matrix is initiated in response to the now changing soil concentration

gradient, defined by the gradient between the chamber headspace and the atmosphere. The system therefore is transformed from a one dimensional, pre-deployment diffusion problem to a two dimensional, post-deployment problem. With regards to mixing in the chamber headspace, Livingston et al. [41], in developing their 1-D NSS chamber response model assumed instantaneous uniform mixing to render the problem analytically simpler. In contrast, this work assumes diffusive mixing in the headspace throughout the deployment period.

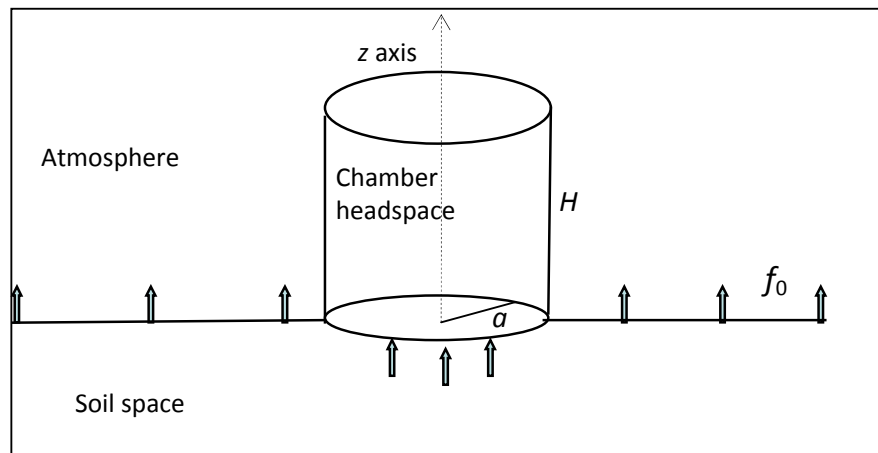


*Fig. 3.1: Schematic diagram of a cylindrical chamber deployed at the surface of the soil matrix. The dashed arrow represents the vertical ( $z$ ) axis in the cylindrical coordinate system. ' $H$ ' and ' $a$ ' are height and radius of the chamber respectively.  $f_0$  is the steady state pre-deployment flux of the trace gas.*

While recognizing that neither approach is entirely satisfactory, it may be noted that diffusive outflow near the chamber walls is a major factor in the so-called back-diffusion effect [82] that results in spatial anisotropy within the headspace. This, however, cannot be addressed by assuming uniform mixing. Both vertical and lateral concentration gradients must be allowed to continue to drive diffusion within the chamber headspace at all times.

Now, considering a partition corrected zero-order production rate density,  $S(z)$ , (where  $S(z)$  is allowed to vary with depth in such a way that the total production in soil is bounded for stable gases) and a first order loss rate constant,  $\lambda$  ( $s^{-1}$ ), (which may be taken as zero for stable gases and is the radioactive decay constant in the case of radon) in the air space of the soil pore, the non-steady state equation describing the gas concentration change over time in the soil space may be written as:

$$\frac{\partial C_s}{\partial t} = D_s \left[ \frac{1}{r} \frac{\partial}{\partial r} \left\{ r \frac{\partial C_s}{\partial r} \right\} + \frac{\partial^2 C_s}{\partial z^2} \right] - \lambda C_s + S(z), \quad 0 \leq r < \infty, \quad -\infty < z \leq 0. \quad (3.13)$$

Since there is no production of trace gas in the chamber headspace, the corresponding concentration,  $C_c$  (moles or Becquerel of target gas per  $m^3$  of air), satisfies the following non-steady state diffusion equation:

$$\frac{\partial C_c}{\partial t} = D \left[ \frac{1}{r} \frac{\partial}{\partial r} \left\{ r \frac{\partial C_c}{\partial r} \right\} + \frac{\partial^2 C_c}{\partial z^2} \right] - \lambda C_c, \quad 0 \leq r \leq a, \quad 0 \leq z \leq H. \quad (3.14)$$

The Boundary Conditions (BC's) of the problem may be written as:

$$C_s(r, -\infty, t) = \text{bounded}, \quad 0 \leq r < \infty, \quad (3.15a)$$

$$C_s(r, 0, t) = C_c(r, 0, t), \quad 0 \leq r \leq a, \quad (3.15b)$$

$$C_s(r, 0, t) = 0, \quad a \leq r \leq \infty, \quad (3.15c)$$

$$-n_e D_s \frac{\partial C_s(r, z, t)}{\partial z} \Big|_{z=0} = -D \frac{\partial C_c(r, z, t)}{\partial z} \Big|_{z=0}, \quad 0 \leq r \leq a, \quad (3.15d)$$

$$\frac{\partial C_c(r, z, t)}{\partial r} \Big|_{r=a} = 0, \quad 0 \leq z \leq H \quad \text{and} \quad (3.15e)$$

$$\frac{\partial C_c(r, z, t)}{\partial z} \Big|_{z=H} = 0, \quad 0 \leq r \leq a. \quad (3.15f)$$

The initial conditions are:

$$C_s(r, z, 0) = C_s^{(0)}(z), \quad -\infty < z < 0, \quad 0 < r < \infty \quad \text{and} \quad (3.16a)$$

$$C_c(r, z, 0) = 0, \quad 0 < z < H, \quad 0 < r < a, \quad (3.16b)$$

where  $C_s^{(0)}(z)$  (moles or Becquerel of target gas per  $\text{m}^3$  of air) denotes the steady state concentration profile of the trace gas in the soil pore space prior to chamber deployment as given in Eq. (3.11).

It may be noted that the concentrations of the gas in the atmosphere (exterior to the chamber), as well as that in the chamber headspace prior to deployment, are assumed to be zero. Although ambient atmospheric concentration ( $C_0$ ) of a stable gas may be significant, it merely results in an additive term in any model for the concentration increase in the chamber headspace over time and does not affect the flux density. This results because the ambient concentration in the atmosphere (and in the chamber headspace) prior to deployment would have pervaded uniformly in the entire soil system and therefore would not induce subsequent concentration gradients. In contrast, for radon or thoron, a non-zero initial concentration affects, in principle, their subsequent time evolution into the chamber. In practice, however, this effect is negligibly small since their atmospheric concentrations are negligible relative to their concentrations in soil pore space. In the unified treatment that is attempted here, it is assumed that the initial trace gas concentration is zero so as to avoid tedious mathematical terms with negligible effects.

### 3.3. Derivation of the Solution

It is evident from the formulation in Eqs.(3.13 to 3.16b) that the two dimensional treatment of the non-steady state chamber problem is a mathematically challenging task, as it combines mixed boundary conditions across multiple regions with time dependence. The available classical techniques based on transform calculus and eigen function expansion are

generally geared to address homogeneous boundary conditions. On the other hand, for the problem involving mixed boundary conditions as in the present case, it is necessary to employ dual integral equation techniques originally developed in the context of potential theory. A comprehensive classical treatise by Sneddon [92] on mixed boundary value problems and that by Mandal & Mandal [93] provide excellent expositions on the subject of dual integral equations. As this method cannot be directly applied to transient diffusion problems, we eliminated the time dependence by Laplace transform method [94]. The solution obtained in the Laplace transformed domain was inverted by using contour integration as well as numerical techniques [95]. We would like to note that this technique has considerable potential in a wider context of trace gas behavior in soils such as accumulation under seals and other artifacts, emissions from cracks in seals and flux density modifications around concrete buildings, etc [43].

For mathematical tractability, we recast our problem in terms of the following dimensionless variables:

$\rho = r/a$  (dimensionless radial coordinate so that  $0 < \rho < 1$  in the chamber region and  $0 < \rho < \infty$  in the soil region),

$\zeta = z/a$  (dimensionless axial coordinate so that  $0 < \zeta < \Delta$  in the chamber region and  $-\infty < \zeta < 0$  in the soil region),

$\Delta = H/a$  (dimensionless height of the chamber),

$\tau_s = a^2/D_s$  (dimensionless relaxation time in the soil matrix) and

$\tau_c = a^2/D$  (dimensionless relaxation time in chamber headspace).

Upon defining the Laplace transform [94] of the concentration profiles with respect to time ( $t \rightarrow p$ ) as

$$\tilde{C}_{s,c}(\rho, \zeta; p) \equiv \int_0^{\infty} C_{s,c}(\rho, \zeta, t) \exp(-pt) dt, \quad (3.17)$$

the set of differential equations (Eqs. (3.13) and (3.14)) may be transformed as

$$\frac{1}{\rho} \frac{\partial}{\partial \rho} \left\{ \rho \frac{\partial \tilde{C}_s}{\partial \rho} \right\} + \frac{\partial^2 \tilde{C}_s}{\partial \zeta^2} - \tau_s (\lambda + p) \tilde{C}_s + \tau_s \left[ \frac{S(\zeta)}{p} + C_s^0(\zeta) \right] = 0, \quad 0 \leq \rho < \infty, \quad -\infty < \zeta \leq 0 \quad (3.18)$$

and

$$\frac{1}{\rho} \frac{\partial}{\partial \rho} \left\{ \rho \frac{\partial \tilde{C}_c}{\partial \rho} \right\} + \frac{\partial^2 \tilde{C}_c}{\partial \zeta^2} - \tau_c (\lambda + p) \tilde{C}_c = 0, \quad 0 \leq \rho < 1, \quad 0 < \zeta \leq \Delta. \quad (3.19)$$

The boundary conditions (3.15a to 3.15f) can be similarly transformed in terms of the dimensionless variables. Hereafter, we refer to the Laplace transformed concentration and flux as LTC and LTF, respectively.

### 3.3.1. Solution in soil matrix

The effect of the unknown pre-deployment concentration profile in the soil matrix, which in turn is related to the distribution of the source through Eq. (3.13), can be eliminated by using the procedure of Livingston et al. [41]. Upon defining an incremental function

$$\psi(r, z; t) = C_s(r, z; t) - C_s^{(0)}(z), \quad (3.20)$$

it may be readily seen from Eq. (3.11) and Eq. (3.18) that the equation for  $\tilde{\psi}(\rho, \zeta; p)$  will be a homogeneous partial differential equation in variables  $\rho, \zeta$ . This can be easily reduced to an ordinary differential equation (ODE) in  $\zeta$  variable by applying the Hankel transform [96] w.r.t.  $\rho$  using the Bessel function  $J_0(k\rho)$ . Upon solving this ODE and then applying Hankel inversion theorem and then reverting back to Eq. (3.20), we have

$$\tilde{C}_s(\rho, \zeta; p) = \frac{C_s^{(0)}(\zeta)}{p} + \int_0^{\infty} A(k, p) J_0(k\rho) \exp \left[ (k^2 + \tau_s \lambda + \tau_s p)^{1/2} \zeta \right] dk, \quad 0 < \rho < \infty, \quad -\infty < \zeta < 0. \quad (3.21)$$

In the above,  $A(k, p)$  (Hankel coefficient) is a yet unknown function of  $k$  only. Upon setting  $\zeta=0$  in Eq. (3.21) and noting Eq. (3.15b) and Eq. (3.15c), the LTC profile over the soil surface (including that beneath the chamber) may be expressed as

$$\begin{aligned} \tilde{C}_s(\rho, 0; p) &= \int_0^{\infty} A(k, p) J_0(k\rho) dk = 0, & 1 < \rho < \infty, \\ &= \text{non-zero finite}, & 0 \leq \rho \leq 1. \end{aligned} \quad (3.22)$$

Here we invoke the results compiled by Sneddon [92] on the class of functions which satisfy integral equations of the type shown in Eq. (3.22). Upon using the property of Weber-Schafheitlin integrals of the first kind, Sneddon arrived at a family of solutions for  $A(k, p)$  which satisfy Eq. (3.22). The most general solution is a linear combination of these solutions:

$$A(k, p) = \sum_{n=0}^{\infty} g_n(p) 2^{\nu+n} \Gamma(\nu+n+1) k^{-\nu-n} J_{\nu+n+1}(k), \quad (3.23)$$

where  $g_n(p)$  are the coefficients of the expansion,  $\nu$  is an index which may be restricted to  $0 < \nu < 1$ ,  $J_{\nu+n+1}(k)$  is the Bessel function of order  $\nu+n+1$  and  $\Gamma(\nu+n+1)$  is the gamma function. Upon substituting  $A(k, p)$  from Eq. (3.23) in Eq. (3.22), we obtain the following expression for the LTC profile set up beneath the chamber:

$$\tilde{C}_s(\rho, 0; p) = \sum_{n=0}^{\infty} g_n(p) (1-\rho^2)^{\nu+n}, \quad 0 \leq \rho \leq 1. \quad (3.24)$$

This is a significant result since it satisfies the radial continuity requirement (viz,  $\tilde{C}_s(1, 0, p) = 0$ ) at the point  $\rho=1$ . It also implies that  $\nu$  cannot be negative since the concentration cannot diverge at  $\rho=1$ . In addition, Eq. (3.24) indicates that when a NSS chamber is deployed, the trace gas concentration in the chamber headspace acquires a power law profile in the variable  $1-\rho^2$  and the exponent of the power, in its lowest order, may be

fractional (for  $\nu < 1$ ). The smaller the value of  $\nu$ , the sharper will be the lateral gradient in the trace gas concentration at the soil-chamber interface.

Similarly, upon differentiating Eq. (3.21) w.r.t  $\zeta$  and applying Fick's law and using Eq. (3.23), the Laplace transformed vertical soil flux (post-deployment) at the surface, denoted by  $\tilde{f}_s(\rho, 0; p)$  can be expressed as

$$\tilde{f}_s(\rho, 0; p) = \frac{f_0}{p} - \frac{n_e D_s}{a} \sum_{n=0}^{\infty} g_n(p) \phi_n(\rho; p), \quad 0 < \rho < \infty, \quad (3.25)$$

where  $\phi_n(\rho; p)$  is an integral function defined as:

$$\phi_n(\rho; p) = 2^{\nu+n} \Gamma(\nu+n+1) \int_0^{\infty} (k^2 + \tau_s \lambda + \tau_s p)^{1/2} k^{-\nu-n} J_{\nu+n+1}(k) J_0(k\rho) dk. \quad (3.26)$$

The function  $\phi_n(\rho; p)$  cannot be reduced to a closed form. A general functional analysis shows that  $\phi_n(\rho; p) \rightarrow 0$  as  $\rho \rightarrow \infty$  and hence the soil flux density far from the chamber will approach  $f_0$ . However, the function has a complicated singular structure at  $\rho \sim 1$ . In order to analyze this structure it is necessary to fix the parameter  $\nu$ , which in turn, requires one to match the solutions in the chamber headspace.

### 3.3.2. Solution in chamber headspace

From Eq. (3.19), the LTC profile in the chamber headspace may be constructed using the standard eigen function expansion techniques involving a Fourier Bessel series satisfying the impermeability condition (Eq. (3.15f)) on the side and the top of the chamber:

$$\tilde{C}_c(\rho, \zeta; p) = \sum_{k=0}^{\infty} B_k(p) \cosh[\mu_k(p)(\Delta - \zeta)] J_0(q_k \rho) \quad (0 \leq \rho \leq 1, 0 < \zeta \leq \Delta), \quad (3.27)$$

where

$$\mu_k(p) = (q_k^2 + \tau_c \lambda + \tau_c p)^{1/2} \quad (k = 0, 1, 2, \dots) \quad (3.28)$$

and  $q_k$  are the roots of the equation involving the Bessel function  $J_1(x)$ :

$$\begin{aligned} q_k J_1(q_k) &= 0, \quad (k = 0, 1, 2, \dots) \\ (q_0 &= 0, \quad q_1 = 3.8317, \quad q_2 = 7.0156, \dots \text{etc.}) \end{aligned} \quad (3.29)$$

We may relate the expansion coefficients  $B_k(p)$  ( $k=0,1,2,\dots$ ) to the coefficients ( $g_n(p)$ ,  $n=0,1,2,\dots$ ) in the soil matrix by setting  $\zeta=0$  in Eq. (3.27), equating it with Eq. (3.24) and applying the orthogonality relationships of the Bessel function. We skip the details for brevity. From this, the Laplace Transformed Flux (LTF) profile at the interface (from the chamber side) may be given by

$$\tilde{f}_c(\rho, 0; p) = \frac{D}{a} \mu_0(p) B_0(p) \sinh[\mu_0(p)\Delta] + \frac{D}{a} \sum_{n=0}^{\infty} g_n(p) X_n(\rho; p), \quad 0 \leq \rho \leq 1, \quad (3.30)$$

where

$$B_0(p) = \frac{1}{\cosh[\mu_0(p)\Delta]} \left[ \sum_{n=0}^{\infty} \frac{g_n(p)}{\nu + n + 1} \right] \quad (3.31)$$

and

$$X_n(\rho; p) = 2^{\nu+n+1} \Gamma(\nu + n + 1) \sum_{k=1}^{\infty} \frac{\mu_k(p) \tanh[\mu_k(p)\Delta] J_{\nu+n+1}(q_k) J_0(q_k \rho)}{J_0^2(q_k) q_k^{\nu+n+1}}. \quad (3.32)$$

### 3.3.3. Explicit form of Laplace Transformed Concentration and Flux

The unknowns,  $g_n(p)$  and  $\nu$ , must then be determined to express the solutions explicitly by applying flux continuity conditions between  $\tilde{f}_s(\rho, 0; p)$  and  $\tilde{f}_c(\rho, 0; p)$  at the soil-chamber interface. Upon matching Eq. (3.25) with Eq. (3.30) and simplifying, we obtain the flux constraint (matching) equation, viz.,

$$\sum_{n=0}^{\infty} g_n(p) [\alpha X_n(\rho; p) + \phi_n(\rho; p)] = \frac{a f_0}{p \varepsilon D_s} - \alpha \mu_0(p) B_0(p) \sinh[\mu_0(p)\Delta], \quad 0 \leq \rho \leq 1, \quad (3.33)$$

where  $\alpha$  is a crucial coupling parameter defined by

$$\alpha = \frac{D}{\varepsilon D_s}. \quad (3.34)$$

The LHS of Eq. (3.33) is a function of  $\rho$  while the RHS is independent of  $\rho$ . The index  $\nu$  appearing in the definition of  $\{X_n(\rho, p), \phi_n(\rho, p)\}$  and the coefficients  $g_n(p)$  should be so adjusted that this equation is satisfied for all  $\rho$ . A necessary requirement to achieve this is that the function  $\alpha X_n(\rho; p) + \phi_n(\rho; p)$  should atleast be bounded in  $0 < \rho < 1$ . This calls for an examination of the detailed behavior of the functions  $X_n(\rho, p)$  and  $\phi_n(\rho, p)$  in the domain  $0 < \rho < 1$ . It turns out that if we accept the possibility of  $\nu < 1$ , the functions  $X_0(\rho, p)$ , represented by a series and  $\phi_0(\rho, p)$  represented by the integral tend to diverge as  $\rho \rightarrow 1^-$  and the higher order functions  $X_n(\rho, p)$ , and  $\phi_n(\rho, p)$  ( $n = 1, 2, \dots$ ) remain bounded as  $\rho \rightarrow 1^-$ . Hence the lowest terms are most crucial and the form of the singularity of  $X_0(\rho, p)$  may be obtained by using Sneddon's summation theorems [92] and that of  $\phi_0(\rho, p)$  by reducing the integral to a hypergeometric function [82]. The result is

$$\alpha X_0(\rho; p) + \phi_0(\rho; p) \sim \frac{2\Gamma(1-\nu)\Gamma(1+\nu)}{\pi} [(\alpha+1)\cos(\pi\nu) - \alpha] (1-\rho^2)^{\nu-1} + \text{constant}, \rho \rightarrow 1^-. \quad (3.35)$$

As a first requirement of satisfying the flux constraint Eq. (3.33), it is necessary to suppress the singular term of the form  $(1-\rho^2)^{\nu-1}$  ( $0 < \nu < 1$ ) occurring in Eq. (3.35), as one approaches the edge of the inner side of the chamber wall. This is achieved by setting the coefficient multiplying this term, to zero. Since the gamma function cannot be zero for real  $\nu$ , the remaining term  $(\alpha+1)\cos(\pi\nu) - \alpha = 0$ , from which we obtain

$$\nu = \frac{1}{\pi} \arccos\left(\frac{\alpha}{1+\alpha}\right). \quad (3.36)$$

It may be noted from Eq. (3.36) that  $\nu$  decreases from  $\frac{1}{2}$  to 0 as  $\alpha$  increases from 0 to  $\infty$ . As this exponent is the same as that obtained for the steady state case [82], it implies that the

shape of the interface concentration profile (Eq. (3.24)) increases in a self-similar fashion, and the transient effects are contained only in the pre-factors ( $g_n(p)$ ).

Having determined  $\nu$ , we have essentially determined the function  $X_n(\rho, p)$  and  $\phi_n(\rho, p)$ . It is now required to determine the coefficients  $g_n(p)$  such that the constraint equation is completely satisfied. In principle, this may be accomplished by setting the coefficients of the successive higher order terms,  $(1-\rho^2)^{n+\nu}$  ( $n=1,2,..$ ) occurring in Eq. (3.33) to zero, although this is a very tedious task. A simpler approach is to follow an iterative procedure and hope for a fast convergence of the series. In the lowest approximation, we may retain only the leading term of the interface LTC and LTF profiles:

$$\tilde{C}_s(\rho, 0; p) \approx g_0(p)(1-\rho^2)^\nu, \quad 0 \leq \rho \leq 1, \quad (3.37)$$

$$\tilde{f}_s(\rho, 0; p) \approx \frac{f_0}{p} - \frac{\varepsilon D_s}{a} g_0(p) \phi_0(\rho; p), \quad 0 \leq \rho < \infty. \quad (3.38)$$

The flux constraint equation (Eq. (3.33)) now takes the following one-term form:

$$g_0(p) [\alpha X_0(\rho; p) + \phi_0(\rho; p)] = \frac{af_0}{p\varepsilon D_s} - \alpha \mu_0(p) \tanh[\mu_0(p)\Delta] \frac{g_0(p)}{\nu+1}. \quad (3.39)$$

By multiplying both sides of Eq. (3.39) by  $2\rho$  and integrating between 0 to 1 and noting

$\int_0^1 \rho X_0(\rho) d\rho = 0$ , we obtain the following expression for  $g_0(p)$ :

$$\frac{g_0(p)}{\nu+1} = \frac{\left(\frac{f_0 a}{p \varepsilon D_s}\right)}{\chi_\nu \left\{ \frac{(\lambda+p)a^2}{D_s} \right\} + \frac{Da}{\varepsilon D_s} \sqrt{\frac{\lambda+p}{D}} \tanh\left(H \sqrt{\frac{\lambda+p}{D}}\right)}, \quad (3.40)$$

where  $\chi_\nu(\dots)$  is the  $\rho$  averaged function of  $\phi_0(\rho, p)$  (Eq. (3.26), with  $n=0$ ), having the form,

$$\chi_\nu(z) = 2^{\nu+1} \Gamma(\nu+2) \int_0^\infty (k^2+z)^{1/2} k^{-\nu-1} J_{\nu+1}(k) J_1(k) dk. \quad (3.41)$$

It may be shown specifically that

$$\chi_\nu(0) = \frac{\Gamma(\nu)\Gamma(2+\nu)}{\Gamma\left(\frac{1}{2}+\nu\right)\Gamma\left(\frac{3}{2}+\nu\right)}, \quad (3.42)$$

where  $\Gamma(z)$  is the gamma function of  $z$ .

Now, the radial averaged interface LTC ( $\bar{C}_s(p)$ ) and LTF ( $\bar{f}_s(p)$ ), may be evaluated

(within the leading term approximation) as

$$\bar{C}_s(p) = \int_0^1 2\rho \tilde{C}_s(\rho, 0; p) d\rho = \frac{g_0(p)}{\nu+1} \quad (3.43)$$

and

$$\bar{f}_s(p) = \int_0^1 2\rho \tilde{f}(\rho, 0; p) d\rho = \frac{f_0}{p} - \frac{n_e D_s}{a} \frac{g_0(p)}{\nu+1} \chi_\nu\left(\frac{a^2}{D_s}(\lambda+p)\right). \quad (3.44)$$

Since the diffusion mixing process is not instantaneous, it is expected that the rates of rise in headspace concentration will differ at different heights within the chamber headspace. A quantity of practical interest is the volumetrically averaged LTC ( $\bar{C}_c(p)$ ), defined as

$$\bar{C}_c(p) = \frac{1}{\Delta} \int_0^1 \int_0^\Delta 2\rho \tilde{C}_c(\rho, \zeta; p) d\rho d\zeta = \frac{g_0(p)}{\nu+1} \frac{\tanh[\mu_0(p)\Delta]}{\mu_0(p)\Delta}, \quad (3.45)$$

where  $g_0(p)$  and  $\nu$  are defined earlier in Eq. (3.40) and Eq. (3.36) respectively.

This completes the formal solutions (to a leading order) for the chamber problem in the Laplace transformed domain. We must now implement a Laplace inversion of the various quantities to obtain their real time behavior. This can be achieved both analytically and by numerical technique. For the latter, we employed a simple numerical Laplace inversion algorithm [95] based on a 15 point Legendre polynomial expansion technique [97]. This was implemented in Mathematica [98] for obtaining the transient profiles of various quantities presented in Eq. (3.37), Eq. (3.38), Eq. (3.43), Eq. (3.44) and Eq. (3.45).

### 3.3.4. Temporal increase of the headspace concentration

An analytical expression for the temporal increase of the trace gas concentration in the chamber headspace is of considerable value for fitting the experimentally observed data and extracting the pre-deployment flux. Although a simple expression cannot be derived, we provide a quadrature type integral expression for the concentration. The derivation is as follows.

Upon substituting the expression for  $g_0(p)$  and  $\nu$  as given in Eq. (3.40) and Eq. (3.36) into Eq. (3.45), the volumetrically averaged LTC, in explicit notations, can be written as

$$\bar{C}_c(p) = \frac{f_0 / pH}{\frac{n_e D_s}{aH} \left[ (\lambda + p) \frac{H^2}{D} \right]^{1/2} \coth \left[ \left\{ (\lambda + p) \frac{H^2}{D} \right\}^{1/2} \right] \chi_v \left[ (\lambda + p) \frac{a^2}{D_s} \right] + (\lambda + p)} . \quad (3.46)$$

We now use the standard Laplace inversion formula [97] based on contour integration techniques. Since  $\bar{C}_c(p)$  has a simple pole at  $p=0$ , its residue may be easily evaluated and then shifting the line of integration to the left, we obtain

$$\bar{C}_c(t) = C_c(\infty) + \frac{1}{2\pi i} \int_{\gamma' - i\infty}^{\gamma' + i\infty} \bar{C}_c(p) \exp[pt] dp \quad (3.47)$$

where  $\gamma'$  ( $<0$ ), is a line of integration parallel to the imaginary axis lying on its left. The first term on the right hand side of Eq. (3.47) is the final steady state concentration attained in the chamber, having the explicit expression:

$$\bar{C}_c(\infty) = \frac{f_0}{H} \frac{1}{\frac{n_e D_s}{aH} \left[ \frac{\lambda H^2}{D} \right]^{1/2} \coth \left[ \left\{ \lambda \frac{H^2}{D} \right\}^{1/2} \right] \chi_v \left[ \lambda \frac{a^2}{D_s} \right] + \lambda} . \quad (3.48)$$

Further evaluation of the integral in Eq. (3.47) requires one to locate the remaining singularities of  $\bar{C}_c(p)$ . A careful analysis of the integrand shows that it has a branch point of

the type  $p^{3/2}$  at  $p'=0$  (where  $p'=\lambda+p$ ) which occurs in the  $\chi_0(\dots)$  function and branch line extends from zero to  $-\infty$ . Skipping the details of the mathematical steps involved, the final quadrature formula for the time evolution of the mean concentration is given by:

$$\bar{C}_c(t) = \bar{C}_c(\infty) + \frac{f_0 \exp[-\lambda t]}{\pi H} \int_0^\infty \frac{\exp[-xt]}{(\lambda+x)} \frac{B(x) dx}{\{A^2(x) + B^2(x)\}}, \quad (3.49)$$

where

$$A(x) = \left[ -x + (n_e D_s / aH) \chi_\nu(0) G_1(-a^2 x / D_s) (xH^2 / D)^{1/2} \coth \left\{ (xH^2 / D)^{1/2} \right\} \right],$$

$$B(x) = \left[ (n_e D_s / aH) (a^2 x / D_s)^{3/2} G_2(-a^2 x / D_s) (xH^2 / D)^{1/2} \coth \left\{ (xH^2 / D)^{1/2} \right\} \right],$$

$$G_1(z) = {}_2F_3 \left[ \left\{ \frac{1+\nu}{2}, \frac{\nu}{2} \right\}, \left\{ \frac{1}{2}, \frac{1}{2} + \nu, \frac{3}{2} + \nu \right\}, z \right],$$

$$G_2(z) = \frac{{}_1 - {}_2F_3 \left[ \left\{ \frac{1+\nu}{2}, 1 + \frac{\nu}{2} \right\}, \left\{ \frac{3}{2}, 1 + \nu, 2 + \nu \right\}, z \right]}{z} \text{ and}$$

${}_2F_3(\dots)$  is the generalized hypergeometric function defined as

$${}_2F_3[\{a_1, a_2\}, \{b_1, b_2, b_3\}, z] = \frac{\Gamma(b_1)\Gamma(b_2)\Gamma(b_3)}{\Gamma(a_1)\Gamma(a_2)} \sum_{k=0}^{\infty} \frac{\Gamma(a_1+k)\Gamma(a_2+k)z^k}{k!\Gamma(b_1+k)\Gamma(b_2+k)\Gamma(b_3+k)}.$$

Eq. (3.49) represents the temporal evolution of the trace gas concentration in the chamber headspace as a function of system parameters for a specified pre-deployment flux. The functions  $A(x)$  and  $B(x)$  can be evaluated using mathematical software, such as Mathematica [98]. The temporal evolution of the stable gases in the chamber headspace may be easily obtained by setting  $\lambda=0$  in Eq. (3.49).

### 3.3.5. First order correction

To estimate the accuracy of the leading term approximation, we have carried out a higher order correction by including the next higher term for the interface concentration profile given in Eq. (3.24) as follows:

$$\tilde{C}_s(\rho, 0; p) = g_0(p)(1 - \rho^2)^v + g_1(p)(1 - \rho^2)^{v+1} \quad (3.50)$$

To determine  $g_0(p)$  and  $g_1(p)$ , we require two equations and these are obtained by minimizing the deviation of the function on the average as well as at the edge ( $\rho=1$ ). The mathematical steps required are similar to that discussed in section 3.3.3. This gives rise to an improved expression for  $g_0(p)$  and an additional formula for  $g_1(p)$ . In Fig. 3.2, we compare the zero<sup>th</sup> and the first order corrections to the concentration increase over time for radon. There appears very little difference between the two solutions thereby reassuring the accuracy of the zero<sup>th</sup> order result from a practical point of view. Therefore, only the leading term approximation (zero<sup>th</sup> order) is considered in future discussions.

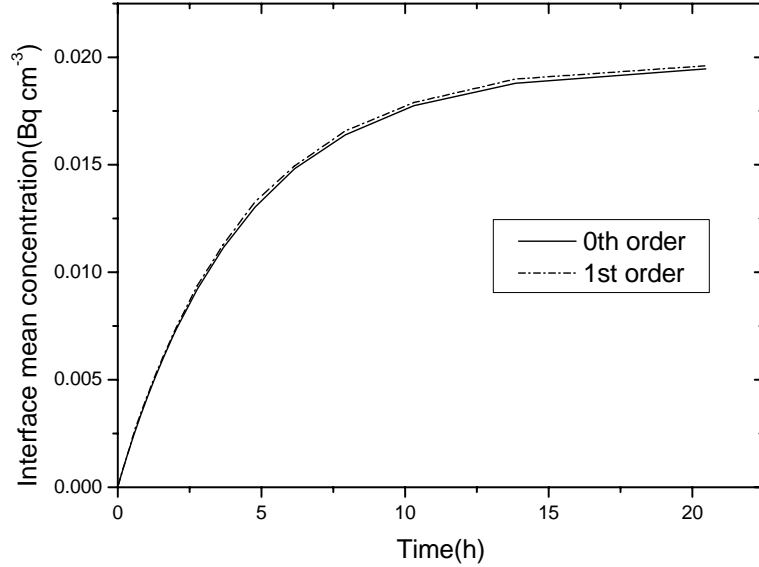


Fig.3.2: Comparison of the 0th and 1st order modeled mean concentration of radon at the chamber-soil interface. (The values of parameters used are:  $a=15$  cm,  $H=30$  cm,  $C_\infty = 1$ ,  $D_s=0.02$  cm<sup>2</sup> s<sup>-1</sup>,  $D = 0.1$  cm<sup>2</sup> s<sup>-1</sup>,  $n_e=0.3$ ,  $\lambda = 2.1 \times 10^{-6}$  s<sup>-1</sup>).

### **3.3.6. Direct numerical solutions of the differential equations:**

To further ensure the correctness of the analytical solutions, the coupled differential equations (Eq. (3.13) and Eq. (3.14)) were solved directly using a two dimensional finite difference scheme [99] written in FORTRAN (Refer Appendix B). The simulation was performed in time steps of  $\Delta t = (\Delta a)^2 / 4D_s$  where  $\Delta a$  is the length of one side of a square grid which was set at 0.5 cm for the final simulation after checking the convergence of the solution with varying grid sizes. Comparisons of the numerical solutions were made for a chamber of 30 cm height and 15 cm radius and the dimensions of the soil domain were: depth: 200 cm and radius: 200 cm. Various quantities, such as the interface concentration and flux profiles, concentration profiles at various depths in the soil matrix and the volumetric mean concentration were evaluated at different time steps. The simulation time for each run of the program required about 1 hour at the resolution mentioned above. For comparison with the analytical technique, we focused on the volumetric mean concentration in the chamber headspace.

### **3.4. Implications of the solution**

Modeling both radial and vertical diffusion processes in chambers highlight several aspects of the chamber system that are not evident in traditional 1-D analysis. To focus on these aspects, it is necessary to first establish confidence in the analytical solutions which contain these features, particularly when those solutions were derived by a series of complicated mathematical steps. The most satisfying way to gain this confidence is to compare the analytical results with the solutions obtained by direct numerical integration of the coupled differential equations. Also, in view of the fact that the analytical solution (Eq. (3.49)) describing the concentration increase in the chamber headspace over time does not

lend itself to easy visualization, we discuss its asymptotic forms. In the limit of an extended deployment period, the saturating exponential approximation provides a simple relationship between the rise time constant of the headspace concentration and the physical parameters of the problem. This not only provides a simple, first approximation to a process-based fitting function, but also serves the present objective of developing and analyzing the implications of our 2-D model. However, in the final analysis, Eq. (3.49) provides the correct fitting function regardless of the chamber dimensions. In a parallel effort, user-friendly software is under development to fit experimental concentration data to Eq. (3.49) to aid researchers in routine flux measurement applications.

#### **3.4.1 Comparison between analytical and numerical solutions:**

Fig. 3.3 compares the temporal increase of the volumetric mean concentration of  $^{222}\text{Rn}$  in the chamber headspace estimated by (i) the finite difference based numerical solution, (ii) the 2-D analytical model (Eq. (3.49)) and (iii) the numerical inversion of Eq. (3.46) of the 2-D theory. The parameters used were:  $a = 15$  cm,  $H = 30$  cm,  $D_s = 0.02$  cm<sup>2</sup> s<sup>-1</sup>,  $D = 0.1$  cm<sup>2</sup> s<sup>-1</sup>,  $n_e = 0.3$  and  $\lambda = 2.1 \times 10^{-6}$  s<sup>-1</sup> and  $f_0 = 0.14$  Bq m<sup>-2</sup> s<sup>-1</sup>, which correspond to a deep soil gas radon concentration of 220 kBq m<sup>-3</sup>. The data shows excellent agreement between all three solutions across the entire concentration profile, thereby reconfirming the accuracy of the analytical formulae obtained with leading term approximation (zero<sup>th</sup> order). Similar agreement was also seen in comparisons of the chamber-soil interface concentration and flux profiles (Data not shown).

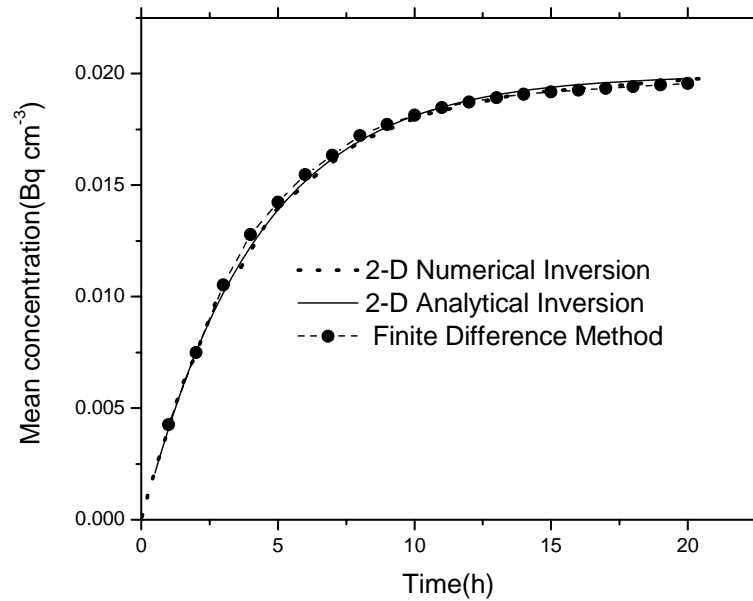


*Fig. 3.3: Temporal variation of mean concentration of radon in the chamber headspace predicted by finite difference method and 2-D analytical and numerical inversion models*

The sharp dip in the concentration profile (predicted by the power-law formula given in Eq. (3.37)) as one approaches the edge of the chamber and the corresponding flux singularity (see section 3.4.5 for more details) were also reproduced by the direct numerical solutions to the differential equations. These agreements place sufficient confidence on the analytical approach so that we may confidently limit our discussions in the succeeding sections to the analytical solutions.

### **3.4.2. Early time behavior: power-law form of the model**

The traditional theory of NSS chambers dwells heavily upon the concentration vs. time response within the chamber headspace immediately following deployment. For example, in their numerical simulations, Hutchinson et al. [68] examined the instantaneous

decrease in the post-deployment flux as a function of the chamber mixing scenarios. Since we have imposed molecular diffusion as the post deployment mechanism of mixing inside the chamber headspace, there is an extreme change in the mixing scenario that should also result in a similar change in flux.

As outlined below, the mean headspace concentration immediately following chamber deployment ( $t=0+$ ) can be easily obtained by examining the large  $p$  behavior of the volumetrically averaged LTC in Eq. (3.46) and then applying Tauberian theorems. As  $p \rightarrow \infty$ , the  $\coth(x)$  function in Eq. (3.46) tends to unity. Further, by detailed asymptotic theory, it can be shown that

$$\chi_\nu(z) \rightarrow z^{1/2} + a_1(\nu)z^{-\nu/2}, \quad (3.51)$$

$$\text{where } a_1(\nu) = \frac{2^{1+\nu} \cos\left(\frac{\nu\pi}{2}\right) \Gamma(2+\nu) \Gamma\left(\frac{3-\nu}{2}\right) \Gamma\left(\frac{\nu}{2}\right)}{\pi^{3/2}(1-\nu^2)}.$$

Upon inserting these, Eq. (3.46) can be expanded in terms of reciprocal powers of  $p$  as  $p \rightarrow \infty$ . The term by term Lapace inversion then yields,

$$\bar{C}_c(t) = \frac{f_0 t}{H(1+\theta)} \left[ 1 - \frac{\theta}{(1+\theta)} \frac{a_1(\nu)}{\Gamma\{(5+\nu)/2\}} \left(\frac{t}{\tau_s}\right)^{\frac{1+\nu}{2}} + \text{higher order} \right]. \quad (3.52)$$

where  $\tau_s (=a^2/D_s)$  is the dimensionless relaxation time in soil space and

$$\theta = n_e \sqrt{\frac{D_s}{D}}. \quad (3.53)$$

This result has the following implications.

1. The first term in Eq. (3.52) is the linear growth law. The effective flux, however, is no longer the pre-deployment flux  $f_0$ , but a modified flux,  $f_0' = f_0/(1+\theta)$ . The drop in flux from a pre-deployment ( $t=0-$ ) value of  $f_0$  to a post deployment ( $t=0+$ ) value of  $f_0'$  occurs

instantaneously. This occurs because, as soon the chamber is deployed, we have assumed that mixing process in the chamber headspace changes from instantaneous to diffusive mixing. As a result, the atoms entering the headspace are not immediately homogenized within the chamber, but instead, they will accumulate at the interface and will be transported only slowly by molecular diffusion. As the accumulation will occur immediately following deployment, it will result in a rapid fall in the concentration gradient across the interface thus manifesting as itself an instantaneous drop in the flux. One can also derive the same formula within a 1-D framework, if only molecular diffusive mixing in the headspace is considered. If we assume a value of  $D_s/D = 0.2$  and  $n_e = 0.3$ , we get  $\theta = 0.134$  and  $f_0' = 0.88 f_0$ , i.e. there is sudden drop of about a 12% in the flux immediately upon chamber deployment for typical soils. Hutchinson et al. (2000) observed a similar flux reduction in their numerical simulation of a 1-D system. It should be noted that the instantaneous reduction in the post-deployment flux resulting from a change in the headspace mixing process differs from the gradient driven change in flux that would occur if the initial headspace concentration were different from the maintained atmospheric concentration outside the chamber. The latter can be readily minimized by equilibrating the air in the chamber headspace with the ambient air prior to deployment.

2. The second term in Eq. (3.52) represents the chamber feedback effect leading to nonlinear growth in the chamber headspace concentration over time. The results suggest a complex dependence of the type  $t^{(3/2+v/2)}$ . It is now interesting to compare the results with the power law form of the 1-D NSS model derived by Livingston et al. [41]. Upon transcribing their formula in currently used notations,

$$\bar{C}(t) = \frac{f_0 t}{H} \left( 1 - \frac{4}{3\sqrt{\pi}} \left( \frac{t}{T_0} \right)^{\frac{1}{2}} + \text{higherorder} \right), \text{ where } T_0 = \frac{H^2}{n_e^2 D_s}. \quad (3.54)$$

The 2<sup>nd</sup> term in Eq. (3.54) (1-D model) yields a  $t^{3/2}$  behavior. However, for the typical case,  $D_s/D = 0.2$ ,  $\varepsilon = 0.3$ , Eq. (3.36) yields  $\nu/2 = 0.05$  i.e. the nonlinear growth exponent in Eq. (3.52) will be about 1.55 instead of 1.5 as projected by the 1-D model. From a practical point of view, the difference is imperceptibly small, and one can take the exponent as almost 1.5. However, there is a vast difference in the pre-factor for the exponent. For example the Livingston et al. [41] formula involves a characteristic time scale that is proportional to the square of the chamber height ( $H=V/A$ ), whereas in this 2-D model it is controlled by the radius ( $a$ ). This difference is primarily due to differences in the respective assumptions regarding the mixing mechanism in the chamber headspace.

At this point, a subtle difference in the non-linear (power-law) terms for the early time behavior in the 1-D model of Livingston et al. [41] and the present 2-D model need to be pointed out. Due to the assumption of an instantaneous mixing process, the power-law term in the 1-D model is relatively robust. In the 2-D model in contrast, this term rapidly crosses over to more complex functional forms due to the assumption of diffusive mixing and it is difficult to estimate the errors in neglecting the cross-over terms. The power-law form is thus less useful as a fitting function in the 2-D theory and is not recommended for use in practical applications for surface deployed chambers.

### 3.4.3. Steady state situation

For radioactive gases such as  $^{222}\text{Rn}$  or  $^{220}\text{Rn}$ , a saturating steady state concentration is expected in the chamber due to the balance between the rate of entry of radon atoms and their decay in the chamber. This may be qualitatively predicted by a fairly simple 1-D treatment [29] of radioactive gases. It is interesting to know whether the concentration inside the chamber would attain a steady state for non-radioactive (stable) gases. For stable gases, the 1-

D model predicts a continuously increasing concentration in the chamber headspace because the system is limited to vertical diffusion and thus the gas produced by the constant source in the soil beneath the chamber must continuously enter the chamber. This is borne out by the solution of Livingston et al. [41] and is precisely why this model is limited to only relatively short duration applications. However, there have been some attempts to predict saturating steady state concentrations within the chamber by implicitly assuming a steady state concentration at the interface [64, 100]. These arguments are basically erroneous since the interface concentrations would also increase as the chamber concentration increased. Saturating steady state for stable gases can only be predicted by a 2-D analysis that allows for radial flow, i.e. a diffusion outflow pathway at the boundary of the chamber-soil interface (see section 4.4.5). As a result, the unperturbed soil flux into the chamber will be exactly counterbalanced by a diffusive outflow at the boundary thereby leading to a steady state concentration. The situation for  $^{222}\text{Rn}$  is very similar to that for a stable trace gas because of its long half life. The resulting steady state value is controlled almost entirely by the outflow rate rather than by radioactive decay. It is only in the case of thoron (half-life = 55.4 s) that radioactive decay would dominate over diffusive outflow in governing the steady state concentration. In fact, a quick calculation shows that for thoron, the chamber feedback effect is negligible in most practical situations, and the steady state value is almost equal to  $f_0 / \lambda H$ , i.e. that obtained by balancing the flux entering the chamber with the radioactive decay. These interpretations may be confirmed simply by setting typical values for the variables in Eq. (3.48).

To the best of our knowledge, there exists no theoretical or experimental information in the literature addressing steady state concentrations in chambers. It is generally believed to be of no practical relevance in view of the large times required to reach steady states in most

chambers and the environmental variations which would take place in that time. However, the situation does not appear overly daunting if smaller chambers are used. In Chapter 4, the occurrence of a steady state has been demonstrated experimentally using a small chamber on a time scale of an hour consistent with the 2-D theory.

For a non-radioactive stable gas, the steady state concentration is obtained in the limit of  $\lambda \rightarrow 0$  in Eq. (3.48):

$$\bar{C}_c(\infty) \approx f_0 \frac{a}{n_e D_s \chi_v(0)} . \quad (3.55)$$

It may be noted from Eq. (3.55) that the steady state concentration of a trace gas inside the chamber headspace is directly proportional to the chamber radius ( $a$ ) and does not depend upon the height of the chamber. For soils with high tortuosity (e.g. say  $\tau \sim <0.4$ ), the formula may be given a simpler form. For example when  $\tau$  is small, the function  $\chi_v(0) \sim (2D/n_e D_s)^{1/2} = (2/n_e \tau)^{1/2}$  and hence

$$\bar{C}_c(\infty) \sim \frac{f_0 a}{D \sqrt{2n_e \tau}} . \quad (3.56)$$

An interesting consequence of Eq. (3.56) pertains to the joint estimation of fluxes of two different stable gases (say  $\text{CO}_2$  and  $\text{CH}_4$ ) in a single experimental setting [100]. Upon denoting the two gases by superscripts (1) and (2), the ratio of their steady state concentrations is

$$\frac{\bar{C}_c^{(1)}(\infty)}{\bar{C}_c^{(2)}(\infty)} = \frac{f_0^{(1)} D^{(2)}}{f_0^{(2)} D^{(1)}} . \quad (3.57)$$

i.e., the ratio is directly proportional to the ratio of their fluxes and inversely proportional to their molecular diffusivities. This result may be useful in testing the model if information on fluxes is available.

Eq. (3.55) is almost valid for radon in view of its long half-life. Upon expressing the flux in terms of the deep soil concentration of radon, it may be recast as

$$\frac{\bar{C}_c(\infty)}{C_\infty} = a \sqrt{\frac{n_e \lambda}{2D}} . \quad (3.58)$$

This suggests that the steady state chamber concentration is independent of the soil diffusion coefficient and has a square root dependence on the air-filled soil porosity. Assuming a typical value for porosity, Eq. (3.58) suggests a non-invasive method of estimating the soil gas concentration from chamber measurements.

**The steady state flux:** The expression for the radial averaged interface LTF (flux) into the chamber is given in Eq. (3.44). After inserting the expression for  $g_0$  and  $\nu$  into Eq. (3.44), we may write

$$\bar{f}_s(p) = \bar{C}_c(p) H(\lambda + p) . \quad (3.59)$$

Upon multiplying by  $p$  on both sides of Eq. (3.58) and applying the final value theorem of Laplace transform, (i.e., taking the limit as  $p \rightarrow 0$ ), the following relationship between the final steady state flux and the concentration inside the chamber is obtained:

$$\bar{f}_s(\infty) = \lambda H \bar{C}_c(\infty) . \quad (3.60)$$

For a stable trace gas, the final steady state flux averaged over the interface is zero, i.e., the upward flux  $f_0$  entering the chamber headspace is exactly balanced by the net diffusive flux out of the chamber headspace. For a radioactive gas, a nonzero steady state flux is sustained by the loss due to radioactive decay in the chamber headspace.

#### 3.4.4. Exponential approximation of the model

A saturating exponential model of concentration increase in the chamber headspace is a practically useful assumption in experiments for extracting the pre-deployment flux from

observed concentration vs. time data [63]. This approach assumes that the concentration increase within the chamber headspace occurs with an effective rate constant ( $\lambda_e$ ). Within the framework of our present theory, this can be obtained by locating the largest pole in the function  $\bar{C}_c(p)$  (Eq. (3.45)), as was demonstrated by Mayya (2004). Alternatively, we may also arrive at a formula for  $\lambda_e$  by forcing an exponential growth over the entire profile. A general expression for exponential growth (assuming an initial concentration of zero) which leads asymptotically to a steady state concentration ( $\bar{C}_c(\infty)$  defined in Eq. (3.48)) as  $t \rightarrow \infty$  can be written as:

$$\bar{C}_c(t) = \bar{C}_c(\infty) [1 - \exp(-\lambda_e t)]. \quad (3.61)$$

When  $t$  is very small, Eq. (3.61) predicts linear growth and upon comparing this with the linear expression for early time concentration, given in Eq. (3.52), one obtains

$$\bar{C}_c(\infty) = \frac{f_0}{(1+\theta)H\lambda_e}, \quad (3.62)$$

where  $\theta$  is defined in Eq. (3.53).

It may be noted that the term  $1/(1+\theta)$  was missed in the earlier formula by Mayya (2004) since the author did not consider the instantaneous drop in flux upon chamber deployment ( $t=0+$ ). Now upon comparing Eq. (3.61) with Eq. (3.48), we get

$$\lambda_e = \frac{1}{1+\theta} \left( \frac{n_e D_s}{aH} \left[ \frac{\lambda H^2}{D} \right]^{1/2} \text{Cot h} \left[ \left\{ \lambda \frac{H^2}{D} \right\}^{1/2} \right] \chi_v \left[ \lambda \frac{a^2}{D_s} + \lambda \right] \right). \quad (3.63)$$

For stable gases ( $\lambda \rightarrow 0$ ), Eq. (3.63) reduces to

$$\lambda_e = \frac{n_e D_s}{aH} \frac{\chi_v(0)}{1+\theta}, \quad (3.64)$$

where  $\lambda_e$  represents the rate constant ( $s^{-1}$ ) for build-up of concentration in the chamber headspace.

Table 3.1: Comparison of radon growth rate constants estimated using Eq. (53) with those obtained by exponential fitting to the headspace concentration predicted by 2-D theory for the chambers. The text in bold represents the best matching of the rise rate constants predicted by the two approaches.

$aH$ (cm <sup>2</sup> )	$a$ (cm)	$H$ (cm)	Growth rate constant, $\lambda_e$ (h <sup>-1</sup> )		$\frac{\lambda_e _1}{\lambda_e _2}$
			$\lambda_e _1$ : Exp. fitting to 2-D model predicted concentration data	$\lambda_e _2$ : Using directly rate constant formula	
50	4.5	11.2	2.00	2.39	0.84
	7.7	7.7	2.23	2.39	0.93
	9.1	5.5	2.26	2.39	0.95
	<b>10.0</b>	<b>5.0</b>	<b>2.26</b>	<b>2.39</b>	<b>0.95</b>
	11.2	4.5	2.25	2.39	0.94
	15.8	3.2	2.15	2.39	0.89
100	4.5	22.4	0.85	1.20	0.71
	7.1	14.2	1.05	1.20	0.87
	<b>14.1</b>	<b>7.1</b>	<b>1.15</b>	<b>1.20</b>	<b>0.96</b>
	31.6	3.2	1.03	1.20	0.86
450	9.5	47.4	0.20	0.27	0.74
	15.0	30.0	0.24	0.27	0.89
	<b>30</b>	<b>15</b>	<b>0.26</b>	<b>0.27</b>	<b>0.96</b>
	45	10	0.22	0.27	0.81

Since the exponential formula (Eq. (3.61)) is essentially an asymptotic expression, it is instructive to compare its performance vis-à-vis the exact results of the 2-D theory (Eq. (3.49)). In fact, it was found that the exponential model overestimates the rate of increase in concentration as compared to the 2-D theory (not presented). However, the difference between the predictions of the exponential model and 2-D theory gradually decreased when the chamber height ( $H$ ) approached half of the radius ( $a$ ). As the chamber height was

decreased further, the deviation between the two again increased. To quantify these differences, exponential fits were forced to the concentration vs. time curves generated using 2-D theory and compared the rate constants with that predicted by the exponential model for different  $a$  and  $H$  (Table 3.1). As may be seen, the rate constants are closest when  $H \sim 0.5 a$ . Thus it may be more appropriate to deploy chambers with  $H \sim 0.5a$  and fit an exponential model to the concentration data to estimate  $f_0$  and  $\lambda_e$ . The estimation of  $\lambda_e$  offers a practically useful non-invasive technique to determine the value of the soil diffusion coefficient ( $D_s$ ) using Eq. (3.63).

#### **3.4.5. Radial profiles of vertical flux and concentration at the interface**

The 2-D analysis of the chamber response predicts a flux discontinuity that occurs at the boundary line at which the chamber is sealed to the surface. A typical radial profile of the post-deployment flux (expressed relative to pre-deployment flux ( $f_0$ )) at the soil-chamber interface is shown in Fig. 3.4 at early and late ( $\sim$ steady state) deployment times. The case of radon is considered. The value of parameters used for computations were:  $a = 15$  cm,  $H = 30$  cm,  $D_s = 0.02$  cm<sup>2</sup> s<sup>-1</sup>,  $D = 0.1$  cm<sup>2</sup> s<sup>-1</sup>,  $n_e = 0.3$  and  $\lambda = 2.1 \times 10^{-6}$  s<sup>-1</sup>. It may be seen from Fig. 3.4 that in the central region of the soil-chamber interface, the flux is marginally lower than the pre-deployment flux value. However, as one approaches the walls of the chamber, the flux reverses direction towards soil and displays a singular behavior at the edge of the chamber walls. A similar singularity, but directed upwards, is seen just outside the chamber walls.

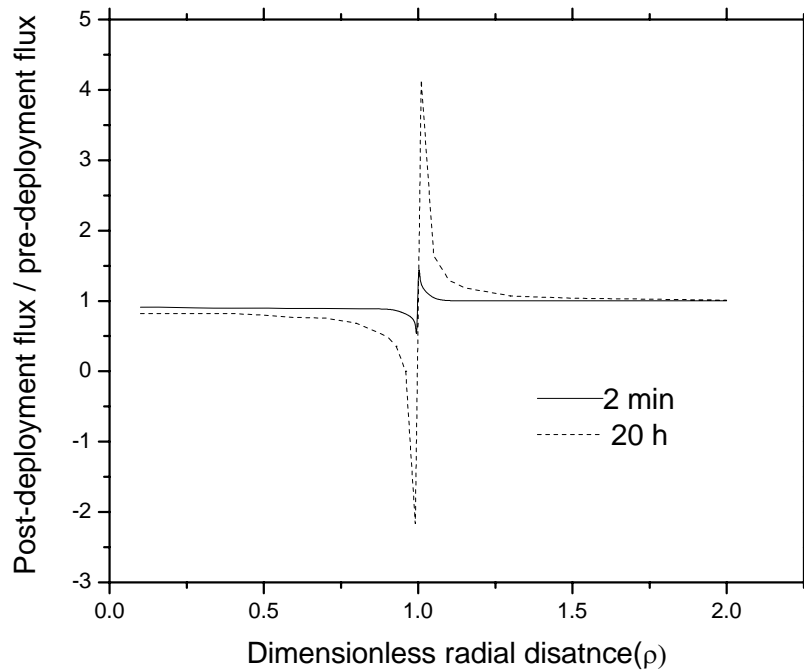


*Fig. 3.4: Variation of radon flux at chamber-soil interface with dimensionless radial distance from the center of the chamber for short and extended deployment times.*

In the region exterior to the chamber, the post-deployment flux rapidly decreases to  $f_0$  within a radial distance of about  $2a$ . The first part, i.e. the decrease in the flux in the central region of the chamber can be easily understood: it is due to the lowering of the vertical gradient as the trace gas entering the chamber headspace accumulates in this region. On the other hand, the explanations for the occurrence of the negative singular vertical flux near the chamber wall and the positive singular flux just outside it are somewhat subtler. The atoms entering the chamber in the central region diffuse only vertically upward at the interface and then diffuse both vertically and radially towards the wall. Since the wall is impermeable, a non-zero concentration will be sustained at the wall. However, the boundary line of the soil-chamber interface acts as a sink since the concentration there is maintained at zero. After

sufficient time, a situation arises at points near the wall and the interface in the headspace, at which the concentration will exceed the interface concentration corresponding to that radial distance. As a result, the flux at this point will be directed vertically downwards with increasing magnitude as one approaches the boundary line both radially and vertically. A similar explanation may be given for the positive singular flux at the soil surface just outside the chamber wall. These changes, along with the instantaneous flux drop discussed in the section 3.4.2., brought about after chamber deployment can be collectively referred to as the “chamber feedback effect”.

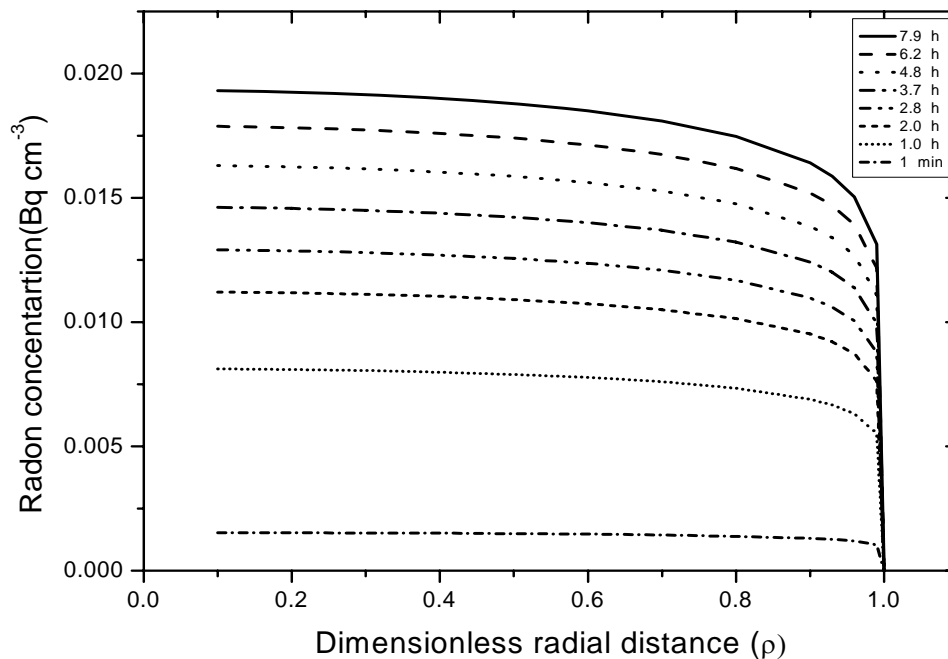


*Fig. 3.5: Spatial variation in radon concentration at the chamber-soil interface as a function of the dimensionless radial distance from the center of the chamber for deployment periods ranging from 1 min to 7.9 h.*

Using the same parameters as used in the flux profile, Fig. 3.5 shows the radial variation in the concentration profile (relative to deep soil concentration) at the soil-chamber interface at different time steps. It may be noted that the concentration decreases gradually with increasing distance from the center of the chamber but decreases sharply upon approaching the boundary. This is a reflection of the power-law nature of the interface concentration profile (Eq. (3.37)) with the index  $\nu$  being quite small ( $\sim 0.1$ ) for the parameters cited above. With increasing deployment time, the concentration increases to its steady state value. The radial profiles at different chamber heights and soil depths were discussed by Mayya [82] for the steady state situation. The radial profile for any other stable trace gas will be similar to that demonstrated here for radon.

#### **3.4.6. Effect of chamber dimension on headspace concentration**

Figs. 3.6 and 3.7 show the effects of chamber radius ( $a$ ) and height ( $H$ ) respectively on the temporal evolution of the headspace concentration. Consider the case for  $\text{CO}_2$  (stable trace gas) and that for radon (long half life radioactive) to be similar. From Hutchinson et al. [68], the parameters used for the calculation were:  $D=0.18 \text{ cm}^2 \text{ s}^{-1}$ ,  $D_s=0.056 \text{ cm}^2 \text{ s}^{-1}$ ,  $n_e=0.3$  and  $f_0=0.5 \text{ g m}^{-2} \text{ h}^{-1}$ . The effective time constant ( $T_c$ ), defined as the reciprocal of effective rate constant ( $\lambda_e$ ), was determined directly by fitting the exponential form of the 2-D model to the respective concentration vs. time curves generated using the exact 2-D theory (Fig. 3.6 and Fig. 3.7).

Fig. 3.6 indicates that the steady state concentration of  $\text{CO}_2$  is independent of chamber height as was predicted from Eq. (3.55), whereas Fig. 3.7 indicates that the steady state concentration and the time ( $T_c$ ) to reach steady state increased in direct proportion to chamber radius ( $a$ ). The smaller the radius ( $a$ ) or height ( $H$ ) of the chamber, the faster will be the rise

and correspondingly smaller will be the time constant for saturation. The ability of the theory to relate the chamber dimensions to its response characteristics has a significant potential in aiding the design of chambers for special applications. For example, one can design a chamber with sufficiently fast response characteristics (for typical soil properties) to attain quick saturation so that one can work near the saturation region of the headspace concentration (steady state). In this mode, it may be possible to track environmentally induced temporal changes in the flux more faithfully.

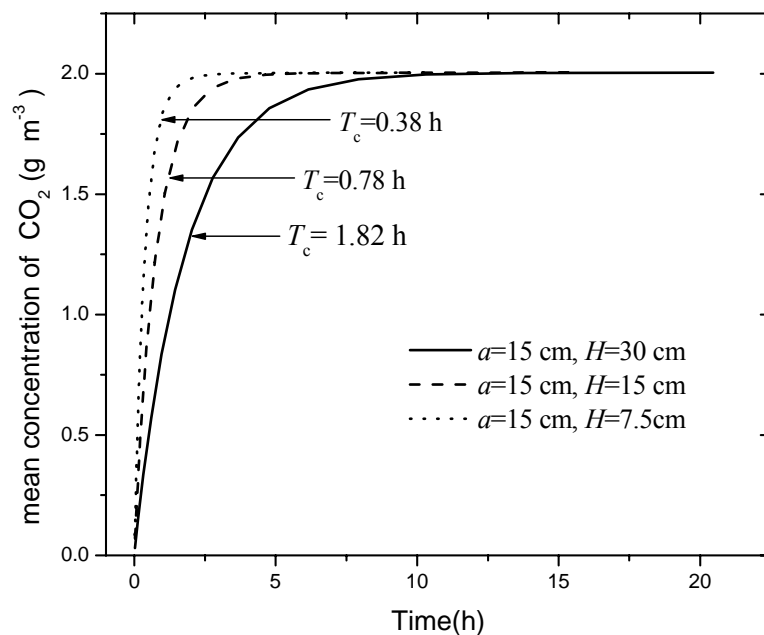


Fig. 3.6: Temporal variation in the mean concentration of  $CO_2$  in the chamber headspace for chambers of different height ( $H$ ) and fixed radius ( $a$ ).

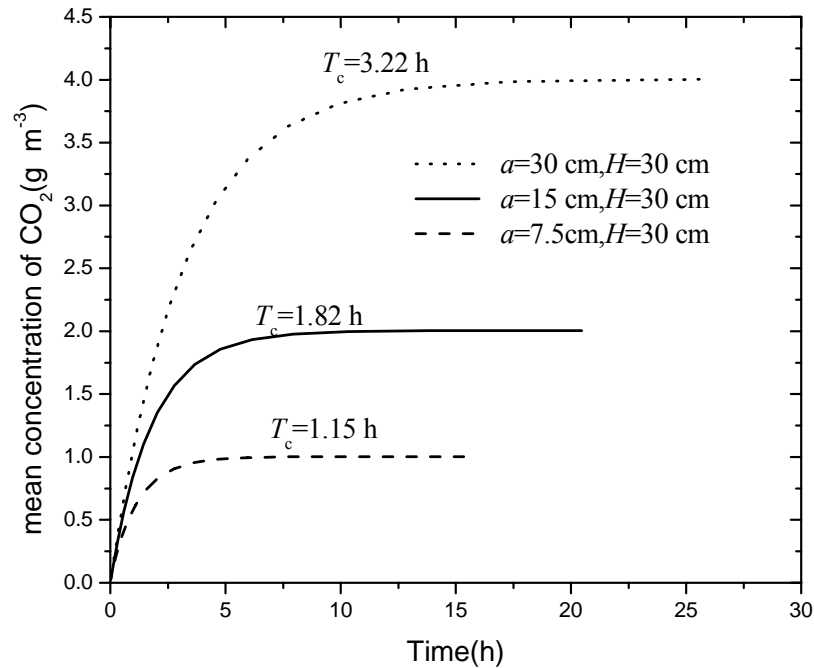
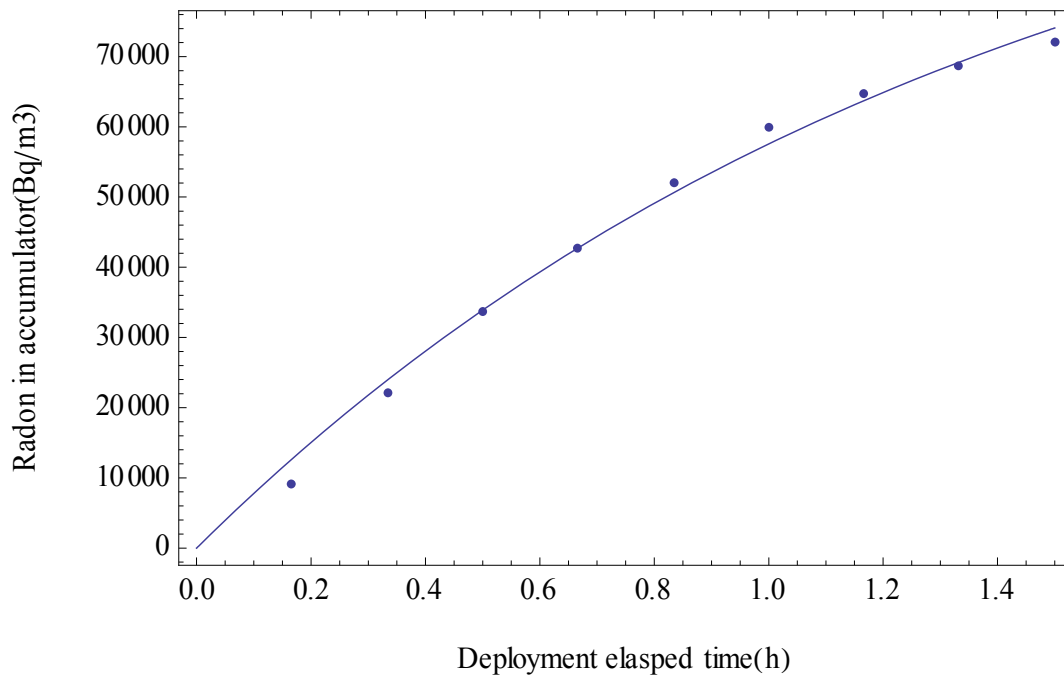


Fig. 3.7: Temporal variation in the mean concentration of CO<sub>2</sub> in the headspace of chambers with different radii ( $a$ ) and fixed height ( $H$ ).

### 3.5. Development of a Least-Square Fitting Algorithm in Wolfram Mathematica

A numerical program is written in Wolfram Mathematica [98] for carrying out least square fitting of exponential approximation version of 2-D model (Eq.3.64) for practical application in experiments. The numerical program of the fitting algorithm is given in Appendix C. The least square fitting in the program to a set of input concentration data is executed by the built-in algorithm of 'Wolfram Mathematica' and the output of the program provides the values of radon flux ( $\text{Bq m}^{-2} \text{h}^{-1}$ ) and effective diffusion coefficient ( $\text{m}^2 \text{h}^{-1}$ ) of trace gas in soil. To carry out the fitting, the program require initial guess of parameters such as radon flux ( $f_0$ ), effective diffusion coefficient ( $D_e$ ), saturating radon concentration in

accumulator ( $C_c$ ) and the time constant of accumulator ( $t_c$ ). If the typical values of these parameters cannot be guessed, then the default parameters given in the program may be used. Besides this, the program also requires minor input parameters such as chamber radius and height and diffusion coefficient of radon in air ( $0.1 \text{ cm}^2 \text{ s}^{-1}$ ). By successive iterations, the actual converged values of parameters will be displayed along with other statistical parameters at the end of the fitting. A sample output of least square fitting of the 2-D model and the derived parameters of interest are shown in Fig 3.8 and Table 3.2 respectively.



*Fig. 3.8: Graph showing least square fitting of 2-D model to the radon build up data in chamber headspace*

Table 3.2: Estimated radon emission parameters after least square fitting of 2-D model to the radon build up data in the chamber parameters

Parameters	Estimated value	<i>t</i> Statistic	P-Value	R <sup>2</sup>
$f_0$ (Bq m <sup>-2</sup> h <sup>-1</sup> )	19215±1031	18.63	3.19 x10 <sup>-7</sup>	
$D_e$ (m <sup>2</sup> h <sup>-1</sup> )	(2.3±0.6) x10 <sup>-4</sup>	3.42	0.011	0.99
$C_c$ (Bq m <sup>-3</sup> )	112275±10809	10.38	1.7 x10 <sup>-5</sup>	
$t_c$ (h)	1.39±0.2	6.86	2.4 x10 <sup>-4</sup>	

### 3.6. Summary

Given the importance of non-steady state chamber methods for gas flux measurements over regional and global scales, it is vital to develop uniform chamber deployment protocols with minimum and unambiguous assumptions. To achieve this, it is important to make use of process-based models derived from basic soil gas transport theory. In this chapter, such a model is developed for the case of surface deployed chambers. Both lateral and vertical diffusion are treated simultaneously in the soil and chamber headspace in post-deployment situation. The theory predicted that there is an instantaneous drop (~ 12 %) of pre-deployment flux density due to change in the mixing phenomena in the headspace at time of deployment of the chamber; subsequently the flux density decreases gradually due to back-diffusion at edge of the chamber-soil interface. To retrieve the pre-deployment flux density from the headspace concentration data, an analytical expression for temporal build up of trace gas concentration in the headspace is developed. Since the analytical expression is in integral form involving higher mathematical functions, an exponential approximation of the model is developed for practical application. Using this exponential version of the 2-D

model, a user-friendly fitting algorithm is written in Wolfram Mathematica to obtain the pre-deployment soil flux and the soil diffusion coefficient, from the experimentally measured concentration data. This development now offers several advantages for trace gas emission studies, such as deployment on untested or hard soils, extended deployment periods for simultaneous estimation of pre-deployment flux and soil diffusion coefficient, steady state operation of the chamber for obtaining time resolved flux data (diurnal variation) and use of smaller radii chamber for obtaining space resolved flux data at smaller length scales. In order to carry out these applications, it is first and foremost required to validate the 2-D model predictions against experimental data obtained under well defined conditions and also from field studies. The next chapter discusses radon emission experiments carried out in three different sites to test the validity of the 2-D model. Two field studies carried out in (i) Uranium tailings pond at Jaduguda and (ii) on the beach sands in coastal region of Kerala, to demonstrate the applicability of the model in real field situations are also presented.

## **4. Experimental Validation and Field Applications of the Chamber Response Model**

---

### **4.1. Introduction**

The use of empirical models (linear, linear quadratic and exponential) coupled with sub-optimal number of observations and use of arbitrary protocols have been the significant sources of uncertainty in chamber-based flux estimates. These models are neither capable of accounting for the possibility of the instantaneous drop in flux that occurs upon chamber deployment, nor capable of assigning physical meaning to the coefficient of non-linear concentration build-up in the chamber headspace and its saturation value. As a result, they are of little value in fitting time-dependent chamber headspace concentration data.

The development of 2-D chamber response model (Chapter 3) which considers both lateral and vertical diffusion as the post deployment mechanism of gas emission into the chamber headspace has overcome the above mentioned inherent limitations of the empirical models. In addition, this development simplifies the deployment strategy of soil chamber by addressing the surface deployment rigorously thereby doing away with the need to insert the chamber walls to greater depths into hard soils. The 2-D chamber response model is applicable over both short and extended deployment periods so that it can be used effectively by following surface deployment chamber protocols. This development opens up new measurement opportunities for soil gas emission studies, such as the simultaneous estimation of pre-deployment flux and soil diffusion coefficient, measurements on untested or hard soils

without any time restriction, steady state operation of the chamber for obtaining time-resolved flux data (diurnal variation) and use of smaller radii chamber for obtaining space resolved flux data at smaller length scales.

However, prior to the practical application of the 2-D chamber response model, it is required to validate its predictions. In chapter 3, the analytical results were compared with numerical solutions with satisfactory agreement between the two. However, it is also required to compare the model prediction directly with experimental results to gain confidence for the practical applicability of the model in real field situations. In this chapter, three different set of experiments conducted at a Uranium mineralized zone at Jaduguda in Jharkhand state of India using chambers of different dimensions are discussed. Subsequently two field campaigns were conducted at Uranium tailing pond, Jaduguda and coastal beaches, Kerala to map radon ( $^{222}\text{Rn}$ ), thoron ( $^{220}\text{Rn}$ ) fluxes from soils respectively. The experimental methods and results of studies are given below.

## **4.2. Experimental Validation**

### **4.2.1. Materials and Methods**

The first set of experiments was aimed at comparing the transient build-up of headspace concentration to its saturation value during an extended deployment period, with that predicted by theory based on measured soil parameters such as  $^{226}\text{Ra}$  content, radon emanation factor, diffusion coefficient, bulk density and moisture content. Observations were made using a cylindrical chamber of radius 7.5 cm and height 15 cm deployed at the soil surface. To prevent superficial leakage, the chamber was inserted into the soil a minimal depth of 1cm. The radon concentration within the chamber headspace was monitored at regular 10 min time intervals by a continuous radon monitor (Alpha GUARD) connected to the chamber. The observations were continued for nearly 12 hours to generate an extended

profile of radon concentration with time. Upon completion of the radon measurement, soil samples were collected by hammering a stainless steel cylinder (with both ends open) into the soil to a depth of 20 cm. The cylinder was removed along with the 20 cm block of soil upon which various soil parameters required for the theoretical computation were measured.

The pre-deployment flux ( $f_0$ ) was estimated using the modified version of the UNSCEAR flux formula [14] developed by Zhuo et al. [101] as given below:

$$f_0 = R\rho_b E \left( \frac{T}{273} \right)^{0.75} \sqrt{\lambda D_{MA} n_T \exp(-6mn_T - 6m^{14n_T})}, \quad (4.1)$$

where

$R$  is the  $^{226}\text{Ra}$  content in soil ( $\text{Bq kg}^{-1}$ ),  $D_{MA}$  is the binary molecular diffusion coefficient of radon in air at ambient temperature and pressure, which has a value of  $0.1 \text{ cm}^2 \text{ s}^{-1}$  [30],  $E$  is the radon emanation factor (grain to pore air space),  $n_T$  the porosity of the soil matrix,  $T$  is temperature ( $^{\circ}\text{K}$ ) and  $m$  is the moisture saturation in the soil. The standard gamma spectrometric technique [102] was used to measure  $^{226}\text{Ra}$  in soil ( $R$ ). The mass exhalation rate estimation procedure of Sahoo et al. [89] was followed using the soil sample (immediate after collecting the sample, i.e. without drying) to obtain the radon emanation factor ( $E$ ). Soil porosity ( $n_T$ ) and moisture saturation ( $m$ ) were estimated from dry and wet bulk densities, and using these, the radon diffusion coefficient in soil ( $D_s$ ) was estimated from the relations given by Rogers and Nielson [30]. Soil temperature ( $T$ ) was measured at a depth of 10 cm.

The measured soil parameters  $n_T = 0.3$ ,  $D_s = 2.0 \times 10^{-6} \text{ m}^2 \text{ s}^{-1}$  and  $f_0 = 504 \text{ Bqm}^{-2} \text{ h}^{-1}$  (which corresponds to a deep soil radon concentration of  $220 \text{ kBq m}^{-3}$ ) were used as inputs to

simulate the headspace concentration data at different time steps by implementing the proposed 2-D model (Eq. 3.49) using the software “Mathematica” [98]

The second set of experiments was aimed at examining, how well the observed concentration data, fitted to the 2-D model, returned the values of the flux and the soil diffusion coefficient (as estimated in the first experiment). This experiment was conducted using a chamber of radius 15 cm and height 30 cm at two neighbouring locations within 2 m radius of the first experiment. It is thus reasonable to assume that the soil parameters and the radioactivity content of these locations were similar to that measured in the first experiment. The radon concentration data observed after 50 minutes and extending up to 10 hours were used for fitting. The early time data were ignored since it is expected to take a few tens of minutes for radon to diffuse vertically throughout the chamber. The resultant concentration versus time data were then fitted to Eq. (3.61) (exponential form of the 2-D model) independently to estimate the pre-deployment fluxes and soil diffusion coefficients. (Since a fitting algorithm for the exact solution is not yet developed, Eq. (3.61) was used as it represents a close approximation to the exact solution Eq. (3.49)).

The third validation experiment was aimed at comparing the radon fluxes and soil diffusion coefficients obtained by using different chambers having different chamber feedback relaxation times. For this case, experiments were conducted in same location using three chambers of different dimensions in same experimental environment. The chambers are deployed and radon concentration build up data collected and the following parameters are calculated for each accumulator, pre-deployment radon flux from soil surface ( $f_0$ ), effective diffusion coefficient ( $D_e$ ), saturation concentration of the radon ( $C_e$ ) and effective time constant ( $t_c$ ) for radon growth which are then analyzed.

#### 4.2.2. Results and discussion

Fig. 4.1 shows the temporal variation of the radon concentration in the chamber headspace (i) observed experimentally, and (ii) predicted by the 2-D model (Eq. (3.49)). The results indicate reasonably good agreement between the experimental observations and the headspace concentration predicted by the 2-D model throughout the deployment period. A noteworthy feature is the fact that the 2-D model is able to correctly predict the observed saturation concentration. The model predictions deviated from the reference data by only about  $\pm 20\%$  throughout the deployment period. These results demonstrate the unique capabilities of the 2-D theory and reinforce confidence in the analytical results. It may now be possible to evolve measurement protocols using chambers deployed in diffusion controlled steady state mode (i.e. unventilated chamber) to monitor real time flux variations and transients due to possible changes in the environmental and source parameters.

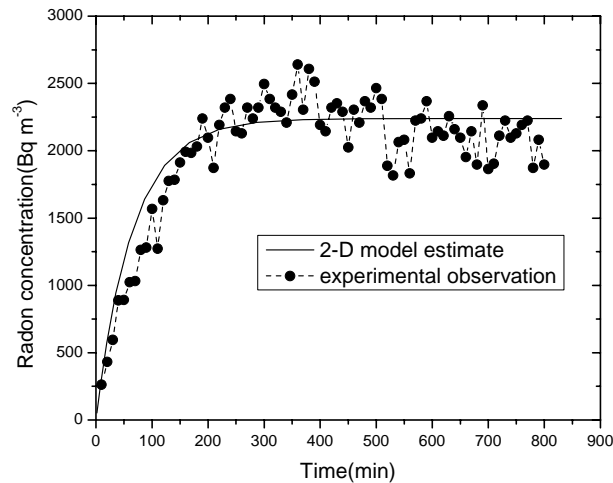


Fig. 4.1: Comparison of experimental data on the temporal increase of radon concentration in the headspace with that predicted by 2-D theory based on measured soil parameters. Chamber dimensions are: radius 7.5 cm and height 15 cm. Observed data points are connected with lines for guiding the eye.

The observed and fitted data are shown in Fig. 4.2, the resultant estimated parameters are shown in Table 2. The soil diffusion coefficient ( $D_s$ ) and pre-deployment flux ( $f_0$ ) were estimated from the fitting parameters ( $\bar{C}_c(\infty), \lambda_e$ ) using Eq. (53) and Eq. (52) respectively, assuming  $D = 0.1 \text{ cm}^2\text{s}^{-1}$  and  $n_T = 0.3$  (measured in experiment no.1). The data in Table 4.1 indicates that both the derived pre-deployment flux and soil diffusion coefficient are in close agreement with their respective estimates from experiment no.1. These results demonstrate the mathematical validity of the proposed 2-D model to describe trace gas emission into chambers deployed at the soil surface under both non-steady state and steady state conditions driven by diffusive transport.

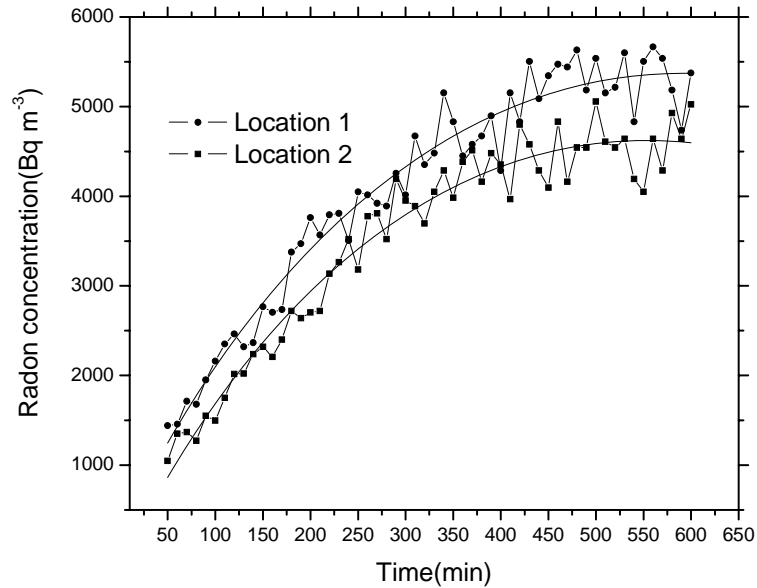


Fig. 4.2: Least square fit of the exponential form of the 2-D model (Eq. (3.61)) to the experimental observations data for radon concentration in the chamber headspace as outlined in experiment no. 2. Observed data points are connected with lines for guiding the eye.

Table 4.1: Parameters ( $\bar{C}_c(\infty)$  and  $\lambda_e$ ) obtained by fitting the exponential form of the 2-D model (Eq.(51)) to the data points shown in the Fig. 9 and the derived pre-deployment flux ( $f_0$ ) and soil diffusion coefficient ( $D_s$ ) from these parameters.

Location No	$\bar{C}_c(\infty)$ (Bq m <sup>-3</sup> )	$\lambda_e$ (h <sup>-1</sup> )	$f_0$ (Bq m <sup>-2</sup> h <sup>-1</sup> )	$D_s$ (m <sup>2</sup> s <sup>-1</sup> )
Location 1	5610	0.26	508	$2.4 \times 10^{-6}$
Location 2	4920	0.28	480	$2.7 \times 10^{-6}$
Average	$5265 \pm 488$	$0.27 \pm 0.02$	$494 \pm 20$	$(2.5 \pm 0.2) \times 10^{-6}$

The results for third set of experiment are shown in Table 4.2. As expected, it can be inferred from the above table that radon flux from the surface of the soil ( $f_0$ ) and inferred radon diffusion coefficient remains almost same even though chamber dimensions are varying significantly. Thus, it can be concluded that both parameters are independent of chamber dimensions which is in complete accordance with 2-D model.

Table 4.2: Comparison of estimated pre-deployment flux density and time constant for different chambers used in the third set of experiments

Parameters	Chamber 1	Chamber 2	Chamber 3
$a$ (cm)	3.65	17	7.75
$H$ (cm)	39.9	9.68	23.51
$f_0$ (Bq/m <sup>2</sup> /h)	21.45	23.16	22.32
$t_c$ (h)	15.18	12.23	20.39

Table 4.3 presents the percentage change of effective time constant ( $t_c$ ) as multiplicative term ( $a.H$ ) varies while, Table 4.4 presents the radon saturation concentration observed in the chamber headspace of different radii. As may be seen from these tables, the observed change in the time constant (response) and saturating radon concentration in the chamber is following the prediction by 2-D diffusion theory indicating an internal consistency between observations made by three different chambers. This demonstrates the validity of the model over different sizes of the chamber.

*Table 4.3: Relative variations in time constant with respect to change in multiplicative term  $a.H$  (Product of chamber radius and height)*

<b>Observation between</b>	<b>% Change in (<math>a.H</math>)</b>	<b>% Change in (<math>t_c</math>)</b>
Chamber 1 and Chamber 2	10%	50%
Chamber 1 and Chamber 3	12%	21%
Chamber 2 and Chamber 3	21%	29%

*Table 4.4: Variations in radon saturation concentration with respect to radius of chamber*

<b>Radius of Chamber (cm)</b>	<b>Saturating radon concentration (<math>Bq/m^3</math>)</b>
3.65	1195
7.75	1934
17	2921

### 4.3. Field study at Uranium Tailing Ponds, Jaduguda

A field study involving multi-parametric measurements was carried out on a uranium waste repository at Jaduguda, India to evaluate the performance of 2-D model in a radon rich environment. The tailings produced from the uranium mill at Jaduguda are segregated into coarse and fine fractions at the ore-processing facility before disposal. The coarse fraction is used for backfilling the mine, while the fine fraction (slurry form) is placed into a repository known as a *tailings pond*. The tailings accumulate to form a compact mass minimum cracks or cavities likely to develop over time. This condition favored the use of a diffusion based model for predicting the radon releases.

This study illuminates some of the results presented in the previous sections, by comparing predicted flux by means of empirical equations, and also directly measured using a chamber.

The radon flux densities were predicted using two approaches, namely:

- (1) using in-situ measured values for radon emanation coefficient ( $E$ ) and radon diffusion length in the tailings ( $L(m) = \sqrt{\frac{D}{\lambda}}$ ), and
- (2) using the empirical correlations given for the radon diffusion coefficient ( $D(\text{m}^2\text{s}^{-1})$ ) by Rogers and Nielson [30] and radon emanation coefficient ( $E$ ) by Zhuo et al. [101].

#### 4.3.1. Materials and Methods

##### 4.3.1.1 Measuring radon flux directly at the tailings surface

In-situ radon fluxes from the residue surface were measured using the chamber technique.

The set up (Fig. 4.3) consisted of a cylindrical accumulator (15 cm diameter and 15 cm

height) attached to a continuous radon monitor. The accumulator was inserted into the residue surface to a depth of approximately 1 cm to prevent superficial leakage. Radon concentrations inside the accumulator were monitored at 10 minute time intervals for about 3 hours at each location. The concentration data were fitted to an exponential approximation of the 2-D model (Eq. 3. 61) to simultaneously obtain the in-situ radon flux and diffusion coefficient. Typical data on the build-up of radon concentration in the accumulator deployed at one location at the site is shown in Fig. 4.4.

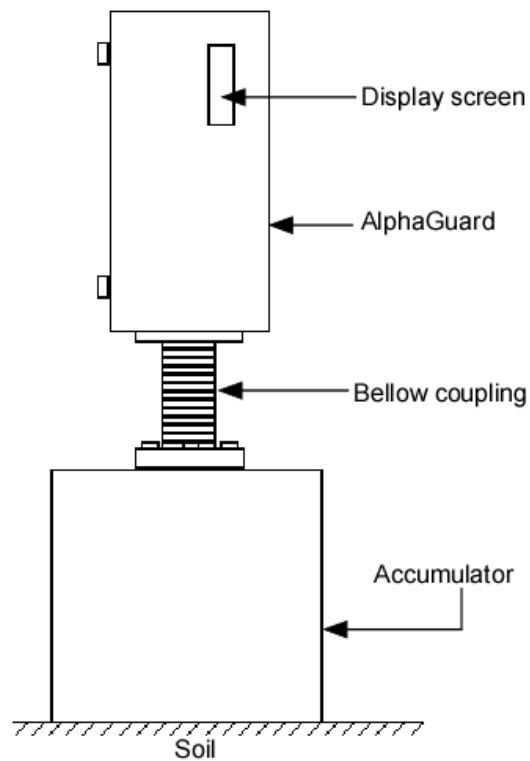


*Fig. 4.3: Soil chamber attached with AlphaGUARD continuous radon monitor set up for radon flux measurement.*

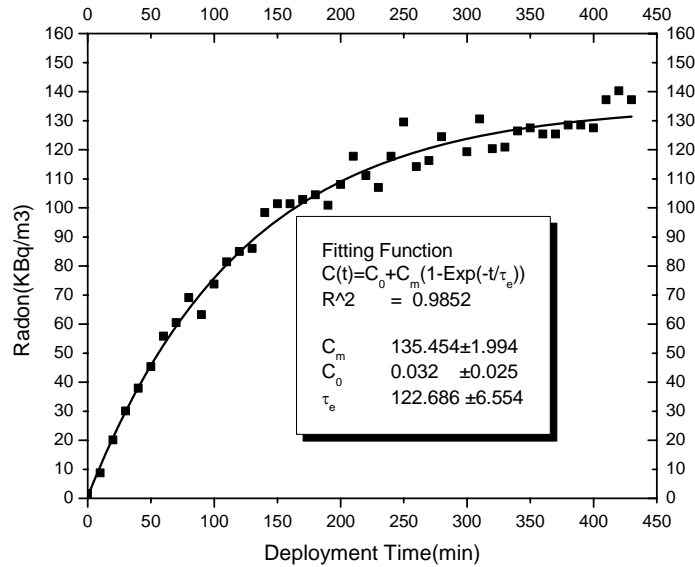


Fig.. 4.4. Typical build up data of radon concentration in the chamber along with least square fitting of Equation (3.61) for an accumulator of radius,  $a=7.5$  cm and  $V=3.4$  L deployed on the Uranium Tailings Pond.

#### 4.3.1.2 Measurement of radon diffusion length ( $L$ )

The in-situ radon diffusion lengths were determined by analyzing the depth profile of radon concentration in the tailings matrix [103]. The schematic diagram of the measurement set up is shown in Fig. 4.5. Radon concentrations were measured at different depths from 20 to 150 cm, using a soil probe with a flow rate of about  $0.5 \text{ l min}^{-1}$ . According to diffusion theory, the radon concentration  $C(z)$  at depth  $z$ , follows the equation [15]:

$$C(z) = C_{\infty} (1 - \exp(-z/L)) \quad (4.2)$$

where

$C_{\infty}$  is the radon concentration at large depth ( $\text{Bq m}^{-3}$ );

$z$  is the thickness of the material (m);

$L$  is the radon diffusion length (m).

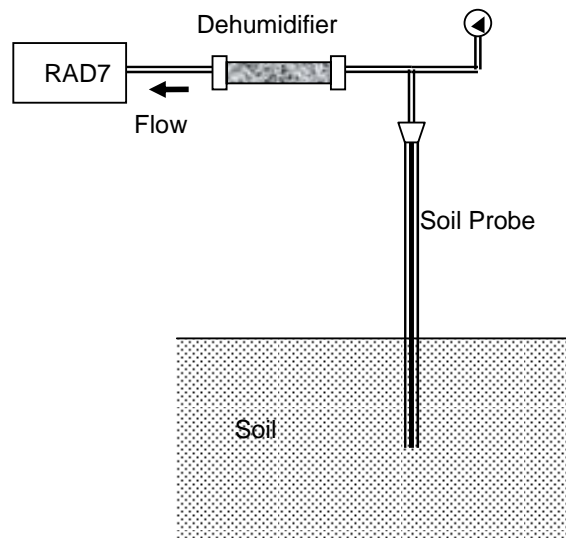


*Fig. 4.5: Schematic diagram of soil probe method for the measurement of radon concentration in tailings using a continuous radon monitor.*

At end of the experiment, the radon concentration data at different depths were fitted to Equation 4.2 by the method of least squares and the in-situ radon diffusion length was obtained from the fitting coefficients. Typical fit to the data is shown in Fig. 4.6. The in-situ diffusion lengths were also estimated by the technique based on the radon build-up in the accumulator deployed for flux measurements using the 2-D model developed in Chapter 3.

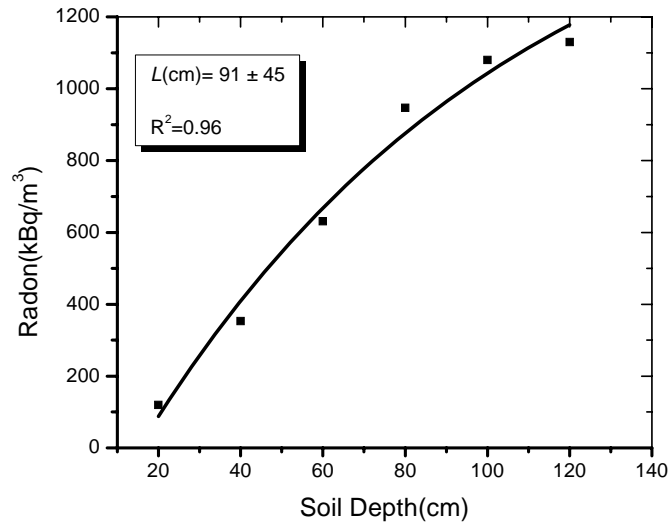


Fig 4.6: Least square fitting of radon depth profile equation to the radon concentration data in soil gas at various depths.

#### 4.3.1.3 Measurement of radium content ( $R$ ) and radon emanation coefficient ( $E$ )

Tailings samples were collected from 40 locations of the tailings pile by inserting a 1000 cm<sup>3</sup> stainless steel cylindrical tube into the residue matrix. The samples were processed and dried in an oven at 110°C to attain constant weight. Then the samples were packed in a 300 cm<sup>3</sup> leak-proof plastic container and stored for about 30 days to ensure secular equilibrium between <sup>226</sup>Ra and its decay products. A gamma spectrometry technique [102, 104] was used to measure the dry weight specific <sup>226</sup>Ra content in the samples. The samples were subjected to radon mass exhalation rate measurement [89]. The radon emanation coefficient ( $E$ ) was then determined by the equation:

$$E = J_m / \lambda R \quad (4.3)$$

Where

$J_m$  is the mass exhalation rate ( $\text{Bq kg}^{-1} \text{ s}^{-1}$ );

$R$  is the dry weight radium activity concentration ( $\text{Bq kg}^{-1}$ ); and

$\lambda$  is the decay constant of  $^{222}\text{Rn}$  ( $\text{s}^{-1}$ ).

The tailings porosity ( $n_T$ ) was estimated using the equation:

$$n_T = 1 - \rho_b / \rho_g \quad (4.4)$$

where

$\rho_g$  is the grain density of the tailings material ( $2700 \text{ kg m}^{-3}$ ) [14]; and

$\rho_b$  is the measured dry bulk density of the tailings ( $\text{kg m}^{-3}$ ).

Moisture content ( $m$ ) was estimated from the measured soil water content,  $M_w$  (dry weight percent) as  $m = \rho_b M_w / 100 \rho_w n_T$  where  $\rho_w$  is density of water ( $\text{kg m}^{-3}$ ). The in-situ temperature ( $T$ ) at a depth of 10 cm from tailings surface was measured by a sensor.

The radon emanation coefficient ( $E$ ) in the tailings was determined by measuring the mass exhalation rates using fresh samples without subjecting them to drying. These experiments were performed at the site itself immediately after collecting the samples and hence the results are expected to be close to the values corresponding to in-situ moisture conditions.

#### 4.3.1.4. Estimating flux by measurement of $L$ and $E$

The radon flux density,  $f$ , ( $\text{Bq m}^{-2} \text{ s}^{-1}$ ) at the tailings surface was estimated using the following formula [14]

$$f = \lambda LR\rho_b E \quad (4.5)$$

where

$R$  is the radium content in tailings ( $\text{Bq kg}^{-1}$ );

$\lambda$  is the decay constant of  $^{222}\text{Rn}$  ( $\text{s}^{-1}$ );

$\rho_b$  is the bulk density of tailings ( $\text{kg m}^{-3}$ );

$L$  is the measured radon diffusion length (m);

$E$  is the measured radon emanation factor for freshly collected tailings samples

#### 4.3.1.5. Estimating flux by calculating $L$ and $E$ via empirical formulae

The third, and least exact, approach to estimating the radon flux at the surface used Equation 4.5 again, but instead of experimentally measured values of  $L$  (and thus  $D$ ) and  $E$ , empirical relations were used for  $D$  and  $E$ . The diffusion coefficient was estimated using Equation 4.6 [30], including a temperature correction:

$$D = D_{MA} n_T \exp(-6mn_T - 6m^{14n_T}) \left(\frac{T}{273}\right)^{0.75} \quad (4.6)$$

The following empirical equation [101] was employed to estimate  $E$ :

$$E = E_0 [1 + 1.85(1 - \exp(-18.8m))] \quad (4.7)$$

The variables in the above equations are defined as:

$D_{MA}$  is the diffusion coefficient of radon in air at ambient temperature and pressure ( $1.1 \times 10^{-5} \text{ m}^2 \text{ s}^{-1}$ );

$n_T$  is the soil porosity;

$m$  is the fraction of pore space filled with water (moisture saturation);

$T$  is the absolute temperature (K); and

$E_0$  is the radon emanation coefficient of tailings in dry conditions.

Once these equations were computed, they were substituted into equation 4.5 to generate the flux estimate.

### **4.3.2. Results and Discussion**

#### **4.3.2.1. Determination of exhalation flux**

Table 4.5 presents a summary of various parameters measured for the repository. Fig. 4.7 shows the measured and predicted (by the two approaches mentioned in section 4.3) radon fluxes over 10 locations of the tailings pond. There is an overall agreement within deviations of about 20 %, between the measured and the predicted radon fluxes. A closer statistical analysis (not shown) indicates that the radon fluxes predicted using the in-situ diffusion lengths and emanation coefficients are closer to the measured values than the fluxes predicted from the moisture corrected empirical functions given in Equation 4.6 and 4.7. This could be due to the fact that the moisture content estimated from the top layer of the repository may not represent values down to a depth of about one metre [35] thereby affecting the parameter values based on empirical correlations.

Table 4.5: The mean of measured tailings parameters along with standard deviation in winter, summer and rainy seasons for 40 locations of the tailings pile.

Parameters	Winter	Summer	Rainy	Average
Radium content, $R$ ( $\text{Bq kg}^{-1}$ )	5124±2348	5144±2256	5081±2244	5166±2282
In-situ $^{222}\text{Rn}$ diffusion length, $L$ (m)	0.81±0.15	0.90±0.14	0.72±0.14	0.81±0.14
In-situ $^{222}\text{Rn}$ emanation coefficient, $E$	0.24±0.05	0.20±0.02	0.28±0.07	0.24±0.05
Dry $^{222}\text{Rn}$ emanation coefficient, $E_0$	0.09±0.04	0.10±0.03	0.09±0.03	0.09±0.03
Dry bulk density, $\rho_b$ ( $\text{kg m}^{-3}$ )	1790±66	1786±52	1801±37	1792±52
Total porosity, $n_T$	0.34±0.02	0.34±0.03	0.33±0.04	0.34±0.03
Moisture fraction, $m$	0.54±0.05	0.35±0.04	0.74±0.06	0.54±0.05

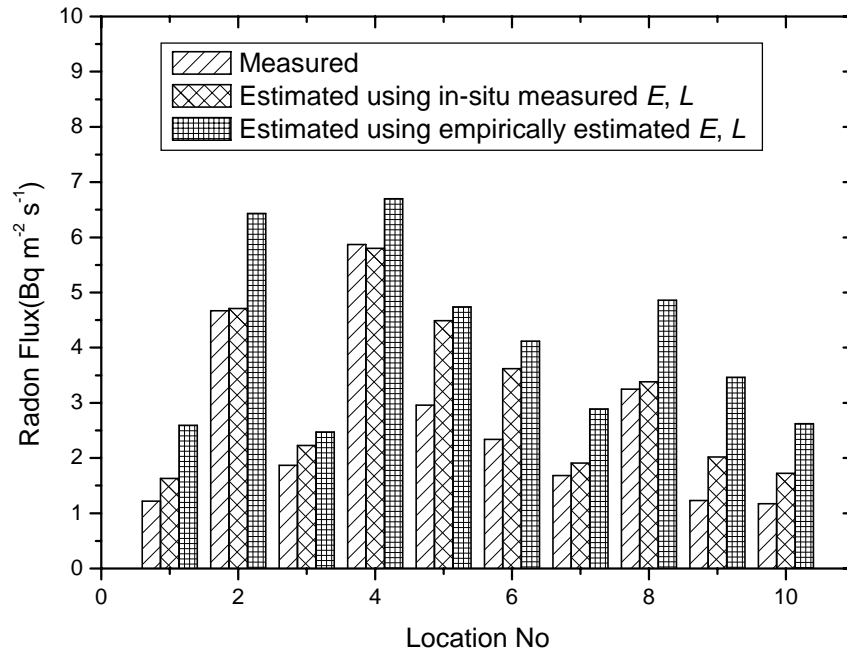
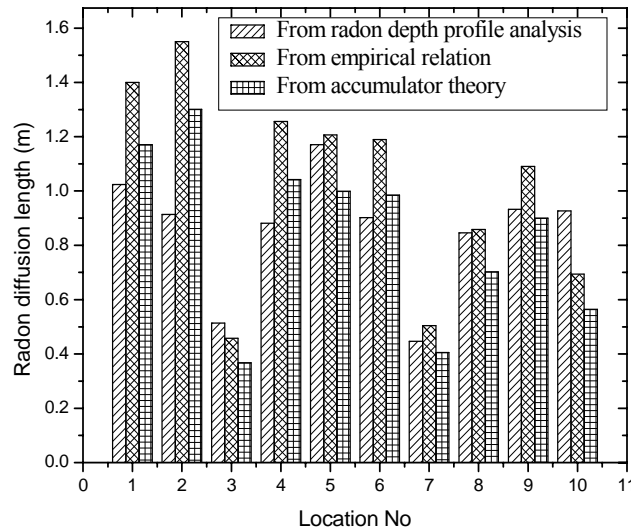


Fig. 4.7: Comparison between measured and predicted radon flux densities at 10 locations of the Uranium Tailings Pond

#### 4.3.2.2. Determinations of radon diffusion length

At times, it is required to estimate the diffusion length, given a known exhalation flux. For this purpose, the results can be obtained by comparing measurement-estimated and empirical-formula-estimated values of  $L$  with its measured value. Figure 4.8 shows the comparison of radon diffusion lengths obtained from the three methods, the accumulator method, the depth profile analysis of soil-gas radon and the empirical relation given in Equation 4.6. Overall agreement between the three methods was within 20%. The diffusion lengths estimated from the empirical correlation method were generally higher than the other two, thereby supporting the moisture content effect mentioned above. The study also demonstrates that the accumulator method is a useful tool not only for deriving flux but also for estimating in-situ diffusion coefficient in soil.



*Fig. 4.8: Comparison of radon diffusion length in uranium tailings obtained by three different methods at 10 locations of the Uranium tailing pond.*

### 4.3.2.3. Relating radium content to radon flux

Apart from the above analysis, Fig. 4.9 shows the relation between radium content and the season averaged radon fluxes at over 40 locations on the repository. The linear fit shows a strong correlation between radium content and radon flux in the repository. The slope yields a ratio of  $(8.3 \pm 0.4) \times 10^{-4} \text{ kg m}^{-2} \text{ s}^{-1}$ . This ratio also represents the product of radon decay constant,  $\lambda$ , ( $2.1 \times 10^{-6} \text{ s}^{-1}$ ), and average values of the radon diffusion length ( $L$ ), soil density ( $\rho_b$ ) and in-situ radon emanation coefficient ( $E$ ) (from Equation 4.7). Using the measured value of above parameters (Table 4.4), this ratio works out to be  $7.3 \times 10^{-4} \text{ kg m}^{-2} \text{ s}^{-1}$ . The slope  $(8.3 \pm 0.4) \times 10^{-4} \text{ kg m}^{-2} \text{ s}^{-1}$  may be used as a conversion factor to quickly estimate the radon flux ( $\text{Bq m}^{-2} \text{ s}^{-1}$ ) using the  $^{226}\text{Ra}$  content ( $\text{Bq kg}^{-1}$ ) for the uranium waste residue repository at Jaduguda.

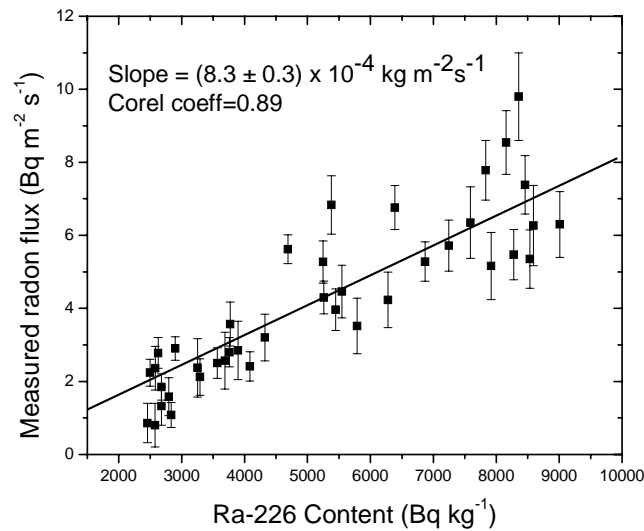


Fig. 4.9: Correlation between measured radon fluxes and  $^{226}\text{Ra}$  content at 40 locations of the Uranium Tailings Pond

#### **4.4. Field study at coastal beaches, High Background Radiation Areas**

As mention in the chapter 1 (section 1.3), thoron problem is of unique significance to India in view of thorium deposits in form of monazite along the coastal beaches of Kerala (So called High Background Radiation Areas) and future nuclear power programme involving thorium based fuels. A crucial part of thoron problem pertains to the understanding of its emission and transport characteristics from thorium rich matrices. Although chemically same as radon, the short half-life causes thoron to be essentially emitted from the crustal layers of matrices, which is more closely linked to the atmospheric parameters. Hence one can expect major quantitative differences in the emission characteristics between thoron and radon. The beach sands of Kerala provide a natural setting for carrying out thoron studies, exclusively. Also, the measurements of the thoron exhalation rates from these sands will be helpful in quantifying the thoron source term in HBRA's for investigating dosimetric issues in a more effective manner. The development of chamber technique equipped with automatic, fast monitoring instruments and process based data interpretation algorithms, has opened up application for large-scale mapping of thoron emissions in fields. Taking this opportunity and to demonstrate the applicability of the chamber technique in thoron emission studies, a study was taken up to measure thoron exhalation fluxes from monazite containing beach sand at about 26 different locations spanning over a distance of about 30 kilometers on the beaches in Karunagapally-Kollam area of coastal Kerala. The same is presented below.

##### **4.4.1. Materials and Methods**

An in-house developed accumulator set up was used for the measurement purpose. Unlike the case of radon, a relatively small accumulator (5 cm diameter and 7 cm height) was used for measurement of thoron exhalation so that the assumption of uniform concentration

in the accumulator holds good. Besides this, thoron sampling from the accumulator was carried out in a flow mode to minimize loss in the sampling path and detection was carried out using the spectroscopy based RAD-7 detector [105] to avoid radon interference. A representative location for a particular site was selected based on the gamma survey meter readings. The accumulator was deployed by inserting its edge 2 cm into the sand matrix. Following the deployment, measurements were carried out by RAD-7 detector, every five minutes up to 20 minutes. The initial 5 minutes were utilized to ensure mixing throughout the detector and accumulator. Following this, the equilibrium thoron concentration was measured by taking three readings, each of 5 min duration. These readings were observed to be close to each other, as is expected from theory. The average was taken to estimate the equilibrium thoron concentration ( $C_{eq}$ (Bq m<sup>-3</sup>)) in the accumulator. The value of  $C_{eq}$  was used later to compute the thoron exhalation rate ( $f_t$  (Bq m<sup>-2</sup> s<sup>-1</sup>)) using Equation (4.8) [106].

$$f_t = C_{eq} V \lambda / A, \quad (4.8)$$

where,  $\lambda$  is the thoron decay constant (s<sup>-1</sup>),  $V$  is the total volume i.e. sum of accumulator, RAD-7 detector and tubing volume (m<sup>3</sup>) and  $A$  is the enclosed surface area of the sand matrix by the accumulator (m<sup>2</sup>).

#### 4.4.2. Results and Discussion

Fig.4.10 shows the histogram plot of thoron exhalation rate measured at various locations on the beaches in Karunagapally-Kollam area of coastal Kerala. It was observed that the thoron exhalation rates measured were in the range of 1-18 Bq m<sup>-2</sup> s<sup>-1</sup> with an average of  $8 \pm 4$  Bq m<sup>-2</sup> s<sup>-1</sup>. The average value is about 10 times higher than that of model predicted global average thoron exhalation rate indicating that substantial thoron emission is taking place from the monazite sand. A good linear correlation was observed between gamma field

and thoron exhalation rate (data are not presented) which ensured the measurement consistency of the two parameters. One of the important features that was noticed was that the variation of thoron exhalation rate for a particular beach is not significantly large indicating thoron exhalation rate is a stable index parameter unlike the case of atmospheric thoron concentration which varies considerably within a small distance.

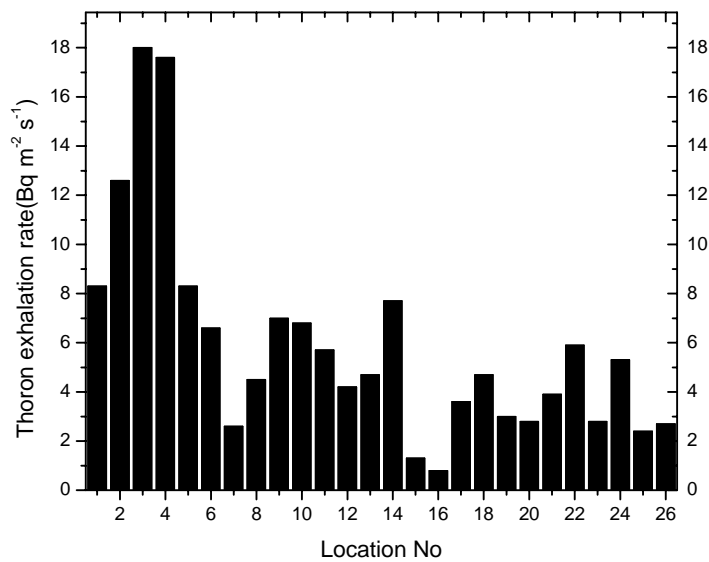


*Fig. 4.10: Histogram plot of measured thoron exhalation rate at various locations on monazite beach sands, Kerala.*

#### 4.5. Summary

The validation experiments indicated that there is a reasonably good agreement between the experimental observations and the headspace concentration predicted by the 2-D model throughout the deployment period. A noteworthy feature is that the 2-D model is able to correctly predict the observed saturation concentration. The model predictions deviated

from the reference data by only about  $\pm 20\%$  throughout the deployment period. These results demonstrate the unique capabilities of the 2-D theory and reinforce confidence in the analytical results. It may now be possible to evolve measurement protocols using chambers deployed in diffusion controlled steady state mode (i.e. unventilated chamber) to monitor real time flux variations and transients due to possible changes in the environmental and source parameters. The derived pre-deployment flux and soil diffusion coefficient from the headspace concentration data through least square fitting of 2-D model are in close agreement with their respective estimates using soil parameters. These results demonstrate the mathematical validity of the proposed 2-D model to describe trace gas emission into chambers deployed at the soil surface under both non-steady state and steady state conditions driven by diffusive transport.

The chamber was deployed at several locations of a uranium tailings repository and the measured chamber concentration data were fitted to the analytical formula derived in the previous chapter to elicit both the pre-deployment flux and the effective diffusion coefficient. The chapter presents the details of the alternative method [14] of estimating these two quantities based on the measurements of several soil parameters at the same locations. An excellent matching was found between the model predicted and measured radon fluxes as well as the effective diffusion coefficient. Similarly, the field study at Coastal beaches of High Background Radiation Areas of Kerala also demonstrated the applicability of chamber technique in thoron emission studies. However, the study indicated that a small accumulator ( $\sim 150$  cc volume) should be used for measurement of thoron flux in order to meet the assumption of uniform concentration in the chamber headspace. The thoron flux is found to be about 10 times higher than that of normal regions.

## **5. Studies on Radon Emission Perturbations due to Soil Seals**

---

### **5. 1. Introduction**

As discussed in section 2.4 of Chapter 2, the emission perturbation arising out of soil sealing in urban areas will affect the radioactive as well as green house gases emission estimate [42-43]. This is because, the sealed surface tends to inhibit the gas emission from the soil and at the same time, the buildup of gases under the sealed surface would result in enhanced emission fluxes from the cracks as well as from the free surface near the seal. In the latter case, the fluxes will decrease gradually to normal value as one moves away from the seal. Estimates of net emission fluxes contributed from the soil in an urban region based on measurements at arbitrary open locations will be considerably in error, if the effect of seals is not properly taken into account. In view of this, the spatial profiling of fluxes is very important for selecting representative locations for chamber deployment near the vicinity of soil seals. More specifically, it is important to address the question of how far from seal should a chamber be deployed to measure the unperturbed emission flux.

Given the fact that the conventional chamber techniques favor the use of large chambers for minimizing back diffusion effects, it has been a difficult task to prove experimentally the existence of spatial profile around seals which require higher spatial resolutions (~5-10 cms). Such studies require smaller chambers which in turn will have

considerable nonlinear chamber feedback effects. Development of a process based 2-D model (presented in chapter 3) for the chamber method is capable of handling the nonlinear effects regardless of the chamber dimension thereby enhancing the scope of the chamber techniques for conducting spatial profiling experiments across sealed surface.- In this chapter, we demonstrate this application through a study that combines theoretical results for the expected spatial profile of radon flux with experimental measurements conducted using a small chamber. The theoretical part deals with formulating and solving diffusion equations to predict spatial profile of radon fluxes across a semi-infinite, sealed, surface and the experimental study deals with flux profiling near the parapet of a building using a chamber of radius 5 cm and height 10 cm. Apart from demonstrating the enhanced scope, the study provides a quantitative understanding of the perturbation effect of soil seals.

## **5.2. Theoretical aspect to emission perturbation near sealed surfaces**

The covering of the soil surface with impervious materials as a result of urban development and infrastructure construction may be referred as anthropogenic sealing of soil. As a first example, we examine the build-up of a radioactive trace gas underneath large slab placed on soil, i.e. a semi-infinite seal. It is required to find the concentration build up of a trace gas under the seal and fluxes around its periphery. This problem does not have a bounded steady-state solution for stable gases having a uniform source in the soil because of inhibitive escape over an infinite area. However, solution will be bounded for radioactive gases such as radon and thoron having finite diffusion lengths.

If the seal dimensions are much larger than the diffusion length of radon ( $\sim 1\text{m}$ ), it is sufficient to analyse the problem in the vicinity of its edge. This is then a 2-D problem with depth as one variable and distance from the edge of the seal as the other. Several contexts

involving semi-infinite seals may be given namely, radon flux just outside a concrete building having parapets, flux outside concrete pavements and flux around large boulders on soil etc. This is among the few exactly solvable problems having simple solutions and can often be used as a validation exercise for more complex situations. We obtain exact analytical solutions to the perturbed fluxes as well as concentration build-up underneath the seal.

In order to set up the equation of radon diffusion, some general considerations are in order. The soil is assumed to be homogeneous containing a uniform distribution of radium-226. Let  $R$  be the specific activity ( $\text{Bq kg}^{-1}$ ) of radium-226 in soil. A fraction ( $E$ ) of the radon atoms emanated from the grains containing Ra-226 migrates into the air filled pores present in the soil. Let us denote the concentration of radon in the pore space by  $C_s$  ( $\text{Bq/m}^3$ ). In the deep soil several meters below the ground, other than radioactive decay, no other mechanism of loss is expected for radon, and hence there must be equilibrium between the radon atoms escaping into the pores and those decaying. If we denote pore space concentration of radon in the deep soil by  $C_s(-\infty) = C_\infty$ , one relates it to  $R$  through the relation:

$$C_\infty = \frac{R\rho_b E}{n_e} \quad (5.1)$$

where,  $\rho_b$  is the bulk density of soil (wt per unit bulk vol:  $\text{kg/m}^3$ ),  $E$  is the emanation fraction of radon and  $n_e$  is the effective porosity of soil. However, as one approaches soil surface, the concentration  $C_s$  begins to deplete due to exhalation from the surface. If the surface is free, i.e, radon atoms reaching the surface are rapidly carried away by the atmospheric currents and hence are irreversibly lost from the soil matrix, we refer to it as free exhalation. On the other hand, if the surface is covered with seals and radon escapes through cracks and holes in the seals or by diffusing around its edges, we may refer to it as obstructed exhalation.

It is required to provide solution to the exhalation rate in the presence of such obstructions on the surface.

### 5.2.1. Formulation of diffusion equation

Consider a slab placed on the positive side of X-axis on a soil surface as shown in Fig. 5.1. The Z-axis is perpendicular to the slab.  $z = 0$  defines the soil and slab-soil interface and  $z < 0$  defines the soil region. The region  $x < 0$  on the surface is free soil and that corresponding to  $x > 0$  is the slab-soil interface. This system possesses only one characteristic length namely the diffusion length, given by

$$l_s = (D_s/\lambda)^{1/2}, \quad (5.2)$$

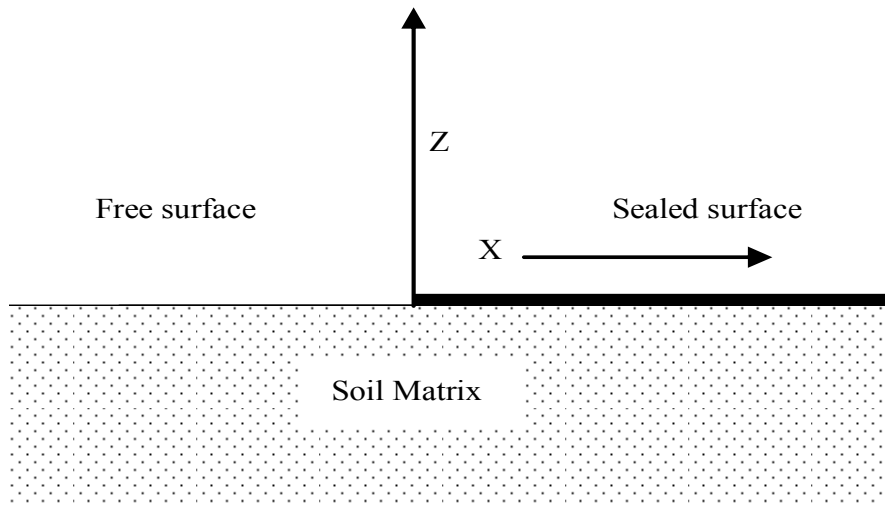


*Fig. 5.1: Schematic diagram of a semi infinite seal on soil surface and coordinate system taken for the problem formulation*

In view of this, it is appropriate to scale all distances in terms of  $l_s$ :

$$\left. \begin{aligned} \xi &= x/l_s, & -\infty < \xi < \infty \\ \zeta &= z/l_s, & -\infty < \zeta \leq 0 \end{aligned} \right\} \quad (5.3)$$

In rectangular coordinate system, the diffusion equation for radon concentration in the soil may be written in terms of the dimensionless variables as

$$\frac{\partial^2 C_s}{\partial \xi^2} + \frac{\partial^2 C_s}{\partial \zeta^2} - (C_s - C_\infty) = 0, \quad -\infty < \xi < \infty, \quad -\infty < \zeta \leq 0 \quad (5.4)$$

Unlike the standard problem of exhalation from a free surface, the present problem will have different boundary conditions on the seal and free parts of the surface. On the free part ( $\xi < 0$ ), the concentration will be zero and beneath the seal, ( $\xi > 0$ ) the flux will be zero. This is the well-known mixed boundary value problem discussed by Sneddon [92]. Hence

$$C_s(\xi, 0) = 0, \quad \xi < 0 \quad (5.5a)$$

$$\frac{\partial C_s(\xi, 0)}{\partial \zeta} = 0, \quad \xi > 0 \quad (5.5b)$$

$$\text{In addition, we have, } C_s(\xi, -\infty) = C_\infty, \quad -\infty < \xi < \infty \quad (5.5c)$$

### 5.2.2. Derivation of the Solution

Upon taking the Fourier transform [107] of the Eq.(5.4) w.r.t  $\xi$  variable and then inverting the solution, we have,

$$C_s(\xi, \zeta) = C_\infty [1 - \exp(\zeta)] + \frac{1}{2\pi} \int_{-\infty}^{\infty} A(k) \exp(-ik\xi) \exp\left\{(k^2 + 1)^{1/2} \zeta\right\} dk \quad (5.6)$$

$$-\infty \leq \xi < \infty, \quad -\infty < \zeta \leq 0$$

where,  $k$  is the  $\xi$  conjugate variable and  $A(k)$  is the unknown spectral function to be determined.

For convenience, we convert the integral on the real line in  $k$  space to that along the imaginary axis in  $s$ -space through the transformation,

$$s = -ik \quad (5.7)$$

Eq.(5.6) now becomes

$$C_s(\xi, \zeta) = C_\infty [1 - \exp(\zeta)] + \frac{1}{2\pi i} \int_{-i\infty}^{i\infty} A(s) \exp(s\xi) \exp\left\{(1-s^2)^{1/2} \zeta\right\} ds \quad (5.8)$$

$-\infty \leq \xi < \infty, \quad -\infty < \zeta \leq 0$

### 5.2.2.1 Determination of Coefficient, $A(s)$

Upon applying the BCs given in Eq. (5.5a) and Eq. (5.5b), we obtain

$$C_s(\xi, 0) = \left. \begin{aligned} \frac{1}{2\pi i} \int_{-i\infty}^{+i\infty} A(s) \exp(s\xi) ds = 0, & \quad \xi < 0 \\ = g(\xi), & \quad \xi > 0 \end{aligned} \right\} \quad (5.9)$$

where  $g(\xi)$  is the concentration (yet unknown) right below the seal ( $\zeta=0, \xi < 0$ ). Since  $C_s(\xi, 0)$  needs to be continuous at  $\xi=0$ ,  $g(0)$  must be zero. It implies that any pole existing in  $A(s)$  on the imaginary axis should not contribute to  $g(\xi)$  as  $\xi \rightarrow 0^+$ . This may be achieved by indenting the pole by a semi circle on the right half plane of the imaginary axis. Alternatively, this is equivalent to shifting the line of integration by a small quantity  $c$  to the right of the imaginary axis. With this, Eq.(5.8) may be rewritten as

$$C_s(\xi, \zeta) = C_\infty [1 - \exp(\zeta)] + \frac{1}{2\pi i} \int_{c-i\infty}^{c+i\infty} A(s) \exp\left[s\xi + (1-s^2)^{1/2} \zeta\right] ds, \quad (5.10)$$

$-\infty < \xi < \infty, \quad -\infty < \zeta < 0; \quad c > 0$

Accordingly, Eq.(5.9) may be rewritten as

$$C_s(\xi, 0) = \left. \begin{aligned} \frac{1}{2\pi i} \int_{c-i\infty}^{c+i\infty} A(s) \exp(s\xi) ds = 0, & \quad \xi < 0 \\ = g(\xi), & \quad \xi > 0 \end{aligned} \right\} \quad (5.11)$$

Supposing  $A(s)$  were known, one would evaluate the integral (Eq. (5.11)) by contour integration techniques [108]. Since for  $\xi < 0$ ,  $\exp[s\xi]$  would vanish on a large contour on the positive side, it is appropriate to construct a contour on the right half plane as shown in Fig.5.2.

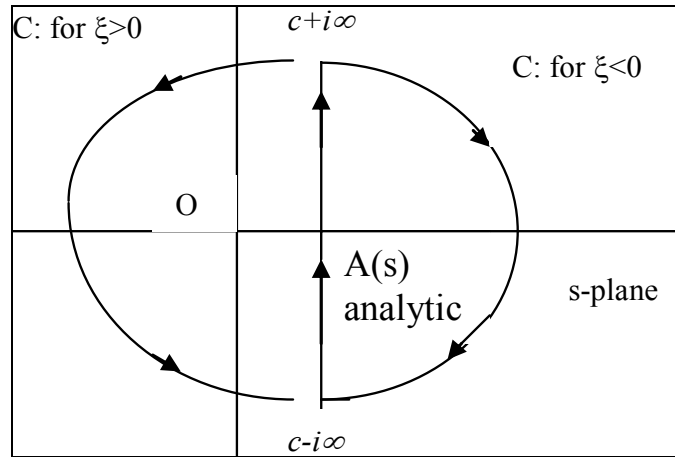


Fig.5.2: A schematic of the contour taken for solving the complex integral equation given in Eq.(5.11)

From the Cauchy's residue theorem, it is evident that the integral would vanish for  $\xi < 0$ , only if the integrand has no singularities on the right half plane. Since  $\exp(s\xi)$  is analytic,  $A(s)$  should also be analytic for  $\text{Re}(s) > 0$ . Proceeding in a similar manner for the region  $\xi > 0$ , one can argue that if the integral (5.11) has to yield a non zero function  $g(\xi)$  for  $\xi > 0$ , the function  $A(s)$  should be non-analytic on the left side. In sum, we have,

(i)  $A(s)$  is analytic on the right half s-plane and non-analytic on left half s-plane.

Next consider the flux at the interface obtained from differentiating Eq.(5.10) wrt  $\zeta$ .

$$j_s(\xi, 0) = -\frac{\varepsilon D_s}{l_s} \frac{\partial C_s(\xi, \zeta)}{\partial \zeta} \Big|_{\zeta=0} = \frac{\varepsilon D_s}{l_s} \left[ C_\infty - \frac{1}{2\pi i} \int_{c-i\infty}^{c+i\infty} A(s) (1-s^2)^{1/2} \exp(s\xi) ds \right], \quad (5.12)$$

$$-\infty < \xi < \infty, \quad -\infty < \zeta < 0; \quad c > 0$$

In view of the BC (Eq.(5.5b)), we have :

$$j_s(\xi, 0) = 0 \text{ for } \xi > 0 \quad \Rightarrow \quad \frac{1}{2\pi i} \int_{c-i\infty}^{c+i\infty} A(s) (1-s^2)^{1/2} \exp(s\xi) ds = C_\infty, \quad \xi > 0 \quad (5.13a)$$

$$= f(\xi), \quad \xi < 0 \quad (5.13b)$$

where,  $c > 0$  and hence the line of integration is to the right of the imaginary axis.  $f(\xi)$  is a non-zero function (yet unknown) representing the flux on the free interface.

We can now shift the line of integration to the left plane at a distance  $c'$  by evaluating the residue at  $s=0$ . Let us suppose that  $A(s)$  has a simple pole at  $s=0$  such that we may write  $A(s)=B(s)/s$ , where  $B(0)$  has a non-zero finite value. The function  $B(s)$  may be non-analytic elsewhere. The integral on  $c$  is equal to the residue at  $s=0$  {i.e.,  $B(0)$ } + integral on  $c'$ . If we choose  $B(0) = C_\infty$  the residue exactly cancels  $C_\infty$  on the right of Eq.(5.13a). With this, Eq.(5.13a, b) reduce to integrals over the line at  $c'$ :

$$\frac{1}{2\pi i} \int_{c'-i\infty}^{c'+i\infty} \frac{B(s)}{s} (1-s^2)^{1/2} \exp(s\xi) ds = 0 \quad \xi > 0 \quad [5.14a]$$

$$= f'(\xi), \quad \xi < 0 \quad [5.14b]$$

where  $f'(\xi)$  is another non-zero function.

The integrals in Eqs.(5.14 (a, b)) may be evaluated through contours as shown in Fig. 5.3 for regions  $\xi < 0$  and  $\xi > 0$ .

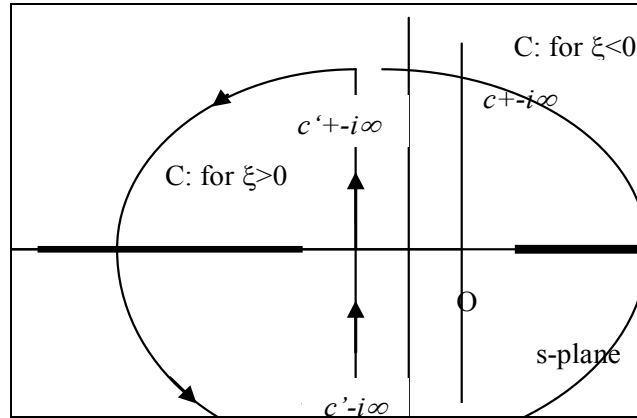


Fig.5.3 A schematic of the contour taken for solving the complex integral equation given in Eq. (5.14 (a, b))

The function  $(1-s^2)^{1/2}$  is analytic only between  $-1 < s < 1$ . This function gives rise to branch lines  $(1, \infty)$  and  $(-1, -\infty)$  along the  $X$ -axis ( $Re(s)$ ) as shown in Fig. 5.3. Considering this, one can now use similar argument as in the earlier case of Eq.(5.11). If the integral has to vanish for  $\xi > 0$  {Eq.(5.14a)}, then the integrand should be analytic on  $s < 0$ . If it were to be non-zero and finite for  $\xi < 0$ , integrand should be non-analytic on  $s \geq 0$ . We thus obtain a second constraint, viz.,

(ii)  $A(s) (1-s^2)^{1/2}$  should be analytic for  $s < 0$  and non-analytic for  $s \geq 0$ .

In order to meet the constraints (i) and (ii) simultaneously, an expression for  $A(s)$  may be written as

$$A(s) = \frac{B(s)}{s} = \frac{B'(s)}{s(1+s)^{1/2}} \quad (5.15)$$

where,  $B'(s)$  is a function which is analytic and bounded everywhere on the complex  $s$  plane. The uniqueness comes from the analyticity and boundedness requirement of  $B'(s)$ . For, only when  $B'(s)$  is analytic that  $A(s)$  will be analytic for  $s > 0$  but is non-analytic for  $s < 0$  in view of its branch line between  $(-1, -\infty)$  {requirement (i)}. On the other hand,  $A(s) (1-s^2)^{1/2} = [B'(s)/s] (1-s)^{1/2}$  will be analytic for  $s < 0$  but is non-analytic for  $s > 0$  in view of its branch line  $(1, \infty)$

{requirement (ii)}. Boundedness of  $B'(s)$  comes because it has to vanish on large contours on both sides to yield finite values for  $\xi=0$ .

If  $B'(s)$  is analytic and bounded in the entire complex plane, then by Liouville theorem [108] it should be a constant. i.e.

$$B'(s) = B(0) = C_\infty. \quad (5.16)$$

With this, the function  $A(s)$  is completely determined.

### 5.2.3. Surface concentration and flux

The concentration  $g(\xi)$  under the seal ( $\xi > 0$ ) may be expressed as {Eq.(5.11)}

$$g(\xi) = \frac{C_\infty}{2\pi i} \int_{c-i\infty}^{c+i\infty} \frac{1}{s(1+s)^{1/2}} \exp(s\xi) ds \quad \xi > 0, \quad c > 0. \quad (5.17)$$

that may be evaluated by standard contour integration methods as

$$g(\xi) = C_\infty \operatorname{erf}(\sqrt{\xi}) = C_\infty \operatorname{erf}(\sqrt{x/l_s}) \quad (5.18)$$

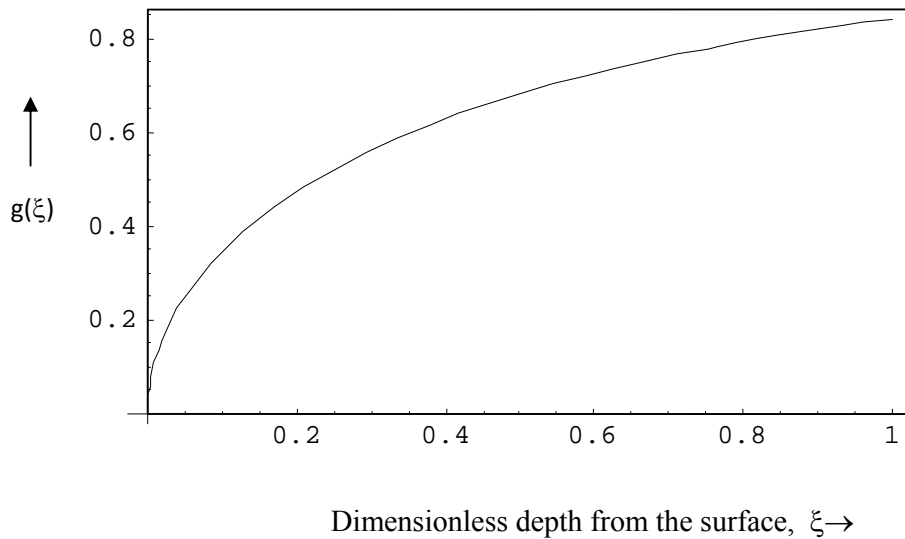


Fig.5.4: Graph showing the radon concentration build-up below the seal as predicted by the model

The profile is shown in Fig. 5.4. The concentration builds up to about 85% of  $C_\infty$  at a distance of one diffusion length from the edge. From the formula, it is clear that the concentration increases as  $(x/l_s)^{1/2}$  in the vicinity of the edge. From Eq.(5.12),and using Eq.(5.15) and Eq. (5.16), the **exhalation flux** profile at the free surface  $\xi < 0$  will be

$$\frac{j(\xi)}{j_\infty} = 1 - \frac{1}{2\pi i} \int_{c-i\infty}^{c+i\infty} \frac{(1-s)^{1/2}}{s} \exp(s\xi) ds; \quad c > 0. \text{ and } \xi < 0 \quad (5.19)$$

where,  $j_\infty$  is the exhalation flux far away from the seal (free surface flux) given by [15]:

$$j_\infty = \lambda n_e l_s C_\infty \quad (5.20)$$

Where,

$n_e$  is the effective porosity as defined in Eq. (3.8) in Chapter 3.

$l_s$  is the radon diffusion length in the soil matrix

$C_\infty$  is the deep soil gas radon concentration

$\lambda$  is the decay constant of radon ( $2.1 \times 10^{-6} \text{ s}^{-1}$ )

Eq.(5.19) may be integrated to yield

$$\frac{j(\xi)}{j_\infty} = \text{erf}\left(\sqrt{|\xi|}\right) + \frac{1}{\sqrt{\pi|\xi|}} \exp\{-|\xi|\} \quad (5.21)$$

The flux shows  $\xi^{-1/2}$  divergence as one approaches the discontinuity at the edge of the seal. The square root law is typical of the Laplacian operator and occurs in electrostatic problems. The deviation from this law at large distance is a result of the radioactive decay term present in the present problem. This term gradually dampens the singular flux at the edge and reduces it to free surface exhalation value at large distances.

Let us now consider a practical situation. Suppose one measures the flux with a small accumulator (inverted cup) of dimension  $2a$  at various distances from the edge of the block.

When the center of the cup is placed at a distance  $\xi_0$ , it would measure a mean flux

$$\bar{j}(\xi_0) = \frac{1}{2a} \int_{\xi_0-a}^{\xi_0+a} j(\xi) d\xi \quad (5.22)$$

For a diffusion length of 100 cm and a rectangular cup of width  $2a=10$  cm, the plot of  $\bar{j}(\xi_0)$  is as shown in Fig.5.5. The mean flux could be 4 times as high if measured at the edge; it would be less than about 1.5 times as we move away beyond 20 cms. From Eq.(5.21), one may compute the total excess current exhaled into the atmosphere due to the edge effect by integrating the excess flux (over the free flux) wrt  $\xi$ . We obtain,

$$i_{\text{excess}} = \int_0^{\infty} \{j(\xi) - j_{\infty}\} d\xi = \frac{1}{2} j_{\infty} l_s \quad (\text{atoms per unit length}) \quad (5.23)$$

This expression is useful for comparing the limiting form of the flux obtained from rigorous methods for rectangular cracks.

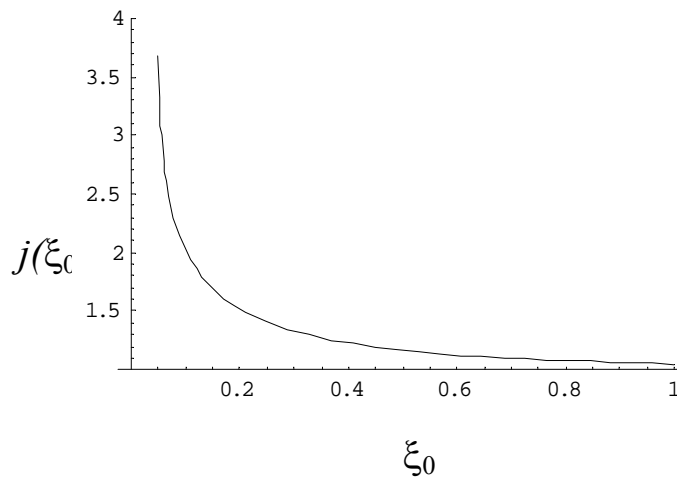


Fig.5.5: Graph showing the variation of mean radon flux ( $j(\xi_0)$ ) with respect to dimensionless distance ( $\xi_0$ ) from edge of the seal.

### 5.2.4. Concentration depth profile

From Eqs (5.10) , (5.15) and (5.16), expression for the soil gas concentration **depth profile** may be written as

$$C_s(\xi, \zeta) = C_\infty [1 - \exp(\zeta)] + \frac{C_\infty}{2\pi i} \int_{c-i\infty}^{c+i\infty} \frac{\exp[s\xi + (1-s^2)^{1/2} \zeta]}{s(1+s)^{1/2}} ds, \quad (5.24)$$

$$-\infty < \xi < \infty, \quad -\infty < \zeta < 0; \quad c > 0$$

This may be converted to the following real integrals:

$$C_s(\xi, \zeta) = C_\infty [1 - \exp(\zeta)] - \frac{2C_\infty}{\pi} \int_0^\infty \frac{\exp[(1+u^2)\xi]}{(1+u^2)(2+u^2)^{1/2}} \sin\left\{u(2+u^2)^{1/2} \zeta\right\} u du, \quad (5.25)$$

$$-\infty < \xi < 0, \quad -\infty < \zeta < 0;$$

and

$$C_s(\xi, \zeta) = C_\infty \left[ 1 - \frac{2}{\pi} \int_0^\infty \frac{\exp[-(1+u^2)\xi]}{(1+u^2)} \cos\left\{u(2+u^2)^{1/2} \zeta\right\} du \right], \quad (5.26)$$

$$0 < \xi < \infty, \quad -\infty < \zeta < 0;$$

Where  $u$  denote a variable of integration.

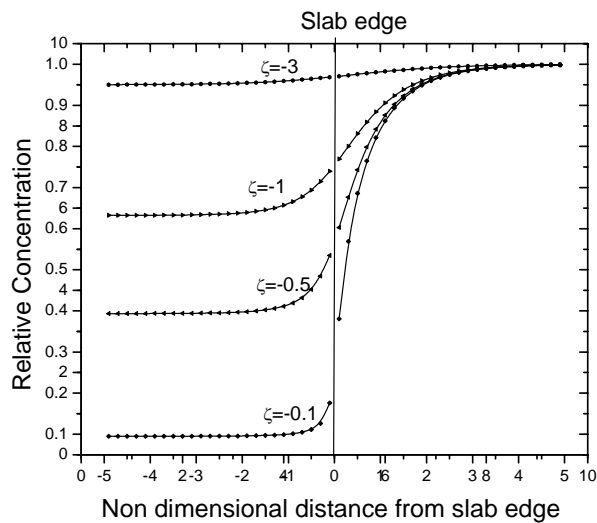


Fig.5.6: Depth profile of the relative radon concentration below the seal, predicted by model

These have been numerically evaluated. Typical depth profiles are shown in Fig. 5.6. Also shown are the concentration values at these depths for unperturbed soil. The perturbations subside beyond about 1.5 diffusion lengths away from the slab side.

### **5.2.5: Implications of study to flux mapping**

At this point, an interesting implication of the results for practical radon flux measurement may be mentioned. Suppose, one deploys an accumulator over a surface for measuring the flux. A low value of the measured flux (as compared to that expected by known radioactivity of the soil) would be a strong hint on the possible presence of a block (say a large boulder, or a slab rock) just underneath the soil surface. Also, an unusually large flux would also imply that one is measuring the flux at the edge of a block just underneath the soil. Although the theory needs to be modified for blocks occurring in the sub-soil region, the qualitative predictions made here would be helpful in alerting to such possibilities, which should be looked into in analyzing the data.

## **5.3. Experimental Validation**

### **5.3.1. Materials and Methods**

A series of in-situ experiments were conducted near a concrete sealed surface (Fig. 5.7) to study radon flux behavior at its vicinity. The theoretical prediction of the radon flux variation with respect to the distance measured from the sealed surface is given by Eq. (5.21). The plot of the radon flux with varying distance from edge of the seal for a case problem is shown in Fig.5.7. The in-situ radon fluxes were measured at various distances from the sealed surface following the process-based accumulator methods [106] described in Chapter 3 and 4. A chamber of radius 2.5 cm and height of 10 cm connected to an AlphaGUARD radon monitor [109] was employed for measurements of radon flux. AlphaGUARD was set to

diffusion mode and measurement cycle time was kept to 10 minutes. The chamber was kept for about 3 to 5 hours to allow sufficient build-up of  $^{222}\text{Rn}$  concentration in it. After sufficient rise of  $^{222}\text{Rn}$  concentration in the accumulator, AlphaGUARD was disconnected and data from AlphaGUARD was retrieved. The data were then subjected to least square fitting of the 2-D model to estimate the radon flux. Experiments were repeated in a similar manner at various distances from the edge of the seal.



AlphaGUARD

Accumulation Chamber

Concrete Seal

*Fig. 5.7: In-situ measurement of radon flux from soil surface at edge of a concrete seal using a chamber connected to AlphaGUARD radon monitor.*

On the other hand, radon concentration in soil gas at various depths from soil surface (upto 1.2 meter) was measured in the unperturbed locations following the procedure described in section 4.3.3. The measured depth profile data of radon concentration was then utilized to estimate the deep soil gas radon concentration ( $C_{\infty}$ ) and radon diffusion length ( $l_s$ ) in the soil matrix. Few other soil parameters such as density ( $\rho$ ), effective porosity ( $n_e$ ) were measured using the soil samples collected from the experimental locations. Then, the unperturbed radon flux (far away from the sealed surface) was predicted using Eq. (5.20)

which requires input parameters such as deep soil gas radon concentration, radon diffusion coefficient length and effective porosity. The flux profile at the sealed surface was then generated using unperturbed radon flux and radon diffusion length by applying Eq. (5.21)

### 5.3.2 Results and discussion

Table 5.1 provide the values of various measured/estimated parameters of soil used for generating the radon flux profile in the vicinity of a sealed surface and Table 5.2 presents the radon fluxes predicted through model (Eq. 5.21) vs. directly measured using chamber technique at various distances from edge of the sealed surface.

*Table 5.1: Various parameters of soil estimated using soil samples and measured radon concentration in the pore space of the soil matrix*

<b>Parameters of soil</b>	<b>Estimated value</b>
$\rho$ , Bulk density of soil	1359.5 kg/m <sup>3</sup>
$n_e$ , effective porosity of soil	0.497
$C_\infty$ , (Radon concentration at deep depth)	10,703 Bq/m <sup>3</sup>
$l_s$ , radon diffusion length	1.28 m
$j_\infty$ , Unperturbed radon flux	52 Bq/m <sup>2</sup> /h

Fig. 5.8 presents the plot of model predicted and measured radon flux at various distances from the edge of the seal. As may be seen from numerical value in Table 5.2 as well as the profile trend in Fig 5.8, there is a fairly good matching between the radon fluxes obtained from model using the measured soil parameters and that obtained directly from chamber experiments. The linear correlation between measured and model predicted radon

fluxes (Fig.5.9) at the vicinity of the seal yielded a slope value of 1.07 with correlation coefficient of 0.97, indicating the validity of the diffusion based seal theory proposed in this chapter.

It may be noted that there is a strong experimental evidence of the radon emission perturbation as predicted by the diffusion model. Radon flux at edge of the seal is very high (about 7 times higher than normal) and it decreases gradually to normal value at a distance of about 1 diffusion length ( $\sim 1$  m for soil)). This suggests that for measurement of unperturbed radon flux at the vicinity of a sealed surface, one should deploy the accumulator at least 1 meter away from the edge of the seal. It is hoped that this emission perturbation model will be quite useful to assess the extent of emission flux perturbation near a sealed surface and to select representing locations for emission mapping in urban regions.

*Table.5.2: Model predicted and experimentally measured radon fluxes at various distances from edge of the seal*

Distance (cm)	Radon fluxes ( $\text{Bq m}^{-2} \text{h}^{-1}$ )	
	Theoretically predicted	Experimentally measured
5	291	315
10	165	157
15	139	154
20	124	149
30	108	112
50	93	86
70	86	62
100	81	60

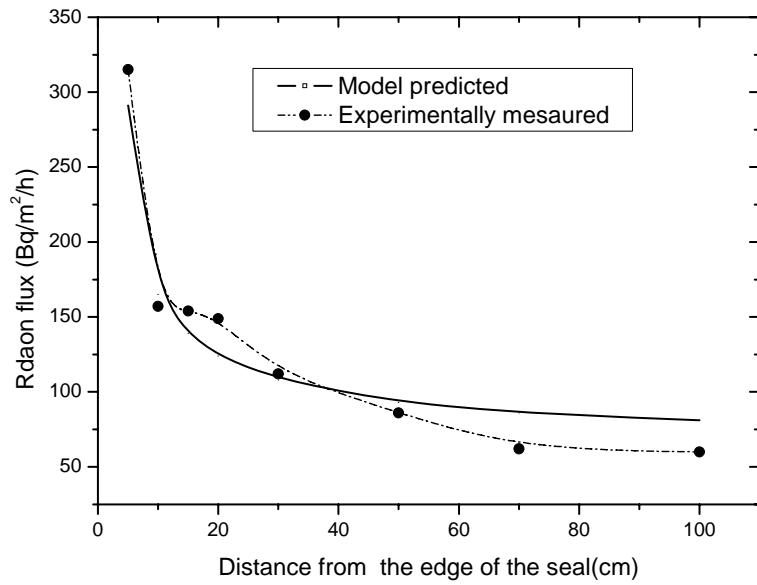


Fig. 5.8: Plot of model predicted and measured radon flux at various distances from the edge of the seal. Data points are connected with dot lines for guiding the eye

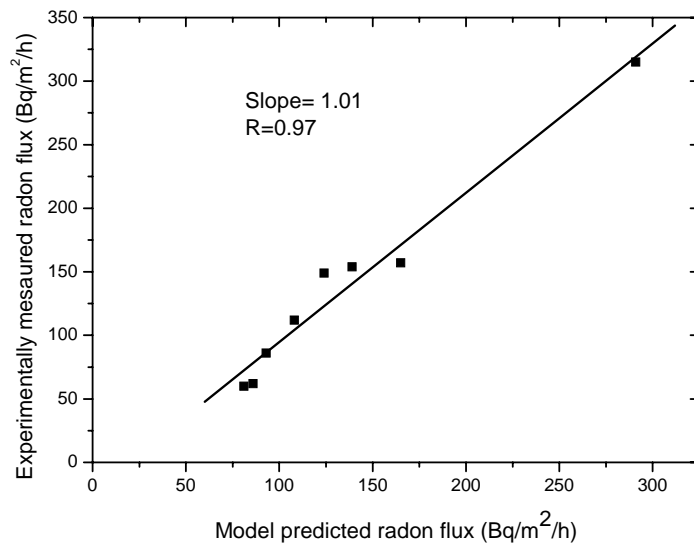


Fig. 5.9: Linear correlation of model predicted and experimentally measured radon fluxes near the sealed surface

#### 5.4 Summary

The study demonstrated the existence of a radon flux profile at the vicinity of a sealed surface. This fact has been predicted from the diffusion based modeling as well as directly observed from in-situ experiments. A closed form solution for predicting radon flux profile is derived from the diffusion theory. The model prediction is validated successfully against experimental observations of radon emission fluxes made at a concrete seal surface. For this, a small chamber of radius 5 cm and height 10 cm was used for which nonlinear effect is expected to be high. The development of 2-D non-steady state model for chamber method, which is capable of handling the nonlinear effects regardless of the chamber dimension, made it possible to conduct spatial profiling experiments across sealed surface. It was observed that there is a very high radon flux at the edge of the seal and it decreases with increase of distance from the edge of the sealed surface. The radon flux at the edge of the seal is observed to be as high as 7 times of that observed at a distance of about 1 meter away from the edge of the seal. In view of this, measurement of unperturbed radon flux near soil seals should be carried out about 1 meter away from the edge of the seal.

This far, we addressed the realistic modeling of the response of the chamber for radon flux measurements, through 2-D diffusion theory (Chapter 3), conducted a series of experiments (Chapter 4) to validate the model, and demonstrated special application (Chapter 5) of the model to spatial profiling near soil seals. With this, the existing shortcoming of an absence of a process based model for outdoor emission measurement method is resolved. As mentioned in the introduction, radon problem includes both outdoor and indoor emission issues. In the next chapter, we address the case of indoor emission with a view to provide an improved model to estimate the radon emission fluxes of building materials and a recipe to extrapolate this data to emission from walls.

## **6. Studies on Radon Emission from Building Materials to Indoor Air**

---

### **6.1. Introduction**

The work presented in the previous chapters mainly focuses on providing a quantitative basis for the response characteristics of the chamber technique for assessing outdoor radon emissions, principally from soils. Apart from outdoor measurements, the radon problem encompasses indoor issues in which besides soil, there are also other sources of radon, chief among them being various building materials such as bricks, tiles, cement and concrete. As highlighted in Chapter 1, radon emission from these building materials can be a significant source of indoor radon and while choosing these materials for construction, it is necessary to follow the guidelines of international agencies [110, 11] for the acceptance criteria for these materials. This calls for developing reliable techniques for assessing radon emission source term into the indoor environment based on measurement data of building material samples. Literature review in Chapter 2 suggests that, most of the past studies on building materials assumed that the emission from building material samples is same as emission from walls made by these materials and predicted the indoor radon and inhalation dose contributed from these building materials. This assumption is in serious error because of the change in the radon diffusion process from prior to latter configuration. The radon diffusion process in the wall is one dimensional (1-D), while the process in the brick or any other block of building materials is three dimensional (3-D). This leads to different radon exhalation per unit surface area of the matrix per unit time for the two cases. Further, sample

measurements are not unique measures of wall flux in view of possible variations in diffusion lengths of radon from material to material. The correct estimation of wall emission fluxes based on sample measurements requires the use of 3-D diffusion theory and necessitates a model which can predict radon flux from the wall based on radon flux data in samples.

In this chapter, a theoretical analysis and experimental evidence for a significant enhancement in the flux from building material when actually used in construction of a wall is demonstrated. To estimate the radon flux from the wall using measured flux data of building material samples, a semi-empirical model has been proposed. This model has been established by comparing the solution of the three dimensional radon diffusion equation applicable for a cuboidal shaped building material (such as brick) with the solution of the one dimensional radon diffusion equation applicable for a building wall. The semi-empirical model has been successfully validated with the actual measurements at a new construction site. Towards this end, the mathematical development of the brick to wall exhalation model is discussed.

## **6.2. Model development**

### **6.2.1. Formulation and solution to diffusion equation for a building material block.**

Consider a cuboidal shaped building material (such as brick) of dimension  $[2a, 2b, 2h]$ , where  $a, b, h$  are the half-length, half-breadth and half-thickness of the block.  $[x, y, z]$  are coordinates along the direction of length, breadth and thickness of the building material respectively with origin at the center (Fig. 6.1).

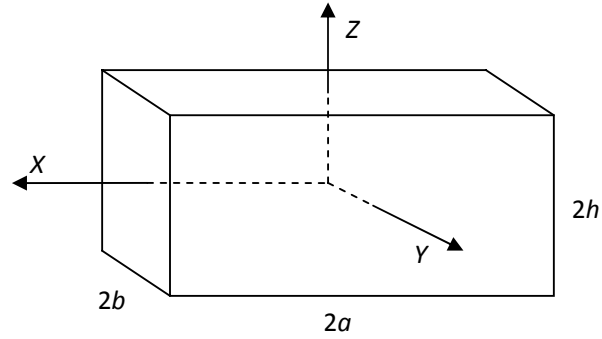


*Fig. 6.1: Schematic diagram of a cuboidal shaped building material and the coordinate system used for the model development.*

It is assumed that radon after emanating into pore spaces from the grains is exhaled to the environment by diffusion through void spaces of the building material. The diffusion equation of radon in the pore space of the building material in steady state may be written as:

$$D \left[ \frac{\partial^2 C}{\partial x^2} + \frac{\partial^2 C}{\partial y^2} + \frac{\partial^2 C}{\partial z^2} \right] - \lambda C + \lambda \left( \frac{R \rho_b E}{n_e} \right) = 0 \quad (6.1)$$

Where,

$C$  is the radon concentration ( $\text{Bq m}^{-3}$ ) in the pore space of the material at point  $(x, y, z)$ ,

$R$  is the radium content ( $\text{Bq kg}^{-1}$ ),

$\rho_b$  is the bulk density of the materials ( $\text{kg m}^{-3}$ ),

$E$  is the radon emanation factor from grain to pore space,

$n_e$  is the effective porosity of the material,

$D$  is the radon diffusion coefficient in the material ( $\text{m}^2 \text{s}^{-1}$ ),

$\lambda$  is the decay constant of radon ( $\text{s}^{-1}$ ).

The boundary conditions of the problem are governed by the fact that the pore space radon concentration at the surfaces of the material is zero, i.e.;

$$C(x, y, z = \pm h) = 0, \quad (6.2a)$$

$$C(x, y = \pm b, z) = 0, \quad (6.2b)$$

$$C(x = \pm a, y, z) = 0. \quad (6.2c)$$

Eq. (6.1) may be solved by using Fourier expansion technique. Considering that there exists a symmetric solution along spatial coordinates as defined in Fig.6.1, we may write the solution using cosine function as:

$$C(x, y, z) = \sum_{m=0}^{\infty} \sum_{n=0}^{\infty} \cos(k_n x) \cos(k_m y) \phi_{nm}(z). \quad (6.3)$$

Where,  $k_n, k_m$  are constants which can be determined using boundary conditions (Eqs. (6.2a: 6.2c) and  $\phi_{nm}(z)$  is a function of  $z$ . Similarly denoting  $\frac{R\rho_b E}{n_e} = C_{\infty}$ , a theoretical quantity referring to the maximum radon concentration ( $\text{Bq m}^{-3}$ ) in pore space that can be attained if the emitted radon atoms are completely confined within the block matrix, we may expand  $C_{\infty}$  in term of cosine function as:

$$C_{\infty} = \sum_{m=0}^{\infty} \sum_{n=0}^{\infty} A_{nm} \cos(k_n x) \cos(k_m y), \quad (6.4)$$

Where the constant  $A_{nm}$  ( $n, m = 0, 1, \dots$ ) can be estimated by applying condition of orthogonality to Eq. (6.4). Skipping the details of derivation of the above constants, the explicit solution for  $C(x, y, z)$  may be written as:

$$C(x, y, z) = \sum_{m=0}^{\infty} \sum_{n=0}^{\infty} 4C_{\infty} (-1)^{n+m} \frac{d_{nm}^2}{l^2} \frac{\cos(k_n x)}{k_n a} \frac{\cos(k_m y)}{k_m b} \left[ 1 - \frac{\cosh\left(\frac{z}{d_{nm}}\right)}{\cosh\left(\frac{h}{d_{nm}}\right)} \right], \quad (6.5)$$

Where,  $l$  is the radon diffusion length in the material defined as

$$l = \sqrt{D/\lambda}$$

and,

$$\left. \begin{aligned} k_n &= \left(n + \frac{1}{2}\right) \frac{\pi}{a}, k_m = \left(m + \frac{1}{2}\right) \frac{\pi}{b}, \\ \frac{1}{d_{nm}^2} &= k_n^2 + k_m^2 + \frac{1}{l^2} \end{aligned} \right\} \quad (6.6)$$

Let us consider a special case where  $a, b$  are relatively large as compared to  $h$  so that the problem becomes identical to the 1-D case of a wall, then under this condition it can easily be shown that  $d_{nm} = l$ . With this, the above series converts to the analytical expression:

$$C(z) = C_\infty \left[ 1 - \frac{\cosh\left(\frac{z}{l}\right)}{\cosh\left(\frac{h}{l}\right)} \right]. \quad (6.7)$$

As may be seen, this is the 1-D solution of the radon diffusion equation in a wall [15]. Hence under the limiting condition, the 3-D solution reduces to 1-D solution indicating the accuracy of the mathematical derivation.

With the 3-D solution (Eq. (6.5)), it is now possible to derive the analytical expression for the radon flux at six surfaces of the building material applying Fick's law of diffusion, which may be written as follows:

$$j_x^+ = j_x^- = \left| -n_e D \left( \frac{\partial C}{\partial z} \right)_{x=a} \right|, \quad (6.8a)$$

$$j_y^+ = j_y^- = \left| -n_e D \left( \frac{\partial C}{\partial z} \right)_{y=b} \right|, \quad (6.8b)$$

$$j_z^+ = j_z^- = \left| -n_e D \left( \frac{\partial C}{\partial z} \right)_{z=h} \right|, \quad (6.8c)$$

Where,

$j_x^+$ ,  $j_x^-$  denote radon flux at surface along positive and negative directions of the  $X$  axis respectively, with similar definitions for the fluxes in the  $Y$  and  $Z$  directions respectively. However, the quantity of practical interest is the mean flux ( $J_b$ ) from the building material defined by:

$$J_b = \frac{\iiint (j_x^+ + j_x^-) dydz + \iiint (j_y^+ + j_y^-) dzdx + \iiint (j_z^+ + j_z^-) dxdy}{8(ab + bh + ha)}. \quad (6.9)$$

Using Eqs. (6.5, 6.8, 6.9) and solving  $J_b$  finally can be expressed as :

$$J_b = \lambda R \rho_b E \sum_{n,m=0}^{\infty} \frac{4d_{nm}^3}{ab + bh + ha} \left[ \left\{ \left( \frac{h}{d_{nm}} \right) - \tanh \left( \frac{h}{d_{nm}} \right) \right\} \left\{ \frac{\left( \frac{b}{a} \right)}{(m+1/2)^2 \pi^2} + \frac{\left( \frac{a}{b} \right)}{(n+1/2)^2 \pi^2} \right\} + \left\{ \tanh \left( \frac{h}{d_{nm}} \right) \frac{\left( \frac{ab}{d_{nm}^2} \right)}{(n+1/2)^2 (m+1/2)^2 \pi^4} \right\} \right] \quad (6.10)$$

Eq. (6.10) represents the required analytical expression to estimate the radon flux from any cuboidal shaped building material. As may be seen, the computation using Eq. (6.10) requires certain input parameters. These mainly include radium content, radon emanation factor, bulk density and radon diffusion length. Though the solution contains series of terms that have to be summed up, the series is found to be rapidly convergent and can be computed very easily with the help of a numerical program written in the standard software like Mathematica.

### 6.2.2. Comparison between 3-D and 1-D solution

It is interesting to compare the 1-D and 3-D solutions using the same set of input parameters to assess the relative differences between the radon flux from building material sample and that from wall made up by these samples. As stated earlier, Eq. (6.10) represents the formula for calculating mean radon flux from a block of building material. From the solution of 1-D radon diffusion equation, the radon flux from wall ( $J_w$ ) can be expressed as [15]:

$$J_w = \lambda l R \rho_b E \tanh \frac{d}{l} \quad , \quad (6.11)$$

where,  $d$  is the half -thickness of the wall.

It is now required to examine the variation of  $J_w/J_b$  as a function of radon diffusion length ( $l$ ), dimension of building material sample ( $2a$ ,  $2b$ ,  $2h$ ) and thickness of wall ( $2d$ ) using Eq. (6.10) and Eq. (6.11). Let us consider four typical cases with different combinations of  $a$ ,  $b$ ,  $h$ ,  $d$  which includes both thick and thin walls made by building materials of both cubic and cuboidal shape. The physical dimensions selected for the computation are given as follow. Case I:  $a=b=h=d=5$  cm, case II:  $a=b=h=d=10$  cm, case III:  $a=b=10$  cm,  $h=d=2.5$  cm and case IV:  $a=b=5$  cm,  $h=d=15$  cm. Since the ratio  $J_w/J_b$  does not depend upon  $R$ ,  $\rho_b$  and  $E$ , we considered their values as unity.

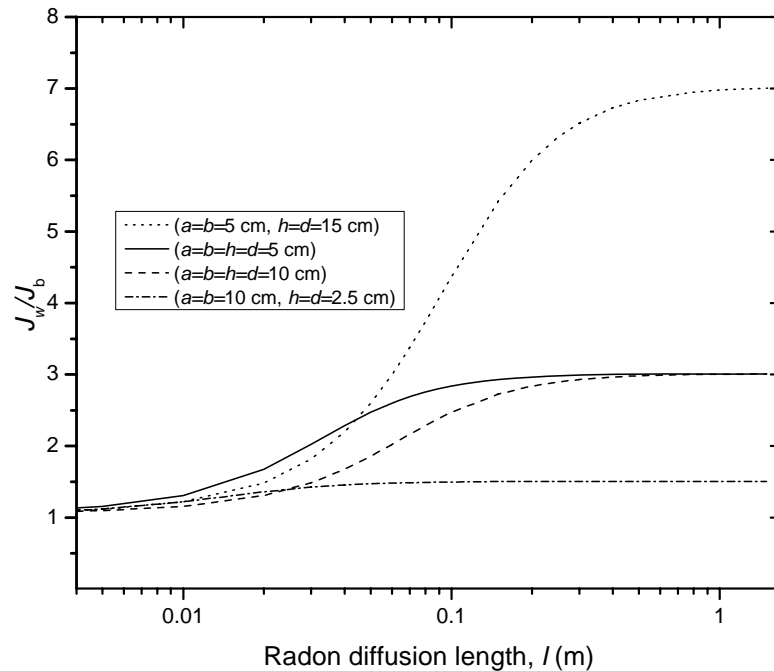


Fig. 6.2: Variation of ' $J_w/J_b$ ' with respect to radon diffusion length ( $l$ ).

With this, computations were made for  $J_w/J_b$  using Mathematica software (to sum the series given in Eq.(6.10)) by varying radon diffusion length( $l$ ) from 0.1 cm to 100 cm. Fig. 6.2 shows the plot of  $J_w/J_b$  with  $l$ . From Fig. 6.2, it is observed that  $J_w/J_b$  has a lower limit of unity (when diffusion length is very small) and increases gradually to a saturation value (when diffusion length is very large). The  $J_w/J_b$  is observed to be as high as 7 indicating a large difference in radon flux from building material sample and that from wall. When the radon diffusion length is very large, then  $J_w/J_b$  is mainly governed by the fraction of the surface area of the building material that has been blocked while constructing the wall and it can be shown theoretically by simple mass balancing considerations that:

$$\frac{J_w}{J_b} = \frac{S_b d}{V_b}, \quad (6.12)$$

where  $S_b$  and  $V_b$  are the surface area and volume of the building material sample respectively. In fact, the saturation value of  $J_w/J_b$  in the numerical evaluation by Eq. (6.10) and Eq. (6.11) as shown in Fig. 6.2 is in exact agreement with this. The factor  $S_b d/V_b$  is similar to the correction factor introduced by Stoulos et al., [53] in their procedure of calculation of indoor radon concentration which corresponds to the surface fractional usage of the building material during the construction of wall. However, this factor alone is not sufficient to infer  $J_w$  from  $J_b$  since in practical situations, the diffusion length ( $l$ ) is comparable to the thickness of the wall. Hence, there is a need to develop a general expression that accounts for the finite  $l$ .

### 6.2.3. Empirical extrapolation

Since there is no exact simple expression (except the full use of Eq. (6.10)) that relates  $J_b$  to  $J_w$ , an empirical extrapolation has been attempted. From the discussions in the preceding section, it is evident that we may now set two limiting conditions for  $J_w/J_b$  namely:

$$(i) \quad \frac{J_w}{J_b} = 1, \text{ when } l \ll d \quad (6.13a)$$

$$(ii) \quad \frac{J_w}{J_b} = \frac{S_b d}{V_b}, \text{ when } l \gg d \quad (6.13b)$$

We seek an empirical extrapolation by comparing 1-D and 3-D solutions to arrive at a model which will satisfy the above two limiting conditions. While several fitting functions are possible, a reasonably simple form of the function consistent with the above limits may be chosen as:

$$\frac{J_w}{J_b} = \left( \frac{S_b d}{V_b} - 1 \right) \exp\left( -k \frac{d}{l} \right) + 1, \quad (6.14)$$

where

$k$  is the regression parameter to be determined from least square fitting to the data points plotted between  $J_w/J_b$  and  $d/l$ .

The data points obtained from Eq. (6.10) and Eq. (6.11) for different cases having several combinations of dimensions of building material samples and wall thickness were least-square fitted to the function given in Eq. (6.14) and the parameter ' $k$ ' was extracted. The fitted functions are shown in Fig. 6.3 vis-a-vis the data points. Table 6.1 lists the value of parameter ' $k$ ' obtained for the different combination of dimensions. The average value of  $k$  is estimated to be  $0.31 \pm 0.05$ .

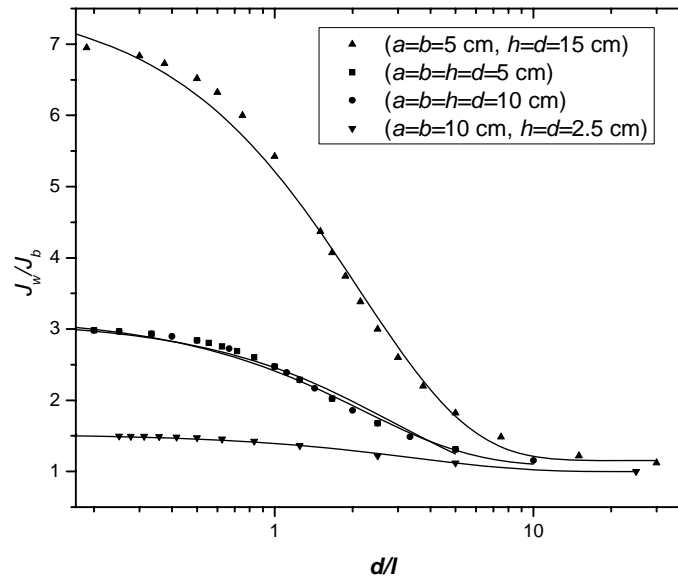


Fig. 6.3: Least Square fitting of the empirical model (Eq. (6.14)) to the data on  $J_w/J_b$ , plotted against  $d/l$  for different combinations of  $a$ ,  $b$ ,  $h$ ,  $d$ . The estimated fitting parameter  $k$  and the corresponding  $R^2$  value showing the goodness of fit are listed in Table 6.1 for each combination.

Table 6.1: List of estimated parameter 'k' from the fitting procedure in Fig. 6.3 and the corresponding  $R^2$  showing the goodness of fit.

Sr. No	Combination	$k \pm SD$	$R^2 \pm SD$
1	$a=b=5$ cm, $h=d=15$ cm	$0.30 \pm 0.04$	$0.97 \pm 0.03$
2	$a=b=h=d=5$ cm	$0.36 \pm 0.03$	$0.98 \pm 0.02$
3	$a=b=h=d=10$ cm	$0.35 \pm 0.03$	$0.98 \pm 0.02$
4	$a=b=10$ cm, $h=d=2.5$ cm	$0.25 \pm 0.04$	$0.99 \pm 0.01$
Average		$0.31 \pm 0.05$	$0.98 \pm 0.008$

It may be noted that the empirical model developed here (Eq. (6.14)) is applicable to both  $^{222}\text{Rn}$  and  $^{220}\text{Rn}$ . For example, if we considered the case of  $^{220}\text{Rn}$ , then under the

condition of small diffusion length, the formula reduces to  $J_w / J_b = 1$  which demonstrates that the  $^{220}\text{Rn}$  exhalation from wall may be considered same as that from building material. However, the same is not true for the case of  $^{222}\text{Rn}$ .

Let us compare the performance of the proposed semi-empirical model (Eq. (6.14)) with respect to the model proposed by Berkvens et al. [111] in the limiting case where latter is applicable. The latter model in our notation can be expressed as:

$$\frac{J_w}{J_b} = \frac{d_e}{d} \cdot \frac{\tanh(d/l)}{\tanh(d_e/l)} \cdot \frac{S_b}{8ab} \quad (6.15)$$

where

$$d_e = h \left( 1 - \frac{h}{3a} - \frac{h}{3b} + \frac{h^2}{6ab} \right) \text{ and the remaining symbols have been defined earlier.}$$

As the above model (Eq. (6.15)) is applicable for  $h=d$  and  $l$  is order of  $d$ , consider a typical case where  $a=b=h=d=l=10$  cm. With this, using Eq. (15) the ratio ' $J_w/J_b$ ' is turned out to be 2.47 against the prediction of 2.46 by the proposed semi-empirical model (Eq. (6.14)) indicating a fairly good matching between the two approaches. However, it was observed that smaller the diffusion length, the model proposed by Berkven et al. [111] underestimates the wall radon exhalation from the absolute value while, the present semi-empirical model correctly predicts the required value within a deviation of less than 2% from the absolute value. This has been demonstrated in section 3.1.

As the focus of this study is on the development of a generalized model to relate the radon flux measured from building material sample to the flux from wall which can be used as substitute to conventional 1-D model, we do not address some of the other practical issues such as effect of plastering and painting on the wall. These issues are basically common to both 1-D and the semi-empirical model developed here. The plastering on wall will reduce the radon concentration in the room which does not increase the risk further. In

this context, the prediction by the proposed semi-empirical model may be treated as an upper bound estimate of indoor radon. The effect due to plastering and painting is a different topic and the same is kept for future work.

### **6.3. Validation of the model**

Using the semi-empirical model given in Eq. (6.14), one can now estimate the enhanced radon flux from a wall using the directly measured radon flux from its building material sample provided the information of radon diffusion length is available. As stated earlier, this model does not require information on radium content, radon emanation factor, density and porosity which are not always very easy to measure. Hence the model may be used as an alternative simple tool to predict radon flux from wall. However, before its application, the model needs to be validated. Towards this end, we have discussed the validation exercise of the model that has been carried out by comparing its results with the absolute 1-D model and the experimental observations.

#### **6.3.1 Comparison with 1-D model prediction**

To test the validity of the semi-empirical model and find the percentage of deviation from the absolute 1-D model, we have compared the two solutions taking few practical examples. For this, we computed the radon fluxes from building materials by summing the series (Eq. (6.10)) in Mathematica software to a converging value. Radon fluxes from the wall were determined using the semi-empirical model (Eq. (6.14)) based on the above converged value and using the 1-D flux model (Eq. (6.11)). In both cases, same set of input parameters were used for computation. The comparison of the 1-D model and empirical model predicted radon fluxes is shown in Fig. 6.4. It may be observed that the deviation between the two is almost negligible (< 2 %) indicating the accuracy of the fitting parameter ' $k$ '. This also ensures the

validity of the semi-empirical model to estimate radon flux from wall as a substitute to 1-D model.

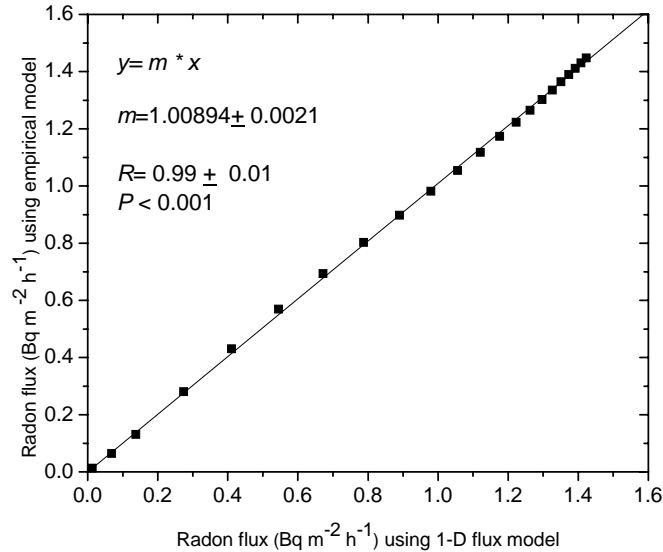


Fig 6.4: Comparison of the radon flux estimated using 1-D flux model and empirical model.

### 6.3.2. Comparison with experimental observations

It is necessary to validate the semi-empirical model by comparing the model prediction directly with experimental observations to gain confidence on the practical applications. However, before validating the semi-empirical model, it is first required to validate the 3-D model (Eq. (10)), which forms the basis of the semi-empirical model. In view of this, two sets of experiments were conducted at a building construction site: (i) to test the validity of the 3-D model (Eq. (6.10)) to predict radon (<sup>222</sup>Rn) flux from building material sample and (ii) the validation of the semi-empirical model (Eq. (6.14) to predict <sup>222</sup>Rn flux from wall. These are described below.

In the first experiment, few cubes of concrete blocks (20 cm x 20 cm x 20 cm) were collected from the construction site. The closed chamber method [53,106] was then used to measure the surface exhalation rates (flux) of  $^{222}\text{Rn}$  from these samples. Standard procedures [104, 112] were used to measure input parameters such as  $^{226}\text{Ra}$  content,  $^{222}\text{Rn}$  emanation factor, bulk density and  $^{222}\text{Rn}$  diffusion length required for the 3-D model. These techniques are briefly described below.

For the exhalation flux measurement, closed chamber technique was followed [89]. The concrete sample block was enclosed in a leak proof chamber (25 cm x 25 cm x 25 cm) to study the build up of  $^{222}\text{Rn}$  in the chamber volume. The build up data were recorded in every one hour interval by a continuous  $^{222}\text{Rn}$  monitor (AlphaGUARD) connected to the chamber. The experiment was continued for about 10 days until saturation was achieved in the growth curve. The  $^{222}\text{Rn}$  flux,  $J_b$  ( $\text{Bq m}^{-2} \text{ h}^{-1}$ ), from the concrete block was estimated by fitting the experimental values of  $^{222}\text{Rn}$  concentration ( $C(t)$ ) vs. elapsed time ( $t$ ) to the following equation (Sahoo et al, 2007).

$$C(t) = \frac{J_b A}{V \lambda_e} (1 - e^{-\lambda_e t}) + C_0 e^{-\lambda_e t} \quad , \quad (6.16)$$

Where,  $V$  is effective volume of the set up i.e. sum of AlphaGUARD and chamber volume excluding the sample volume occupied in the chamber ( $\text{m}^3$ ),  $\lambda_e$  is the effective removal rate ( $\text{h}^{-1}$ ) of  $^{222}\text{Rn}$  for the given set up which is sum of  $^{222}\text{Rn}$  decay constant and back diffusion rate into the sample,  $A$  is the surface area of the concrete block ( $\text{m}^2$ ) and  $C_0$  is the  $^{222}\text{Rn}$  concentration inside the chamber at  $t = 0$ . The experiment was repeated for the other sample blocks as well. At the end of these experiments, each block was crushed into fine particles. To measure  $^{226}\text{Ra}$  content ( $R$ ) in the concrete the standard gamma spectrometric technique [102] was used. The  $^{222}\text{Rn}$  emanation factor ( $E$ ) was estimated from the measured data on

the mass exhalation rates and  $^{226}\text{Ra}$  content of the crushed samples using the procedure of Sahoo et al. [89]. The  $^{222}\text{Rn}$  diffusion lengths in the samples were estimated from the measured bulk density using the standard formula given by Rogers et al. (1994).

Table 6.2 lists the average value of measured input parameters and  $^{222}\text{Rn}$  flux, measured and predicted for the concrete samples. Among all the input parameters,  $^{222}\text{Rn}$  diffusion length and emanation fraction are two critical parameters. The obtained values of these parameters were compared with the values reported in earlier studies [113-114, 45, 53] and confirmed that they fall within the reported range. For example, the diffusion length in concrete estimated from the present experiments was  $0.28 \pm 0.11$  m which is fairly comparable to 0.26 m reported by Stoulos et al. [53].

*Table 6.2: Measured and predicted radon fluxes for concrete block samples using measured physical parameters. Each sample has dimensions:  $a=b=h=10$  cm.*

Sample No	Ra-226 content ( $R$ ) (Bq kg <sup>-1</sup> )	Radon emanation factor ( $E$ )	Density ( $\rho_b$ ) (kg m <sup>-3</sup> )	Radon diffusion length ( $l$ ) (m)	Radon flux ( $J_b$ ) (Bq m <sup>-2</sup> h <sup>-1</sup> )	
					Predicted	Measured
1	20	0.12	2242	0.15	1.3	0.85
2	25	0.09	2180	0.19	1.2	1.8
3	28	0.14	1985	0.35	1.9	2.3
4	22	0.08	1850	0.54	0.8	1.3
5	31	0.11	2063	0.27	1.7	1.4
6	32	0.12	2090	0.25	1.9	2.6
7	24	0.11	2035	0.30	1.3	1.5
8	25	0.08	2258	0.15	1.1	1.3
9	27	0.07	2180	0.19	1	0.5
10	33	0.13	1978	0.36	2.1	3
Average	$27 \pm 4$	$0.11 \pm 0.02$	$2086 \pm 123$	$0.28 \pm 0.11$	$1.4 \pm 0.42$	$1.7 \pm 0.74$

Subsequently, the measured parameters were used in the 3-D model (Eq. (6.10)) to estimate the  $^{222}\text{Rn}$  flux from the concrete blocks. A comparison between the experimental and

the 3-D model estimated fluxes is shown in Fig. 6.5 and a linear fit to the data shows a correlation coefficient of 0.81 and slope of 0.8, implying that the measured values are about 20% higher than the predicted values. Considering the large number of parameters involved and the fact that the diffusion length used for predicting the flux was based on an empirical formula of Roger's et al. [114], the agreement may be considered quite satisfactory. This validation reinforces confidence on the derived semi-empirical model (Eq. (6.14)) to predict  $^{222}\text{Rn}$  flux from the building wall.

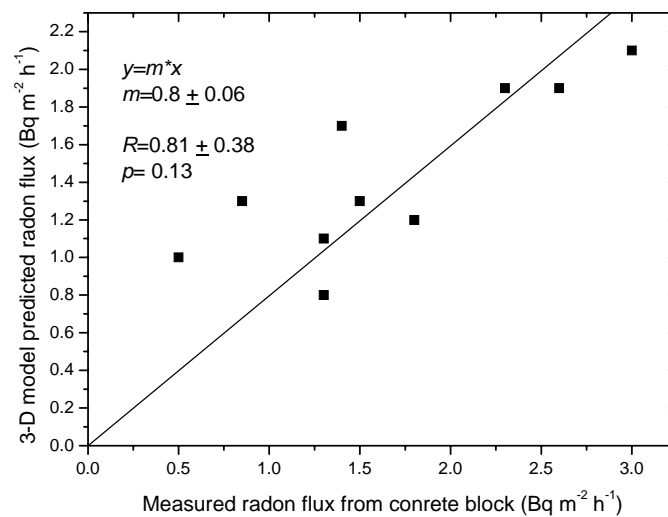


Fig. 6.5: Comparison of the measured and 3-D model predicted radon fluxes from cubic concrete blocks.

Second experiment was mainly aimed at validating the semi-empirical model (Eq. (6.14)) proposed to predict radon flux from building wall based on the flux from building material samples. For this, the in-situ  $^{222}\text{Rn}$  flux was measured from the concrete roof of the building constructed using similar concrete blocks that were collected from the site for first experiment. The accumulator technique was employed for measuring the flux from the roof. The accumulator having a radius of 30 cm and a height of 10 cm was placed on the surface of

the roof. The open mouth of the accumulator which was placed on the surface had a neoprene gasket to prevent superficial leakage from accumulator volume to outside air. The leak was further prevented by placing a load on top of the accumulator. The  $^{222}\text{Rn}$  concentrations in the accumulator were monitored at regular one hour interval using an AlphaGUARD. The accumulator was deployed for time varying from 30 to 60 hours. At the end of the experiment, the  $^{222}\text{Rn}$  flux ( $J_w$ ) from roof was estimated by fitting the buildup data of  $^{222}\text{Rn}$  concentration ( $C(t)$ ) with elapsed time ( $t$ ) to the following equation [63, 82]:

$$C(t) = \frac{J_w A}{V \lambda_e} (1 - \exp(-\lambda_e t)), \quad (6.17)$$

Where  $V$  is total volume (internal volume of AlphaGUARD + volume of the accumulator) ( $\text{m}^3$ ),  $\lambda_e$  is the effective removal rate ( $\text{h}^{-1}$ ) of  $^{222}\text{Rn}$  for the given set up (radioactive decay constant of  $^{222}\text{Rn}$  + back diffusion rate),  $A$  is the surface area of roof covered with accumulator ( $\text{m}^2$ ).

The measurements were carried out at 10 different locations on the roof and the average value of  $^{222}\text{Rn}$  flux from the roof was estimated to be  $5.2 \pm 2.3 \text{ Bq m}^{-2} \text{ h}^{-1}$  which is nearly three times higher than the flux obtained for the concrete block ( $1.7 \text{ Bq m}^{-2} \text{ h}^{-1}$ ). This strongly supports our contention about the enhancement of  $^{222}\text{Rn}$  flux after actual construction of the roof as compared with the concrete block. Thus, calculating indoor  $^{222}\text{Rn}$  concentration [44, 48, 54] by treating the measured  $^{222}\text{Rn}$  flux from building material as same as the  $^{222}\text{Rn}$  flux from the wall, is fundamentally a questionable approach.

Let us now predict the  $^{222}\text{Rn}$  flux from concrete roof by the proposed semi-empirical model (Eq. (6.14)) using the average value of measured  $^{222}\text{Rn}$  fluxes from concrete blocks ( $1.7 \text{ Bq m}^{-2} \text{ h}^{-1}$ ). For this, half thickness of roof ( $d$ ) may be taken as 0.1 m,  $^{222}\text{Rn}$  diffusion length ( $l$ ) as 0.28 m and  $S_b/V_b$  for the cubic concrete block as  $30 \text{ m}^{-1}$ . With this, the predicted  $^{222}\text{Rn}$  flux is found to be  $4.7 \text{ Bq m}^{-2} \text{ h}^{-1}$ , which is very close to measured value of  $5.2 \pm 2.3 \text{ Bq}$

$\text{m}^{-2} \text{h}^{-1}$  from the roof. This validation places considerable confidence on the practical applicability of the proposed empirical model (Eq. (6.14)) for predicting indoor  $^{222}\text{Rn}$  fluxes and (hence concentrations) from the measured  $^{222}\text{Rn}$  flux from building materials.

#### **6.4. A case study from literature on inhalation dose assessment**

Let us consider the case of Ujic et al. [54] wherein they have been calculated the inhalation dose due to  $^{222}\text{Rn}$  and  $^{220}\text{Rn}$  based on the measured surface exhalation rate (flux) of various building materials. It is illustrative to re-compute the inhalation dose based on the corrections obtained with the present empirical model. Although the authors have examined several types of building materials, we take the example of their data on concrete (block 1). The  $^{222}\text{Rn}$  surface exhalation rate reported by the authors for this case is  $290 \pm 50 \mu\text{Bq m}^{-2} \text{s}^{-1}$  which corresponds to  $1.04 \pm 0.18 \text{ Bq m}^{-2} \text{h}^{-1}$ . The authors estimated a corresponding inhalation dose of  $64 \mu\text{Sv y}^{-1}$  considering a model room made by this concrete block, assuming the following parameters: (i) surface area to volume ratio for the room =  $1.6 \text{ m}^{-1}$ , (ii) ventilation rate =  $0.63 \text{ h}^{-1}$ , (iii) dose conversion factor =  $9 \text{ nSv h}^{-1} / \text{Bq m}^{-3}$ , (iv) equilibrium factor = 0.4 and (v) occupancy factor = 0.75.

Now, in order to apply the present model, we need information on dimensions of the concrete block, thickness of the wall and radon diffusion length in concrete. Unfortunately, the paper does not provide information on the dimensions of the building material. However, considering the dimensions of the chamber (20 cm x 20 cm x 40 cm) used for the radon exhalation measurement, we assume that a reasonable dimension for the concrete block is about 20 cm x 20 cm x 20 cm. If the actual dimensions of the blocks were smaller, the correction factors will be even higher. Wall thickness ( $2d$ ) may be taken as 20 cm as reported by authors and we assume a typical value of  $^{222}\text{Rn}$  diffusion length ( $l$ ) in concrete as 0.28 cm

(also estimated in this study). With this, the modified  $^{222}\text{Rn}$  flux from the wall is estimated to be  $3.85 \text{ Bq m}^{-2} \text{ h}^{-1}$  (using Eq. (6.14)), which is nearly 3.5 times of the measured flux from the concrete block. With this, the  $^{222}\text{Rn}$  concentration in the room attributable to concrete turns out to be  $10 \text{ Bq m}^{-3}$  and the corresponding inhalation dose is  $231 \mu\text{Sv y}^{-1}$  which is nearly 3.5 times the value reported by the authors ( $64 \mu\text{Sv y}^{-1}$ ).

### 6.5. Summary

A semi-empirical model has been established by comparing the solution to diffusion equation for a cuboidal shaped building material (3-D) with the solution to diffusion equation for wall (1-D). The model predictions have been validated against experimental observation. This model may be used as a substitute to conventional 1-D model to estimate radon flux from wall without requiring the information on  $^{226}\text{Ra}$  content, radon emanation factor from grain to pore volume of the building material matrix, density and porosity. It, however, requires the information of radon diffusion length and flux from the building material.

This study showed that there exists a large difference (up to a factor of 7) in the radon flux from building material and that from wall made by this building material, depending upon the dimensions of the building material sample and thickness of the wall. Therefore, it is strongly recommended that the indoor radon concentration and inhalation doses should not be directly taken to be the measured radon surface exhalation rate of the building material sample, but should be based on the empirical model presented here. The model provides a useful step towards developing building codes to predict radon concentration in a room and to help in selecting the appropriate building materials from the point of view of reducing the indoor radon concentrations to levels below the reference levels recommended by various international bodies such as WHO [11].

## 7. Concluding Remarks of the Thesis

---

The quantification of the radon source terms in the environment requires accurate techniques for the measurement of emission rates from various Naturally Occurring Radioactive Materials (NORMs) such as soil, building materials etc. The most commonly used techniques, which are also simple and convenient for large scale deployment, are based on measuring the build-up of radon in soil chambers for the case of emissions from soil and closed cans for the case of building materials. The performance of these systems for retrieving the original fluxes from the measured data crucially depends upon understanding quantitatively their responses to impressed radon flux from soil and other matrices. Through a careful study of literature, it was found that there exist several shortcomings in the models used for the analysis of the response of systems. In the context of chamber techniques used for soil flux measurements, no process based model, capable of explaining the chamber response regardless of the chamber size and deployment time, was available. As a result, linear models were employed which placed severe restrictions on chamber dimensions, deployment times and insertion depths. To overcome these limitations, one requires process-based models that can be used primarily for flux retrieval and also for benchmarking the domains of validity of other empirical models. Besides, a well-founded model enables one to obtain additional information on the soil characteristics from the radon concentration build up data.

In the course of the modeling and measurement of radon emissions from soils, an issue of certain significance is the perturbation in emissions due to anthropogenic sealing of

the soil surface such as roads, pavements, buildings and concrete grounds, especially in urban areas. These perturbations introduce certain level of arbitrariness in selecting representative locations by an experimentalist. The establishment of a criterion on the distance of the sampling locations to be maintained from seals requires quantification of the extent of flux perturbations in the vicinity of soil seals. Again one should validate the emission perturbation models by space resolved measurements of fluxes, as one moves away from the seal.

The topic of emission of radon into indoor air from the walls of buildings is of equal importance in assessing radon exposures to populations. Quite often, the radon emission fluxes from walls of the buildings are assessed from the emission data of building material samples assuming that emission fluxes from building material samples and that from walls made up of these materials are the same. This assumption can lead to erroneous estimates of radon fluxes from wall and corresponding indoor radon concentrations. In order to put the issue in proper perspective, it is necessary to carry out systematic modeling of radon emission from building materials samples *vis a vis* the walls made up of those building materials.

With a view to providing improved models and insights into the issues mentioned above, this thesis primarily addresses the development of process based models, analysis of their implications and experimental validations for the flux measurements techniques. The highlights of the various contributions, conclusion arrived at from these studies and the future scopes of works are discussed below.

### **7.1. Contributions**

(i) A two dimensional, two-region, diffusion process based, Non Steady State (NSS) model is developed and solved analytically to quantify the response of the soil chamber deployed on soil surface. The solutions take into account radial diffusion and nonlinear chamber

feedback effects, thereby being applicable to chambers of any size operated continuously without time restriction on the measurement period. The 2-D model enables a simple surface chamber deployment protocol as compared to the deep insertion protocol, commonly used to meet the assumptions of the case of 1-D model. Another important aspect of the 2-D model is that it provides simultaneous information of pre-deployment emission flux and soil diffusion coefficient. The model predicts an instantaneous flux drop due to change in the gas mixing process during deployment of the chamber. The model also predicts other parameters such as saturating concentration in the chamber and its time response, useful parameters for selecting appropriate size of chamber for different applications in environmental specific studies.

(ii) Experimental validation of the 2-D model has been carried out by conducting systematic experiments at a uranium mineralized zone, Jaduguda. Apart from the fluxes, the radium content and various soil parameters were directly measured as inputs for the model. The experimental results showed non-linear growth of radon concentration in the chamber headspace, in close agreement with the the 2-D model predictions. Also, good agreement was found between the model predicted and measured values of the fluxes and soil diffusion coefficients. This study provided a conclusive evidence for the validity of the 2-D model.

(iii) Practical applicability of the 2-D model is demonstrated by carrying two field studies. The first one deals with radon flux mapping on the surface of a uranium tailings pond, Jaduguda and thoron emission mapping on beach sands in coastal region of Kerala. These studies serve the purpose of illustrating the usefulness and convenience of the chamber technique in conjunction with the 2-D model for measuring the emission flux and soil diffusion coefficients, using surface deployment methods.

(iv) Diffusion theory based model has been developed to predict the profile of radon flux on the free soil surface in the vicinity of a semi-infinite soil seal. The model was validated by experiments in the vicinity of a concrete building, by measuring the flux profile closely along the perpendicular direction to the edge of the wall, using small chambers. Such a high resolution, spatial profiling using chambers is made possible by the availability of 2-D model. This study suggested that the flux falls to the normal unperturbed value (within 5%) at a distance of one diffusion length of the soil. This is useful quantification for selecting representative sampling locations in regions with seals.

(v) To correctly predict the indoor emission source term due to walls, a semi-empirical model is proposed which requires input parameters such as emission rate of building materials samples, radon diffusion length in the materials, dimension of the samples and thickness of the wall. Study indicated that there exists a large difference in the surface emission fluxes from a building materials samples and that from a wall made by these materials. This fact was also supported by experimental results. This study suggests that experimentalists either should measure the wall exhalation fluxes directly or must use the semi-empirical model to predict the wall exhalation fluxes using the emission data of building materials samples for calculating indoor radon contributed by building material. The semi-empirical model may be looked upon as a simple alternative tool (substitute to conventional 1-D model) to estimate radon emission from a wall without relying on  $^{226}\text{Ra}$  content, radon emanation factor and bulk density of the samples. The model provides a quantitative framework for developing building codes for radon regulations in new buildings.

## 7.2. Conclusion

The work presented in this thesis constitute definite progress towards providing mathematical bases for the radon, thoron emission processes in general and to their metrology, in particular. It is no longer necessary to make ad-hoc assumptions and arbitrary protocols in deploying soil chambers, since, precise response function is now made available. The experimental studies amply demonstrate that one can use both small and large chambers, deploy them for short and large times, as demanded by specific experimental requirements, without having to worry about the type of model to fit the data. Similarly, the thesis makes a serious attempt to improve our ability for assessing the indoor radon potentials of building materials by bridging the existing knowledge gap between the emission process from a sample and that from a wall, through systematic theoretical analyses. The resulting semi-empirical formula to relate the two fluxes provides a clear recipe for correctly interpreting the experimental data obtained from samples. It may not be an exaggeration to say that the thesis combines mathematical reasoning with experimental practicality to put into perspective. Some of the outstanding issues in the area of radon and thoron flux measurements. Considering the increasing concern shown by professional bodies as well as the general public on the radiological risks due to radon exposure, it is important that the metrological aspects are given due consideration in terms of scientific rigor aimed at improving their accuracy while still retaining their simplicity. This forms the recurring theme of this thesis and it is hoped that the various developments presented here will go a long way in strengthening our confidence in the assessment methods, so as to provide a realistic perspective of the radon, thoron issues in the country and elsewhere in the world.

### 7.3. Future Scope

It may be noted that while chamber techniques are in many applications the best available option for emission studies particularly in view of their simplicity and directness, an increasing emphasis on trace gas budgeting in the atmosphere makes it imperative to explore deployment protocols in which higher spatio-temporal resolutions are possible. The development of the 2-D theory brings such a possibility within sight by providing useable rigorous solutions regardless of chamber dimensions and deployment times. With the advancement of online sensing techniques for trace gases and radon, fully automatic dynamic time-resolved flux measurements are not difficult to establish with the help of this theory. One can easily visualize the importance of joint monitoring of radon and stable gas fluxes at automatic flux stations for delineating the environmental effects (e.g. change of source strength, atmospheric temperature, pressure, relative humidity, etc) on the fluxes.. In case of indoor emission studies, there is a scope for developing dynamic method for measurements of radon and thoron emission from samples of building materials or some passive technique based on radon–thoron discrimination procedure. The thoron interference in radon emission measurements is also required to be investigated. There is also scope for developing building codes for radon regulation in new buildings by extrapolating the emission data of building materials samples to a wall using the indoor radon emission model developed in the thesis. To sum up, it is hoped that the various theoretical ideas and experimental illustrations presented in this thesis will stimulate modeling and field studies further, to obtain an accurate and reliable picture of radon exposure to human populations.

## A. List of Symbols

---

### *Roman*

$a$	: Radius of the chamber/ length of the brick
$A$	: Base area of the Canister / Can/Accumulator
$b$	: Width of the brick
$C_\infty$	: Deep soil pore space concentration of radon
$C_a$	: trace gas concentration in air
$C_c$	: Post deployment chamber headspace concentration
$\bar{C}_c(t)$	: Transient profile of mean concentration in the headspace
$\bar{C}_c(p)$	: Volumetrically averaged LTC (concentration) in the headspace
$C_0$	: Gas concentration in the chamber at time $t=0$
$C_p$	: Trace gas concentration in the pore space of the matrix
$C_s$	: Post deployment soil space gas concentration
$C_s^{(0)}$	: Pre-deployment soil space gas concentration
$\bar{C}_s$	: Mean concentration at chamber-soil interface
$\tilde{C}_s(\rho, \zeta; p)$	: Laplace transform of $C_s(\rho, \zeta, t) : \{t \rightarrow p\}$
$\bar{C}_s(p)$	: Radial averaged LTC (concentration) at soil-chamber interface
$C_w$	: trace gas concentration in water
$d$	: half-thickness of the wall

---

$D_{MA}$	: Molecular diffusion coefficient in air at ambient temp and Pressure
$D$	: Trace gas diffusion coefficient in the matrix
$D_s$	: Diffusion coefficient in soil ( $D\tau$ )
$E$	: Emanation factor of radon from soil grain to the pore space
$f$	: radon flux density measured using charcoal adsorption technique
$f_0$	: Trace gas flux density from the earth's surface prior to the chamber deployment
$\tilde{f}_s(\rho, 0; p)$	: Laplace Transform of $f_s(\rho, 0, t) : \{t \rightarrow p\}$
$\overline{f}_s(p)$	: Radial averaged LTF (flux) at soil-chamber interface
$f_t$	: Thoron exhalation flux density
${}_2F_3(\dots)$	: Generalized hypergeometric function.
$h$	: Thickness of the brick
$H$	: Height of chamber
$J_n(x)$	: Bessel function of order $n$ .
$j_\infty$	: unperturbed trace gas flux density that exist far away from the seal
$j(\xi)$	: Perturbed trace gas flux density at a distance of $\xi$ from the seal
$J_m$	: Radon mass exhalation rate of the sample
$J_b$	: Radon flux density from the brick sample
$J_w$	: Radon flux density from the wall
$K$	: Water to air radon partitioning constant
$L$ ( $l$ )	: Radon diffusion length in the matrix
$M$	: Mass of the sample

---

$m$	: Moisture content in soil
$n_a$	: Air-filled porosity of the matrix
$n_e$	: Partition corrected effective porosity of the soil
$n_T$	: Total porosity of the matrix
$n_w$	: water filled porosity of the matrix
$N$	: net count rate, after background subtraction,
$P(z)$	: Production rate of trace gases in the soil matrix
$R$	: Ra-226 content in soil
$r$	: Radial coordinate
$S(z)$	: $\frac{n_T}{n_e} P(z)$ , partition porosity corrected source term
$S_b$	: Surface area of the brick sample
$t$	: Time since chamber deployment / measurement time
$t_c$	: counting period
$t_d$	: the delay period from the end of exposure
$t_e$	: period of exposure of the charcoal in the canister
$T$	: Temperature in soil
$T_c$	: Effective time constant of the chamber
$T_0$	: $\frac{H^2}{n_e^2 D_s}$
$V$	: effective volume (volume of chamber+ internal volume of $^{222}\text{Rn}$ monitor –volume of sample)
$V_b$	: Volume of the brick sample
$z$	: Vertical axial coordinate

**Greek**

$\alpha$	: $D / n_e D_s$
$\varepsilon$	: counting efficiency of the charcoal canister
$\Gamma(z)$	: Gamma function of $z$
$\Delta$	: Dimensionless height of chamber ( $H/a$ )
$\lambda$	: Decay constant of radon
$\lambda_b$	: Back diffusion rate constant of the trace gas
$\lambda_e$	: Growth rate constant of the trace gas in the headspace
$\rho$	: Dimensionless radial coordinate ( $r/a$ )
$\rho_b$	: Dry bulk density of the soil
$\rho_g$	: Specific gravity of the soil
$\rho_w$	: Density of water
$\theta$	: $n_e \sqrt{D_s / D}$
$\psi$	: $C_s(r, z) - C_s^{(0)}(z)$
$\xi$	: Dimensionless horizontal coordinate
$\zeta$	: Dimensionless axial coordinate
$\nu$	: $1 / \pi \arccos(\alpha / (1 + \alpha))$
$\tau$	: Soil tortuosity
$\tau_c$	: Dimensionless relaxation time in the chamber headspace ( $a^2/D$ )
$\tau_s$	: Dimensionless relaxation time in the soil space ( $a^2/D_s$ )

## B. Finite Difference Programming of the 2-D Chamber Problem

---

Parameter(MaxNx = 600, MaxNz = 600, MaxVisit = 300)

Common /BLK1/Ivisit,Nx,Nz,NzSoil,NzCup,Dx,Dz,Dt,Dsoil,Dair

Common /BLK2/C(MaxNx, MaxNz),Cb(MaxNx, MaxNz)

Common /BLK3/Omin, Omax

Common /BLK4/ProVert(MaxNz,MaxVisit), ProSurf(MaxNx,MaxVisit),

@ ProCupCross(MaxNx,MaxVisit)

Common /BLK5/Flx(MaxNx, MaxNz)

Common /BLK6/FlxVert(MaxNz,MaxVisit), FlxSurf(MaxNx,MaxVisit),

@ FlxCupCross(MaxNx,MaxVisit)

Dimension TimeProC(MaxVisit),TimeproF(MaxVisit)

C Width and depth of soil layer in cm.

Data Width, Depth/100.0,100.0/

C DeltaX and DeltaZ to be used in the computations (in cm)

Data Dx, Dz/1.0,1.0/

C Diameter and height of the cup in cm

Data CupRad, CupHt/15.0,31.0/

C Maximum Simulation duration (hours)

Data Tmax/5.0/

C Output Interval (in Seconds)

Data OutInt/900.0/

C Diffusivity of Rn inside soil and air (cm<sup>2</sup>/s)

---

```

Data Dair, Dsoil/0.1,0.02/

Data Epsair, Epssoil/1.0,0.25/

C  Decay constant for Rn (s-1)

Data Alemda/2.1E-06/

C  Cinf (Bq/m3)

Data Cinf/1.0/

C  Fix Nx and Nz

Nx = (Width/Dx) + 1

NzSoil = (Depth/Dz)+1

NzCup = (CupHt/Dz)

Nz = NzSoil + NzCup

If(Nx.gt.MaxNx.or.Nz.gt.MaxNz)

@Stop' Abnormal Stop: Check dimensions'

D = Dsoil

if(D.lt.Dair) D = Dair

Dspa = Dx

if(Dspa.gt.Dz) Dspa = Dz

Dt = (Dspa * Dspa)/(4.0 * D)

Itime = (Tmax * 3600.0)/Dt

TimeSim = 0.0

TimeOut = 0.0

IcupNx = (CupRad/Dx) + 1

C  Printout the information

Do I = 1 , 5

write(*,*) '

```

```

End Do

write(*,10)Nx, NzSoil, NzCup, Nz, IcupNx, Dt, Itime
10 format(2X,'*****',/,
@ 2X,' Number of grids in X-direction: ',I3,/,
@ 2X,' Number of vertical grids in Soil layer: ',I3,/,
@ 2X,'Number of vertical grids inside the cup: ',I3,/,
@ 2X,' Number of vertical grids: ',I3,/,
@ 2X,' No. of X Grids inside the cup: ',I3,/,
@ 2X,' DeltaT (in seconds): ',F5.2,/,
@ 2X,' Total Number of time steps: ',I5,/,
@ 2X,'*****')
Do I = 1 , 5
write(*,*) ' '
End Do

C Initialize the array including bottom boundary
Do Ix = 1 , Nx
Do Iz = NzSoil+1 , Nz
C(Ix,Iz) = 0.0
End Do
End Do

Dlength = Sqrt(Dsoil/Alemda)
Do Ix = 1 , Nx
Do Iz = 1 , NzSoil
Dist = (Iz - 1) * Dz
C(Ix,Iz) = Cinfi * (1.0 - Exp((Dist-Depth)/Dlength))

```

```

End Do

End Do

Ivisit = 0

Do 9999 It = 1 , Itime
    TimeSim = TimeSim + Dt
    TimeOut = TimeOut + Dt
Do 999 Ix = 2 , Nx-1
Do 99 Iz = 2 , Nz-1
C If you are not inside soil or cup, then please don't fly in air!!!
if(Ix.ge.IcupNx.and.Iz.ge.NzSoil)Go To 99

C Radial 1st term of Eq
if(Iz.le.NzSoil)then
Diff = Dsoil
    Eps = Epssoil
else
Diff = Dair
    Eps = Epsair
End if
FflxX = Eps * Diff * ((C(Ix+1,Iz) - C(Ix,Iz))/Dx)
BflxX = Eps * Diff * ((C(Ix,Iz) - C(Ix-1,Iz))/Dx)
if(Ix.eq.2) BflxX = 0.0
if(Ix.eq.Nx - 1)FflxX = 0.0
if(Ix.eq.IcupNx - 1.and.Iz.gt.Nzsoil)FflxX = 0.0
flxX = (FflxX - BflxX)/Dx

C Radial 2nd term of Eq

```

---

```

if(Ix.eq.2)then
  C1 = C(Ix,Iz)
else
  C1 = (C(Ix,Iz)+C(Ix-1,Iz))/2.0
end if

if(Ix.eq.IcupNx-1.and.Iz.ge.NzSoil)then
  C2 = C(IcupNx-1,Iz)
else if(Ix.eq.Nx-1.and.Iz.lt.Nzsoil)then
  C2 = C(Ix,Iz)
else
  C2 = (C(Ix,Iz)+C(Ix+1,Iz))/2.0
End if

Odist = (Ix - 1) * Dx
Radial = ((C2 - C1)/(Dx)) * ((Diff * Eps)/Odist)

C  Z part of the Eq
if(Iz.le.NzSoil)then
  Diff = Dsoil
  Eps = Epssoil
elseif(Iz.gt.Nzsoil)then
  Diff = Dair
  Eps = Epsair
end if

FflxZ = Diff * ((Eps * C(Ix,Iz+1) - Eps * C(Ix,Iz))/Dz)
BflxZ = Diff * ((Eps * C(Ix,Iz) - Eps * C(Ix,Iz-1))/Dz)
if(Iz.eq.Nz - 1)FflxZ = 0.0

```

---

```

    flxZ = (FflxZ - BflxZ)/Dz
C   Decay Term
    DecayTerm = - Alemda * Eps * C(Ix,Iz)
C   Production term, depending upon the location
    Production = Alemda * Eps * Cinf
    if(Iz.gt.NzSoil)Production=0.0
    RHS = FlxX + Radial + FlxZ + DecayTerm + Production
    C(Ix,Iz) = C(Ix,Iz) + Dt * RHS
99  Continue
999 Continue
C   Pore conc converted to bulk Conc
    Do 98 Ix = 1 , Nx
    Do 97 Iz = 1 , Nz
    Cb(Ix,Iz)=C(Ix,Iz)*Epssoil
97  continue
98  continue
C   Calling various subroutine
    Call SetBC(C(1:Nx,1:Nz),Nx,Nz,NzSoil,IcupNx)
    if(TimeOut.ge.OutInt)then
    print*,'Now entering TimeOut'
    TimeOut = 0.0
    Ivisit = Ivisit + 1
    if(Ivisit.gt.MaxVisit)Stop' No more visit Please!!'
    Call GetMinMax(Cb(1:Nx,1:Nz),Nx,Nz,Omin,Omax)
    Write(*,30)Omin, Omax

```

---

```
30  Format(//,2X,'Minimum Conc = ',E10.4,' and Max. Conc = ',E10.4)
```

```
    Call PrintData(Cb(1:Nx,1:Nz),1)
```

```
    Call GetFlx(Cb(1:Nx,1:Nz), Flx(1:Nx,1:Nz))
```

```
    Call GetMinMax(Flx(1:Nx,1:Nz),Nx,Nz,Omin,Omax)
```

```
    Write(*,40)Omin, Omax
```

```
40  Format(//,2X,'Minimum Flux = ',E10.4,' and Max. Flux = ',E10.4)
```

```
    Call PrintData(Flx(1:Nx,1:Nz),2)
```

```
    write(*,20)IT,Itime,TimeSim
```

```
20  format(2x,I5,' Time steps, out of ',I5,' are over. Sim. Time:',
```

```
    @    F8.2, 'Seconds')
```

```
C    vertical profile of conc and flux with increasing time steps
```

```
    Do Iz = 1 , Nz
```

```
        ProVert(Iz, Ivisit) = Cb(14,Iz)
```

```
        FlxVert(Iz, Ivisit) = Flx(16,Iz)
```

```
    End Do
```

```
C Horizontal profile of conc, flux at surface and at half of cup level
```

```
    Do Ix = 1 , Nx
```

```
        ProSurf(Ix,Ivisit) = Cb(Ix, NzSoil+1)
```

```
        ProCupCross(Ix,Ivisit) = Cb(Ix, NzSoil+(NzCup/2))
```

```
        FlxSurf(Ix,Ivisit) = Flx(Ix, NzSoil-1)
```

```
        FlxCupCross(Ix,Ivisit) = Flx(Ix, NzSoil+(NzCup/2))
```

```
    End Do
```

```
C Time profile of Mean Conc and Mean Flux
```

```
sumf=0
```

```
sumc=0
```

---

```

Do Ix=1,IcupNx
sumf=sumf+(2*3.14*(Ix-1)*Dx*Flx(Ix,Nzsoil-1)*Dx)
End do

Do Ix=1,IcupNx
    Do Iz=Nzsoil,Nz
        sumc=sumc+(2*3.14*(Ix-1)*Dx*Cb(Ix,Iz)*Dx*Dz)
    End do
End do

TimeProC(Ivisit) =((sumc)/(3.14*CupRad**2*CupHt))
TimeproF(Ivisit) =((sumf)/(3.14*CupRad**2))

End If

9999 Continue

Open(21,File='Vert.Dat')
Do Iz = 1 , Nz
write(21,101)(Iz - 1) * Dz, (ProVert(Iz,INV), INV = 1 , Ivisit)
End Do

Close(21)

Open(21,File='Surf.Dat')
Do Ix = 1 , Nx
write(21,101)(Ix - 1) * Dx, (ProSurf(Ix, INV), INV = 1 , Ivisit)
End Do

Close(21)

Open(21,File='CupCro.Dat')
Do Ix = 1 , Nx
write(21,101)(Ix - 1) * Dx,(ProCupCross(Ix, INV), INV = 1 , Ivisit)

```

---

```
End Do
Close(21)
Open(21,File='TimeProC.Dat')
Do INV = 1 , Ivisit
write(21,102)INV,TimeProC(INV)
End Do
Close(21)
Open(21,File='TimeProF.Dat')
Do INV = 1 , Ivisit
write(21,102)INV,TimeProF(INV)
End Do
Close(21)
101 Format(101(E12.4,2X))
102 Format(I3, 2X, E12.4)
Open(21,File='FVert.Dat')
Do Iz = 1 , Nz
write(21,101)(Iz - 1) * Dz, (FlxVert(Iz,INV), INV = 1 , Ivisit)
End Do
Close(21)
Open(21,File='FSurf.Dat')
Do Ix = 1 , Nx
write(21,101)(Ix - 1) * Dx, (FlxSurf(Ix, INV), INV = 1 , Ivisit)
End Do
Close(21)
Open(21,File='FCupCro.Dat')
```

---

```

Do Ix = 1 , Nx
write(21,101)(Ix - 1)* Dx,(FlxCupCross(Ix, INV), INV = 1 , Ivisit)
End Do
Close(21)
Stop
End

Subroutine GetMinMax(Dummy, Nx, Nz, Omin, Omax)
Dimension Dummy(Nx,Nz)
Omin = 1.0E+37
Omax = -1.0E-37
Do I = 1 , Nx
Do K = 1 , Nz
if(Dummy(I,K).ne.0.0.and.Dummy(I,K).lt.Omin) Omin = Dummy(I,K)
if(Dummy(I,K).ne.0.0.and.Dummy(I,K).gt.Omax) Omax = Dummy(I,K)
End Do
End Do
Return
End

Subroutine PrintData(Dummy,ify)
Character*11 FINm
Common /BLK1/Ivisit,Nx,Nz,NzSoil,NzCup,Dx,Dz,Dt,Dsoil,Dair
Common /BLK3/Omin, Omax
Dimension Dummy(Nx, Nz)
if(ify.eq.1)then
C Print concentration

```

```

    FINm(1:4) = 'CONC'

    else if(ify.eq.2)then
C   Print Flux
    FINm(1:4) = 'FLUX'   else

    Stop' Ify is not identified'

    end if

    FINm(8:11) = '.GRD'

    write(FINm(5:7),'(I3.3)')Ivisit

    Open(31, File = FINm)

    write(31,10)

10  format('DSAA')

    write(31,20)Nx, Nz

20  format(I3,2x,I3)

    write(31,30)0.0, (Nx-1) * Dx

30  format(2(E12.4,1X))

    write(31,30)0.0, (Nz-1) * Dz

    write(31,30)Omin, Omax

    write(31,40)Dummy

40  Format(10(E12.4,1X))

    Return

    End

    Subroutine SetBC(Dummy,Nx,Nz,NzSoil,IcupNx)

    Dimension Dummy(Nx,Nz)

    Do Iz = 1 , Nz

    Dummy(1,Iz) = Dummy(2,Iz)

```

---

```

Dummy(Nx,Iz) = Dummy(Nx-1,Iz)

End Do

Do Iz = NzSoil , Nz

Dummy(IcupNx,Iz) = Dummy(IcupNx-1,Iz)

End Do

Do Ix =IcupNx+1,Nx

Dummy(Ix,Nzsoil)=0

    end do

Return

End

Subroutine GetFlx(Dummy1, Dummy2)

Common /BLK1/Ivisit,Nx,Nz,NzSoil,NzCup,Dx,Dz,Dt,Dsoil,Dair

Dimension Dummy1(Nx,Nz), Dummy2(Nx,Nz)

    Data Eps1,Eps2/0.25,1.0/

Do Ix = 1 , Nx

Do Iz = 1 , Nz-1

Diff = Eps1*Dsoil

if(Iz.ge.NzSoil-1) Diff = Eps2*Dair

Dummy2(Ix, Iz) = -Diff * ((Dummy1(Ix, Iz+1)-Dummy1(Ix, Iz))/Dz)

End Do

End Do

Return

End

```

---

## C. Fitting Algorithm of the 2-D Model in ‘Wolfram Mathematica’

---

```

data=ReadList["Mumbai.txt",{Number,Number}]

tmax=45.25; (* This is upper limit of the elapsed time (h) in the data file *)

f0i=1000; (* This is the initial guess of the flux value (Bq/m2/h) to carry out fitting *)

dsei=.000000000000018;

(* This is the initial guess of the effective diffusion coefficient (m2/h) to carry out fitting *)

cci=1000; (* initial guess of saturating concentration (Bq/m3) to carry out fitting *)

tci=1; (*initial guess of time constant (h) to carry out fitting *)

a=0.0775; (* Radius of the Accumulaor (m) *)

h=0.1946; (* This is effective height of accumulaor (m) = Total volume/ accumulator base
area *)

dc=0.36;(* This is the diffusion coefficient of radon in air (m2/h).Default value may be used
*)

eps=0.25; (* This is the typical porosity of matrix. Default value may be used *)

lam=(0.693/(3.82*24)); (* Decay constant of radon (per h). Default value may be used *)

alp[dse_]:=dc/dse;

nu[dse_]:= (1/Pi) ArcCos[alp[dse]/(1+alp[dse])];

theta[dse_]:=((eps*dse)/dc)^0.5;

chinu0[dse_]:= (Gamma[2+nu[dse]]*Gamma[nu[dse]])/(Gamma[0.5+nu[dse]]*Gamma[1.5+nu[dse]]);

```

---

```

lameff[dse_]:=dse/(a*h)*Sqrt[(lam*h^2)/dc]*Coth[((lam*h^2)/dc)^0.5]*chynu0[dse]+lam)/(
1+theta[dse]);
ccinf[f0_,dse_]:=f0/((1+theta[dse])*h*lameff[dse]);
model1[f0_,dse_,t_]:=ccinf[f0,dse]*(1-Exp[-lameff[dse]*t]);
model2[cc_,tc_,t_]:=cc*(1-Exp[-t/tc]);
fittedmodel1=NonlinearModelFit[data,model1[f0,dse,t],{{f0,f0i},{dse,dsei}},t];
fittedmodel2=NonlinearModelFit[data,model2[cc,tc,t],{{cc,cci},{tc,tci}},t];
Show[ListPlot[data],Plot[fittedmodel1[t],{t,0,tmax}],FrameLabel->{"Deployment    elapsed
time(h)", "Radon in accumulator (Bq/m3)"}, Frame->True]
fittedmodel1[{"ParameterTable","RSquared"}]
Show[ListPlot[data],Plot[fittedmodel2[t],{t,0,tmax}],FrameLabel->{"Deployment    elapsed
time(h)", "Radon in accumulator (Bq/m3)"}, Frame->True]
fittedmodel2[{"ParameterTable","RSquared"}]

```

---

---

## **References**

- [1] Kolthoff, I.M and Philips, J. Elving., 1966. Treaties of analytical chemistry, 4, part II, 219.
- [2] Elster, J., Geitel, H., 1901. Physik Z., 2, 590 – 593.
- [3] Gish, O.H., 1951. Compendium of meteorology, edited by Thomas, P. Matone, American Meteorological Society, Boston Massachusetts, 101.
- [4] ICRP, 1987., International Commission of Radiological Protection Pulication No. 50, Lung cancer risks from indoor exposures to radon daughters, annals of ICRP 16, Pergamon press, Oxford.
- [5] BEIR VI, 1999. Committee on Health Risks of Exposure to Radon. National Academy Press.
- [6] Harting, F.H and Hesse, W., 1879. Sanitatswesen, 30, 296 – 309; 31, 102- 132, 313 - 337.
- [7] Ludewing, P. and Lorenzer, S., 1924. Z. Phys., 22, 178
- [8] Lubin J.H. and Boice J.D.Jr., 1997. Lung cancer risk from residential <sup>222</sup>Rn: meta analysis of eight epidemiologic studies. *J. Natl. Cancer Inst.*, 89, 49.
- [9] Darby S, Hill D, Auvinen A, Barros-Dios JM, Baysson H, Bochicchio F, et al., 2005. Radon in homes and risk of lung cancer: Collaborative analysis of individual data from 13 European case-control studies. *British Medical Journal*, 330 (7485), 223-226.
- [10] Krewski D, Lubin J, Zielinski J, Alavanja M, Catalan V, et al., 2005. Residential radon and risk of lung cancer: A combined analysis of 7 North American case-control studies. *Epidemiology* 16 (2), 137-145.
- [11] World Health Organization (WHO), 2009. Handbook on Indoor Radon: A Public Health Perspective. WHO Press, Geneva

- 
- [12] Mayya YS, Mishra R, Prajith R, Gole AC, Sapra BK, Chougaonkar MP, Nair RR, Ramola RC, Karunakara N, Koya PK, 2012. Deposition-based passive monitors for assigning radon, thoron inhalation doses for epidemiological studies. *Radiation Protection Dosimetry* 152 (1-3), 18–24
- [13] Ramola RC, Gusain GS, Rautela BS, Sagar DV, Prasad G, Shahoo SK, Ishikawa T, Omori Y, Janik M, Sorimachi A, Tokonami S., 2012. Levels of thoron and progeny in high background radiation area of southeastern coast of Odisha, India. *Radiat Prot Dosimetry*, 152(1-3), 62-65
- [14] UNSCEAR, 2000. United Nation Scientific Committee on the Effect of Atomic Radiation., Sources, Effects and Risks of Ionizing Radiation., Report to the General Assembly, United Nation, New York.
- [15] Nazaroff WW, Nero Jr AV., 1988. Radon and its decay products in indoor air, New York: John Wiley and Sons
- [16] Bossus D.A.W., 1984. Emanating power and specific surface area. *Radiat. Prot. Dosim*, 7, 73.
- [17] Semkow T.M., 1990. Recoil-emanation theory applied to radon release from mineral grains. *Geochem. Cosmochim. Acta.*, 54, 425.
- [18] Semkow T.M., Parekh P.P., 1990. The role of radium distribution and porosity in radon emanation from solids, *Geophys.Res. Lett.* 17, 837-840
- [19] Semkow T. M., 1991. Fractal model of radon emanation from solids. *Phys. Rev. Lett.* 66 23, 3012-3015.
- [20] Sasaki, T., Gunji, Y., Okuda, T., 2004. Radon emanation dependence on grain configuration, *J. Nucl. Sci. Technol.*, 41, 993-1002.
- [21] Sasaki T., Gunji Y. and Okuda T., 2005. Theoretical Study of High Radon Emanation. *Journal of Nuclear Science and Technology*, 42, 242.

- 
- [22] Thamer B.J., Nielson K.K. and Felthausen, K., 1981. The effects of moisture on radon emanation. Open-File Report 184-82. Washington, D.C.: U.S. Bureau of Mines, 169.
- [23] Strong K.P., Levins D.M., 1982. Effect of moisture content on radon emanation from uranium ore and tailings, *Health Phys.* 42, 27-32
- [24] Rama and Moore W.S., 1984. Mechanism of transport of U-Th series radioisotopes from solids into ground water. *Geochem. Cosmochim. Acta*, 48, 395.
- [25] Bossew P., The radon emanation power of building materials, soils and rocks, *Appl. Radiat. Isot.* 59 (2003) 389-392
- [26] Sakoda A., Ishimori Y., Hanamoto K., Kataoka T., Kawabe A. and Yamaoka K., 2010. Experimental and modeling studies of grain size and moisture content effects on radon emanation. *Radiation Measurements*, doi: 10.1016/j.radmeas.2010.01.010
- [27] Sakoda, A., Ishimori, Y., Yamaoka, K., 2011. A comprehensive review of radon emanation measurements for mineral, rock, soil, mill tailing and fly ash, *Appl. Radiat. Isot.* 69, 1422–1435
- [28] Tanner, A.B., 1980. Radon migration in the ground: A supplementary review. In: Gessell, T.F.; Lowder, W.M., eds. Proc. Natural radiation environment III. Report CONF-780422. Washington, DC.: U.S. Department of Energy ,1, 5.
- [29] Schery, S.D., Holford, D.J., Wilson, J.L., Phillips, F.M., 1988. The flow and diffusion of radon isotopes in fractured porous media: Part 2, semi-infinite media. *Radiat. Prot. Dosim.* 24, 191-197.
- [30] Rogers, V.C., Nielson, K.K., 1991. Multiphase radon generation and transport in porous materials. *Health Phys.* 60, 807.
- [31] Samuelsson, C., and H. Pettersson. 1984. Exhalation of  $^{222}\text{Rn}$  from porous materials. *Radiat. Prot. Dosim.* 7:95–100.

- 
- [32] Lawrence C.E., Akber, R.A., Bollhofer A., Martin P., 2009. Radon-222 exhalation from open ground on and around a uranium mine in the wet-dry tropics, *J. Environ. Radioact.* 100, 1-8.
- [33] Gruber, V., Bossew, P., Cort, M. De, Tollefsen, T., 2013. The European map of the geogenic radon potential. *J. Radiol. Prot.* 33 51 doi:10.1088/0952-4746/33/1/51
- [34] Jha S., Khan A.H., Mishra U.C., 2001. A study of the technologically modified sources of  $^{222}\text{Rn}$  and its environmental impact in an Indian U mineralized belt, *J. Environ. Radioact.* 53, 183-197.
- [35] Hart K.P. 1986, Radon Exhalation from Uranium Tailings, PhD Thesis, University of New South Wales, Kensington, Australia.
- [36] Considine, D. B., Bergmann, D. J., Liu, H. 2005. Sensitivity of Global Modeling Initiative chemistry and transport model simulations of radon-222 and lead-210 to input meteorological data. *Atmos. Chem. Phys. Discuss.*, 5, 3389–3406.
- [37] Jacob, D. J., Prather, M. J., Rasch, P. J., et al., 1997. Evaluation and intercomparison of global atmospheric transport models using Rn-222 and other short-lived tracers, *J. Geophys. Res.*, 102(D5), 5953–5970.
- [38] Rahman NM, Tracy BL, 2009. Radon control systems in existing and new construction: a review. *Radiat. Prot. Dosimetry* 135(4), 243-255.
- [39] Scivyer CR, 2001. Radon protection for new buildings: a practical solution from the UK. *Sci. of Tot. Environ.*, 272, 91-96.
- [40] International Atomic Energy Agency, 1992. Measurement and Calculation of Radon Releases from Uranium Mill Tailings, Technical Reports Series No. 333, IAEA, Vienna
- [41] Livingston, G.P., Hutchinson, G.L., Spartalian, K., 2006. Trace gas emission in chambers: a non-steady state diffusion model. *Soil Sci. Soc. Am. J.* 70, 1459-1469.

- 
- [42] Scalenghe, R., Marsan, A. F., 2009. The anthropogenic sealing of soil in urban areas. *Landscape and Urban Planning*, 90, 1-10.
- [43] Wiegand, J., Schott, B., 1999. The sealing of soils and its effect on soil-gas migration. *Nuovo Cimento Soc. It. Fisica C* 22, 449-455.
- [44] Chen J, Rahman NM, Atiya IA. Radon exhalation from building materials for decorative use. *J. Environ. Radioactivity* 2010; 101(4):317-322.
- [45] Hassan NM, Ishikawa T, Hosoda M, Iwaoka K, Sorimachi A, Sahoo SK, Janik M, Kranrod C, Yonehara H, Fukushi M, Tokonami S, 2010. The effect of water content on the radon emanation coefficient for some building materials used in Japan. *Rad. Meas.* doi:10.1016/j.radmeas.2010.11.006.
- [46] Keller G, Hoffmann B, Feigenspan, 2001. Radon permeability and radon exhalation of building materials. *The Sci. of Tot. Environ* 272, 85-89.
- [47] Maged AF, Ashraf FA., 2005. Radon exhalation rate of some building materials used in Egypt, *Environ. Geochem. Health* 27(5-6), 485-489.
- [48] Mahur, A.K., Kumar, R., Mishra, M., Sengupta, D., Prasad, R., 2008. An investigation of radon exhalation rate and estimation of radiation doses in coal and fly ash samples. *Applied Radiation and Isotopes*, 66(3), 401-406.
- [49] Petropoulos NP, Anagnostakis MJ, Simopoulos SE, 2001. Building materials radon exhalation rate: ERRICCA intercomparison exercise results. *The Sci. of Tot. Environ* 272(1-3), 109-118.
- [50] Rahman S, Mati N, Matiullah, Ghauri B., 2007. Radon exhalation rate from the soil, sand and brick samples collected from NWFP and FATA, Pakistan. *Radiat. Prot. Dosimetry* 124(4), 392-399.
- [51] Righi S, Bruzzi L., 2006. Natural radioactivity and radon exhalation in building materials used in Italian dwellings. *J. Environ. Radioactivity* 88(2), 158-170.

- 
- [52] Shweikani R, Raja G., 2009. Radon exhalation from some finishing materials frequently used in Syria. *Rad. Meas.* 44(9-10), 1019-1023.
- [53] Stoulos S, Manolopoulou M, Papastefanou C., 2003. Assessment of natural radiation exposure and radon exhalation from building materials in Greece. *J. Environ. Radioactivity* 69, 225-240.
- [54] Ujić, P., Čeliković, I., Kandić, A., Vukanac, I., Đurašević, Dragosavac, D., Žunić, Z.S., 2010. Internal exposure from building materials exhaling  $^{222}\text{Rn}$  and  $^{220}\text{Rn}$  as compared to external exposure due to their natural radioactivity content. *Applied Radiation and Isotopes*, 68(1), 201-206.
- [55] Iimoto T., Akasaka Y., Koike Y., Kosako T., 2008. Development of a technique for the measurement of the radon exhalation rate using an activated charcoal collector, *J. Environ. Radioact.* 99 , 587-595.
- [56] Spehr W., Johnston A., 1983. The measurement of radon exhalation rates using activated charcoal, *Radiat. Protect. Aust.* 13, 113–116.
- [57] Iimoto T., Tokonami S., Morishita Y., Kosako T., 2005. Application of activated charcoal radon collectors in high humidity environments, *J. Environ. Radioact.* 78, 69-76.
- [58] Rolston, D.E. 1986. Gas flux. In A. Klute, Ed., *Methods of Soil Analysis, Part 1—Physical and Mineralogical Methods*, 2nd ed. Soil Science Society of America, Madison, WI, pp. 1103–1119.
- [59] Pattey, E., Edwards, G., Strachan, I.B., Desjardins, R.L., Kaharabata, S., and Wagner-Riddle, C. 2006. Towards standards for measuring greenhouse gas flux from agricultural fields using instrumented towers. *Can. J. Soil Sci.* 86, 373–400.
- [60] Antonopoulos-Domis M, Kritidis P, Raptis C., 1998. Diffusion model of radon exhalation rates. *Health Phys.* 74(5), 574-580.

- 
- [61] Jassal, R.S., Black, T. A., Nestic, Z., Guay, D.G., 2012. Using automated non-steady-state chamber systems for making continuous long-term measurements of soil CO<sub>2</sub> efflux in forest ecosystems, *Agricultural and Forest Meteorology*, 161, 57– 65
- [62] Schery, S.D., Whittlestone, S., Hart, K.P., Hill, S.E., 1989. The flux of radon and thoron from Australian soils. *J. Geophys. Res.* 94, 8567-8576.
- [63] Aldenkamp, F.J., de Meijer, R.J., Put, L.W, Stoop, P., 1992. An assessment of in-situ radon exhalation measurements and the relation between free and bound exhalation rate. *Rad. Prot. Dosim.*, 45(1-4), 449-453.
- [64] Pedersen, A.R., Petersen, S.O., Vinther, F.P., 2001. Stochastic diffusion model for estimating trace gas emissions with static chambers. *Soil Sci. Soc. Am. J.*, 65, 49-58.
- [65] Matthias A. D., Blackmer A. M., Bremne, J.M., 1978. A Simple Chamber Technique for Field Measurement of Emissions of Nitrous Oxide from Soils, *Journal of Environmental Quality*, 9 (2), 251-256
- [66] Hutchinson, G.L., and A.R. Mosier. 1981. Improved soil cover method for field measurement of nitrous oxide fluxes. *Soil Sci. Soc. Am. J.* 45, 311–316.
- [67] Jury, W.A., J. Letey, and T. Collins. 1982. Analysis of chamber methods used for measuring nitrous oxide production in the field. *Soil Sci. Soc. Am. J.* 46, 250–256.
- [68] Hutchinson, G.L., G.P. Livingston, R.W. Healy, and R.G. Striegl. 2000. Chamber measurement of surface–atmosphere trace gas exchange: Dependence on soil, interfacial layer, and source/sink properties. *J. Geophys. Res.* 105, 8865–8875.
- [69] Livingston, G.P., and G.L. Hutchinson. 1995. Enclosure-based measurement of trace gas exchange: Applications and sources of error. p. 14–51. In P.A. Matson and R.C. Harriss (ed.) *Methods in Ecology. Biogenic trace gases: Measuring emissions from soil and water.* Blackwell Science, Malden, MA.

- 
- [70] Davidson, E.A., K. Savage, L.V. Verchot, and R. Navarro. 2002. Minimizing artifacts and biases in chamber-based measurements of soil respiration. *Agric. For. Meteorol.* 113, 21–37.
- [71] Hibbard, K., B.E. Law, M.G. Ryan, and E.S. Takle. 2004. Issues and recent advances in soil respiration. *EOS Trans. AGU* 85, 220.
- [72] Anthony, W.H., G.L. Hutchinson, and G.P. Livingston. 1995. Chamber measurement of soil–atmosphere gas exchange: Linear vs. diffusion-based flux models. *Soil Sci. Soc. Am. J.* 59, 1308–1310.
- [73] Livingston, G.P., G.L. Hutchinson, and K. Spatalian. 2005. Diffusion theory improves chamber-based measures of trace gas emissions. *Geophys. Res. Lett.* 32, L24817 doi:10.1029/2005GL024744.
- [74] Wagner, S.W., D.C. Reicosky, and R.S. Alessi. 1997. Regression models for calculating gas fluxes measured with a closed chamber. *Agron. J.*, 89, 279–284.
- [75] Hutchinson, G.L., Livingston, G.P., 2002. Soil-atmosphere gas exchange. In: Dane, J.H., Topp, G.C.(ed). *Method of soil analysis. Part 4. Soil Sci. Soc. Am. J.*, Madison, WI, 1159-1182
- [76] Pedersen, A.R. 2000. Estimating the nitrous oxide emission rate from the soil surface by means of a diffusion model. *Scand. J. Stat.* 27, 385–403.
- [77] Penman, H.L. 1940. Gas and vapor movements in the soil. I. The diffusion of vapours through porous solids. *J. Agric. Sci.* 30, 437–462.
- [78] Ghildyal, B.P., and R.P. Tripathi. 1987. *Soil Physics*. JohnWiley & Sons, New York.
- [79] Rolston, D.E., and P. Moldrup. 2002. Gas diffusivity. p. 1113–1139. In J.H. Dane and G.C. Topp (ed.) *Methods of soil analysis. Part 4. SSSA Book Ser. 5. SSSA*, Madison, WI.

- 
- [80] Healy, R.W., Striegl, R.G., Russel, T.F., Hutchinsion, G.L., Livingston, G.P., 1996. Numerical evaluation of the static-chamber measurements of the soil-atmosphere gas exchange: Identification of physical processes. *Soil Sci. Soc. Am. J.*, 60, 740-747
- [81] Lund, C.P., Riley, W.J., Pierce, L.L., Field, C.B., 1999. The effects of chamber pressurization on the soil-surface CO<sub>2</sub> flux and the implications for NEE measurements under elevated CO<sub>2</sub>. *Global Change Biology*, 5, 269-281.
- [82] Mayya, Y.S., 2004. Theory of radon exhalation into accumulators placed at the soil-atmosphere interface. *Rad. Prot. Dos.*, 111(3), 305-318.
- [83] Abu-jarad, F. A., 1988. Application of nuclear track detectors for radon related measurements. *Nucl. Tracks Radiat. Meas.*, 15 (1-4), 525-534
- [84] Tokonami, S., Takahashi, H., Kobayashi, Y., Zhuo, W., Hulber, E., 2005. Up-to-date radon-thoron discriminative detector for a large scale survey. *Rev. Sci. Instrum.*, 76, 113505–113509.
- [85] Nikezic, D., Stevanovic, N., 2007. Behavior of <sup>220</sup>Rn progeny in diffusion chamber. *Nucl. Instrum. Methods Phys. Res. A*, 570, 182–186.
- [86] Eappen, K.P., Mayya, Y.S., 2004. Calibration factors for LR-115 (Type-II) based radon thoron discriminating dosimeter, *Rad. Meas*, 38, 5-17
- [87] Jarallah M.I. Al, Abu-Jarad F, Rehman F., 2001. Determination of radon exhalation rates from tiles using active and passive techniques *Rad. Meas.*, 34, 491-495
- [88] Strandén E. Building materials as a source of indoor radon. In: Nazaroff WW, Nero AV, editors. *Radon and its Decay Products in Indoor Air*. New York: John Wiley and Sons, 1988
- [89] Sahoo BK, Nathwani D, Eappen KP, Ramachandran TV, Gaware JJ, Mayya YS, 2007. Estimation of radon emanation factor in Indian building materials, *Rad. Meas.*, 42, 1422-1425.

- 
- [90] Liu, G., Si, B.C., 2009. Multi-layer diffusion model and error analysis applied to chamber-based gas fluxes measurements. *Agric. For. Meteorol.*, 149, 169-178.
- [91] Andersen, C.E., 2001. Numerical modelling of radon-222 entry into houses: An outline of techniques and results, *Sci. Total Environ*, 272, 33-42
- [92] Sneddon, I.N., 1966. Mixed Boundary Value Problems in Potential Theory. North Holland Pub. Co.
- [93] Mandal, B.N., Mandal, N., 1998. Advances in dual integral equations. Chapman & Hall/CRC press, Florida, USA. 17-66
- [94] Carslaw, H.S., Jaeger, J.C., 1959. Conduction of heat in solids. 2<sup>nd</sup> ed. Clarendon Press, Oxford, UK, p. 361.
- [95] Mayya, Y.S., Morthekai, P., Murari, M.K., Singhvi, A.K., 2006. Towards quantifying betamicrodosimetric effects in single-grain quartz dose distribution. *Rad. Meas.* 41, 1032-1039
- [96] Sneddon, I.N., 1972. The Use of Integral Transforms. MCGraw Hill, 292-352.
- [97] Bellman, M.D., Kalaba, R.E., Lockett, J.A., 1966. Numerical inversion of the laplace transform; Applications to biology, economics, engineering and physics. NY: Elsevier.
- [98] Wolfram Research, Inc. 2005. Mathematica, Version 5.2, Champaign, IL.
- [99] Smith G. D. 1969 Numerical Solution of Partial Differential Equations. Oxford University Press, London
- [100] Hossler, K., Bouchard, V., 2008. The Joint Estimation of Soil Trace Gas Fluxes. *Soil Sci. Soc. Am. J.*, 72, 1382-1393.
- [101] Zhuo, W., Iida, T., Furukawa, M., 2006. Modeling Radon Flux Density from the Earth's Surface. *J. Nucl. Sci. and Tech.*, 43(4), 479-482.
- [102] Shukla, V.K., Sartendel, S.J., Ramachandran, T.V., 2001. Natural radioactivity level in soil from high background radiation areas of kerala., *Rad. Prot. and Envir.*, 24, 437-439.

- 
- [103]Jonsson G., 2001. Soil radon depth dependence, *Radiat. Meas.* 34 (1-6), 415–418.
- [104]International Atomic Energy Agency, 2010. Analytical Methodology for the Determination of Radium Isotopes in Environmental Samples, IAEA Analytical Quality in Nuclear Applications Series No. 19, IAEA, Vienna.
- [105]RAD 7 Radon detector User's manual (USA: DurrIDGE Company) (2011)
- [106]Sahoo BK, Mayya YS, 2010. Two dimensional diffusion theory of trace gas buildup in soil chambers for flux measurements. *Agric. and Forest Meteorol.* 150, 1211-1224.
- [107]Arfkin G.B. and Weber H.J., 2005. Mathematical Methods for Physicists, Academic Press
- [108]Spiegel M.R, 1964. Schaum's Outline of theory and problems of complex variables SI(Metric) Edition 1981. MCGraw-Hill Book Company, Singapore
- [109]Genitron Instruments GMBH. Users manual Portable Radon Monitor Alpha *GUARD*
- [110]ICRP, 1993. Protection Against Radon-222 at Home and at Work, ICRP Publication 65 Ann. ICRP 23 (2)
- [111]Berkvens P, Kerkhove E, Vanmarcke H., 1988. Three dimensional treatment of steady-state  $^{222}\text{Rn}$  diffusion in building materials: Introducing a practical modified one dimensional approach. *Health Phys*, 55(5), 793-799.
- [112]Sahoo BK, Mayya YS, Sapra BK, Gaware JJ, Banerjee KS, Kushwaha HS. 2010. Radon exhalation studies in an Indian Uranium tailings pile, *Rad. Meas.*, 45, 237-241.
- [113]Cosma C, Dancea F, Jurkut T, Ristoiu D., 2001. Determination of  $^{222}\text{Rn}$  emanation fraction and diffusion coefficient in concrete using accumulation chambers and the influence of humidity and radium distribution, *Applied Radiation and Isotope*, 54, 467-473.
- [114]Rogers VC, Nielson KK, Holt RB, Snoddy R, 1994. Radon diffusion coefficients for residential concretes. *Health Phys*, 67(3), 261-265.